INTERNATIONAL SCHOOL FOR ADVANCED STUDIES

STATISTICAL PHYSICS

Magneto-transport and localization in disordered systems with local superconductive attraction

Thesis submmitted for the degree of Doctor Philosophiae

Academic Year 2015/2016

CANDIDATE

Thuong Thi Nguyen

SUPERVISOR

Prof. Markus Müller

October 2016

SISSA - Via Bonomea 265, 34136 Trieste - ITALY

Contents

Chapter 1

Introduction

1.1 Superconductor-insulator transition in 2D disordered systems

1.1.1 Disorder versus superconductivity: quantum phase transition

Superconductivity [1, 2] and Anderson localization [3] are both fundamental quantum phenomena in condensed matter physics. Their interplay has been intensely investigated theoretically and experimentally for several decades. More than 40 year after its discovery in Kamerlingh Onnes's laboratory in 1911 [1], superconductivity received its first microscopic theory by Bardeen-Cooper-Schrieffer [2], famously known as BCS theory. In this conventional form, electrons from the vicinity of the Fermi level bind in Cooper pairs [4] and condense into a collective state responsible for superconductivity. The pairing effect is induced by the coupling to lattice vibrations, or in other words, is due to phonon-induced attraction. (In more exotic, unconventional superconductors, including high-T_c superconductors, the origin of the effective attraction that glues electrons together and makes them behave as Cooper pairs is still intensely debated, see for example [5].)

Not long after the breakthrough by Bardeen-Cooper-Schrieffer, Anderson [6], Abrikosov and Gor'kov [7] showed that nonmagnetic impurities have no significant effect on superconductivity and its critical temperature, since Cooper pairs are formed from time-reversed eigenstates of the single-particle Hamiltonian, and time-reversal symmetry is not broken by such disorder. However, this statement holds only for weakly disordered systems in which

electronic wavefunctions are not too strongly localized. In strongly disordered systems the Anderson localization can cause the suppression of superconductivity if the level spacing δ_ξ in the localization volume exceeds the gap energy Δ . In 1985, Ma and Lee presented a scenario for the superconductivity formed from localized states [8]. In that work, they argued that strong disorder gives rise to spatial fluctuations of the superconducting order parameter (the BCS gap parameter) and its overall suppression, eventually leading to the destruction of the superconducting state.

Indeed, it is natural to expect the existence of a phase transition in a system where both a superconductive tendency and Anderson localization are present since they lead to two opposite extremes of conductivity at low temperature. On the one hand, superconductivity arises as a condensation of Cooper pairs into a many-body coherent macroscopic quantum state with zero resistance. In contrast, Anderson localization, the disorder-induced quantum localization of electron's wavefunctions, pushes a system towards an insulating state with vanishing conductivity. That transition is particularly interesting and rich in two dimensional systems where Anderson localization is marginal, since only a small amount of disorder is enough to transform a metal to an insulator in non-interacting systems [9]. Adding to this picture is a question about the role of interactions as, in the 1900s, the observation of metallic behaviors in two dimensional low-density electron systems suggested a metal-insulator transition can happen in strongly interacting disordered 2D system [10, 11]. However, the final answer to that question has not been settled.

As the transition between different ground states of the Hamiltonian happens at zero temperature, the superconductor-insulator transition (SIT) provides a simple example of a quantum phase transition [12]. Quantum phase transitions are usually studied through measurements at non-zero but low temperature where the physics is influenced by quantum fluctuation in the critical region. Understanding the essence of how disorder drives the SIT can help to shed light on other related phase transitions. For example, the physics here is closely related to the superfluid-insulator transition of neutral bosons loaded in an optical lattice in the physics of cold atoms [13, 14], which is an

appealing research area that provides a testbed for several condensed matter phenomena. Recently, a potential deep connection between the SIT and the physics of high T_c superconductors has been surmised as several aspects, including a magnetoresistance peak, observed on the insulating side of some systems close to the SIT are similar to those observed in high T_c superconductors, such as $La_{2-x}Sr_xCuO_4$ and $Bi_2Sr_{2-x}La_xCuO_{6-\gamma}$ [15, 16]. Furthermore, as the SIT is a transition driven by disorder in a many-body system, it may entangle with the concept of many-body localization [17, 18] which attracts a lot of attention in recent years. In particular, it has been argued that the insulator close to the SIT might be a good candidate for a nearly many-body localized system in the solid state.

In the following subsections, we briefly selectively review the current situation in both theory and experiments studying the SIT.

1.1.2 Theoretical scenarios

The presence of electron-electron interactions complicates the interplay between superconductivity and disorder, rendering the SIT phenomenology richer and even more interesting. Depending on the strength of Coulomb repulsions, which compete with the electron pairing, the suppression of superconductivity by disorder can occur along different routes. Two main scenarios, the bosonic and fermionic one, have been discussed for the SIT transition. This classification is based on what actually happens at the phase transition: either the amplitude of the order parameter is fully suppressed to zero, or it is just the loss of phase coherence due to strong phase fluctuations, while locally a pairing amplitude survives.

The fermionic scenario was put forward in Finkel'stein's works [19, 20] using a perturbative microscopic description of uniformly disordered systems without any granularity. The essence of this mechanism is that disorder enhances the Coulomb repulsion among electrons by slowing down their diffusion. This effect leads to a reduction of the effective attraction between electrons in a Cooper pair. As a consequence, the amplitude of the superconducting order parameter is suppressed. At a sufficient disorder strength,

the Cooper pairs are broken up into electrons. However, this still happens before the onset of localization. As a result, one expects the emerging non-superconducting state to be a poor metal that eventually transforms into an insulator at higher disorder strength.

In contrast, the bosonic scenario is mostly concerned with phase fluctuations of the superconducting order parameter. In this case, the SIT occurs with a minimal reduction of Cooper pairing. The amplitude of the order parameter is still finite in the vicinity of this transition, but the phase of the order parameter fluctuates such that the oder parameter averages to zero, and stiffness is lost. As a result, Cooper pairs that behave as bosons are present on both sides of the transition. This scenario trivially occurs in granular superconductor with Josephson junctions, where the superconductivity of the macroscopic sample disappears while the local granules remain superconducting [21, 22, 23, 24]. This mechanism was first explored by Fisher [25], based on the boson-vortex duality. He postulated that on the insulating side of the transition, the system forms a Bose insulator where low energy degrees of freedom are just spatially localized "Cooper" pairs. Recently, an interesting route to this bosonic picture has been put forward [16, 26, 27, 28]. In particular, neglecting Coulomb repulsion, Feigel'man *et al.* [26, 27] propose a mechanism of preforming pairs by a relative strong attraction within single particle orbitals. They then argued that superconductivity is even strongly enhanced closed to the Anderson transition due to the multifractal nature of electronic wavefunctions.

Within the scope of this thesis, we aim to employ a relevant microscopic model to explore the physics of the insulating regime of an SIT. We follow in spirit of Ma-Lee approach assuming a good degree of preformation of pairs.

1.1.3 Experimental data

Experiments studying the SIT have been carried out on various thin films with different structures, techniques, materials and control parameters [29, 30]. They include amorphous InO [31, 32, 33], TiN [34, 35], Bi and Pb [36, 37, 38, 39], NbN [40], MoGe [41] films, or $LaAlO_3/SrTiO_3$ interfaces [42], $SrTiO_3$

surfaces [43], MoS_2 flakes [44], etc. The phenomenology results in different experiments vary widely since several mechanisms may be relevant in different materials. For example, films can be simply amorphous or granular. Both exhibit a transition from superconducting to insulating phases; however, in granular systems the formation of mesoscale clusters leads to a nonmonotonic temperature dependence of the resistance which is not expected for homogeneously disordered systems. Also the choice of the parameter tuning through the transition (disorder, magnetic field, or electronic charge density) matters. The nature of the substrate can influence the physics, e.g. some high dielectric constant substrates may better screen Coulomb interactions. Finally, the presence of the strong spin-orbit coupling in experiments with high-atomic-number elements may distinguish them from materials with negligible spin-orbit coupling, as the nature of pairing is affected.

Despite the above diversity, some of the most notable observations are common to most of these experiments, namely:

(i) Many of experiments report a direct transition from a superconducting to an insulating regime. However, for a certain class of materials such as MoGe, the existence of an intermediate metallic regime has been claimed.

(ii) In the case of a direct transition, the characteristics of the quantum critical regime do not seem fully universal, both with respect to the critical values of the resistance and the critical exponent.

(iii) In the insulating phase, close to a direct SIT, at low temperature, a giant magnetoresistance peak appears exhibiting a nonmonotonic magnetic field dependence of the resistance: a strongly positive magnetoresistance at low field and a strongly negative one at high field [32, 33, 34, 39, 40, 45, 46, 47, 48]. The magnetoresistance peak is often interpreted as being driven by a crossover from a regime of paired electrons to a single-electron dominated regime. This experimental observation supported the idea that local superconducting coherence may persist in the insulating regime where only global phase coherence is lost. In special tailored experiments with structured films, magneto-oscillations with a period corresponding to a superconducting flux quantum $h/2e$ have been reported [39, 49, 50]. This further supports the idea that low

energy degrees of freedom are "preformed pairs" rather than single electrons.

(iv) The transport in those systems (in a wide range of low temperature and low magnetic field below the peak where magnetoresistance is positive) exhibits activated behavior, $R(T) = R_0 \exp(T_0/T)$ in a wide temperature window. This is not usually expected in disordered electron systems where normally Mott or Efros-Shklovskii variable range hopping are observed.

1.1.4 Open issues

Despite a lengthy discussion on both the theoretical and experimental side, a generally accepted scenario for the loss of superconductivity with disorder and for the nature of the non-superconducting state has not yet emerged. Several questions remain open, for example regarding the possible universality classes to which the quantum phase transitions belong, their universal characteristics, and the possible description within a scaling theory. Also the insulating phase presents a number of puzzling and intriguing features. In order to understand the nature of the insulating regime, it seems crucial to explore and understand the physical mechanisms underlying the magnetoresistance peak and the activated transport observed close to the SIT. A better understanding of this physics also provides a clearer picture for the approach to the phase transition.

1.2 Thesis overview

Motivated by the intriguing features of the insulating regime close to an SIT, I carry out a systematic study of magnetoresistance, elucidating a variety of approach that influence it.

In ***Chapter 2*** I introduce a model of hard-core bosons on a two dimensional honeycomb lattice in a magnetic field, as motivated by recent experiments on structured films [38, 39]. This aims at explaining several key features observed in the activated magneto-transport in those experiments. Taking into account long range Coulomb interactions among the bosons, I study the crossover from strong to weak localization of those excitations and how it is

affected by a magnetic field. An effective mobility edge in the excitation spectrum of the insulating Bose glass is identified as the (intensive) energy scale at which excitations become nearly delocalized. Within the forward scattering approximation in the bosonic hopping I find the effective mobility edge to oscillate periodically with the magnetic flux per plaquette [51].

Furthermore, I contrast the magnetoresistance in bosonic and fermionic systems, and thus show convincingly that the magneto-oscillations seen in experiments of SIT systems reflect the physics of localized electron pairs, i.e a Bose glass rather than a Fermi insulator. The bosonic magneto-oscillations start with an increase of the mobility edge (and thus of resistance) with applied flux, as opposed to the equivalent fermionic problem. The amplitude of the oscillations is much more substantial in bosons than in fermions. Bosons exhibit a single hump per flux period, while fermion characteristics undergo two humps. Those are identical for non-interacting fermions, but Coulomb correlations are shown to lead to systematic deviations from this statistical period doubling.

In this approach, only bosonic degrees of freedom are considered. It thus cannot cover the wide range of fields often explored in experiments, where field-induced pair breaking processes certainly take place and are relevant. Therefore, in ***Chapter 3*** I introduce a microscopic model taking both bosonic and fermionic degrees of freedom into account. This model is then used to study the magnetic field driven crossover from pair to single electron regimes and the corresponding resistive transport. This study is motivated by the above mentioned experiments observing a strong magnetoresistance peak on the insulating side of the SIT which reflects that crossover.

Assuming Mott variable range hopping transport, the pair-to-single crossover in transport is driven by the crossover in the characteristic temperature scale T_M governing the stretched exponential growth of the resistance $R(T)$ for pairs and single electrons. Within this work, I consider a system of electrons on a square lattice, subject to strong onsite disorder, a local pairing attraction, a magnetic field, and nearest neighbor hopping. The tuning parameter, the magnetic field, enters both by a (spatially) isotropic Zeeman depairing term

and an anisotropic orbital effect proportional to the perpendicular component of the field incorporated via the complex phase of the hoppings. I found that the former leads to a strong effect on the density of state which causes and dominates the crossover, and thus the magnetoresistance peak. The orbital effect captures the effect of the quantum interference of different types of carriers. It further enhances the peak as the field orientation changes. I also discuss the effect of including Coulomb interactions into this theory.

Having pointed out the peculiarity of two dimensional disordered systems which are marginal in terms of single-particle localization, and in view of our finding of the effective mobility edge above, I address the question of whether Coulomb interactions can give rise to a genuine mobility edge in electronic systems in two dimensions. In ***Chapter 4*** with Coulomb interactions being treated at a more quantum level (but still approximately) within a Hartree-Fock treatment, I carry out a numerical study aiming at addressing the possibility of an interaction-induced delocalization effect. This setting focuses on the multiplicity of electron species, or valley degeneracy, that Punnoose and Finkel'stein [11, 52] predicted to cause delocalization in two dimensional interacting electron system. As I will discuss, by looking at the density-density correlation function, the system with multiple species behaves differently from the system with single species. In the former, the two-stage scale-dependent behavior of the correlation function reflects the scale-dependent resistance predicted in Punnoose and Finkel'stein's renormalization group equations.

Chapter 2

Magneto-oscillations of the mobility edge in Coulomb frustrated bosons and fermions

2.1 Introduction

The interplay between disorder and Coulomb interactions is a crucial element affecting the phenomenology of the superconductor-insulator quantum phase transition. If only disorder and local BCS attraction is considered, and Coulomb repulsion is neglected, numerous theoretical studies [8, 25, 26, 27, 28, 53, 54, 55] have predicted the existence of preformed pairs in the vicinity of criticality, in the sense that the route from the insulating to the superconducting state proceeds directly through a delocalization of attractively bound pairs of electrons. This contrasts with the fermionic scenario first studied by Finkel'stein, in which the transition is driven by the suppression of electron pairing due to disorder-enhanced Coulomb interactions [20]. Under certain circumstances and in specific materials, however, it has been argued that the *local* Coulomb repulsion can be overcompensated by specific attraction mechanisms, resulting in systems with effective negative Hubbard U interactions [56, 57, 58, 59].

On the experimental side, in the early nineties, transport measurements on InO_x by Hebard, Palaanen, and Ruel [31, 45] were interpreted as signatures of Cooper pair insulators, suggesting that the above bosonic mechanism might be at work in that material [25]. Indeed, fermionic and bosonic insulators differ

qualitatively since the exchange statistics affect their localization properties, in particular the interference of scattering paths that determine the decay of the wavefunction. In the presence of a magnetic field, the wavefunctions of fermions and bosons respond in opposite ways [60, 61, 62, 63, 64, 65]. For low energy bosonic excitations, the constructive interference among all paths is suppressed by a magnetic field, which leads to a strong positive magnetoresistance [60]. This contrasts with the subtle mechanism of the field-induced suppression of occasional negative interferences, which dominates the localization properties of localized fermions and results in a negative, but rather weak magnetoresistance [63].

More recent experiments on amorphous thin films of Bi [38, 39, 66], PbBi [67], InO_x [32, 33, 50], TiN [34], or on a single ring of InO_x [68] have strengthened the case of bosonic insulators, and exhibited a variety of intriguing transport characteristics. In particular, transport in the insulating state was observed to have an activated characteristics, with an Arrhenius-type resistance of the form $R(T) \propto \exp(T_0/T)$, over a significant range of temperatures, T_0 being the activation energy [32, 69]. Patterned films with an artificially created superlattice [38, 39] also exhibited activated behavior, with an activation energy oscillating with the applied magnetic field. The observed oscillation period corresponds to one superconducting flux quantum $h/2e$ threading the unit cell of the superlattice, suggesting that the relevant charge carriers are pairs of electrons, which preserve phase coherence beyond the scale of the imposed pattern.

The observation of purely activated transport in these systems is rather surprising in a highly disordered insulator, where generically a stretched exponential dependence of the resistance on temperature is expected, due to variable range hopping transport [70]. The latter, relies however, on a sufficiently efficient bath that allows inelastic transitions of carriers to transport charge through the system. If instead the coupling between phonons and the relevant carriers (pairs or electrons) is weak, and if the low energy sector of electronic excitations is by itself discrete in nature, transport may be dominated by other channels than phonon-assisted variable range hopping. One

possibility is the transport via activation to a mobility edge of the relevant charge carriers [70, 71], which indeed yields an Arrhenius resistance down to relatively low temperatures until eventually variable range hopping will take over, in spite of the inefficiency of the phonon bath. Such a phenomenology may be seen as a precursor of the much more stringent many-body localization, which not only requires a strong decoupling from phonons, but also the full localization of *any* intensive excitations, and in particular the absence of finite-energy mobility edges, which we discuss here.

The above mentioned Arrhenius resistance is also expected in a wide temperature range if the mobility of charge excitations merely exhibits a sharp crossover around an 'effective mobility edge' (in energy), instead of undergoing a genuinely sharp transition from localized to diffusive behavior at a precise energy [70]. This will be discussed in more detail below.

In this chapter we explore the phenomenology of the crossover from weak to strong localization. In particular we ask, how the effective mobility edge behaves in the presence of a magnetic field. At a qualitative level, it is clear that the effective mobility edge follow trends analogous to those predicted for the localization length of low energy excitations: As the localization length increases, the effective mobility edge decreases, and vice versa [60]. Here we investigate this effect more quantitatively and show that a relatively simple model of strongly localized pairs, subject to long range Coulomb interactions, is able to reproduce the salient features reported in the experiments on patterned films.

Long range Coulomb interactions are known to play an important role in disordered insulators. In particular, they induce a depletion of the density of states around the chemical potential, creating a pseudo gap in the single particle density of states [72]. This in turn modifies the localization properties of low energy excitations and promotes the appearance of an effective mobility edge, as was recently analyzed in the context of interacting electrons close to the Anderson-Mott metal insulator transition [73, 74, 75]. In contrast, in the presence of a flat or featureless bare density of states, with purely local repulsive interactions, there is no clear evidence of a mobility

edge in the low energy spectrum of bosonic or fermionic insulators [60, 76]. Rather, the available techniques suggest that the localization length always decreases with increasing excitation energy. However, numerical results suggest that the addition of interactions, which are not strictly local, induces a delocalizing tendency at higher energies, and thus mobility edges [77]. The latter tendency becomes stronger with an increasing range of the interactions. Here we analyze the experimentally relevant case of unscreened, long range Coulomb interactions, and study the effect of magnetic fields on the effective mobility edge. Under the assumption that the effective mobility edge takes the role of the activation energy T_0 that enters an Arrhenius law of transport, we obtain a semiquantitative description of transport in the absence of an efficient thermal bath.

It is a main goal of this work to contrast the magnetoresistance in bosonic and fermionic systems. A particularly clean case can be made by comparing tightly bound pairs, acting as hard core bosons, with unpaired (spinless) fermions, which otherwise are subject to the same potential disorder, interactions and hopping strengths. Indeed, both carriers are hard core particles. The only difference consists in their exchange statistics, which at first sight might seem rather innocuous in insulators. However, they reflect strongly in the magnetoresistance, which probes the quantum interference in the exponential tails of localized excitations.

The remainder of this chapter is organized as follows. In Sec. 2.2 we introduce and motivate the model under study. The magneto-oscillations of the localization length and the effective mobility edge for bosons are presented in detail in Sec. 2.3. Sec. 2.4 establishes the connection of our theory with experimental data. In Sec. 2.5 we contrast the phenomenology of hard core bosons with that of fermions and explain the various effects of quantum statistics on the effective mobility edge. A summary of the central results is given in Sec. 2.6.

2.2 Model

The present study is motivated by the experiments of Refs. [38, 39] on patterned films of Bismuth, with holes punched in a triangular array. Those leave a connected part of Bismuth forming a honeycomb lattice (with lattice constant $a \approx 50$nm), see Fig. 2.1. As those films are made sufficiently thin they undergo a superconductor-to-insulator transition, whereby the transport on the insulating side bears the hallmarks of a bosonic insulator. In particular, it exhibits a strong positive magnetoresistance.

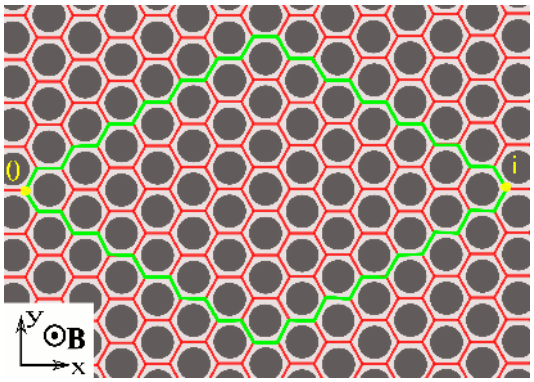

Figure 2.1: Sketch of barely percolating films, with a triangular lattice of holes pinching it. These structures are modelled by a honeycomb lattice of islands hosting preformed pairs. The green lines connecting the two sites 0 and i enclose a diamond-shaped region containing all the shortest paths that connect those sites.

To model such films, we introduce a simplified model of interacting hard-core bosons [8] living on a two-dimensional honeycomb lattice of tunnel-coupled islands, governed by the Hamiltonian

$$\begin{aligned} H &= \sum_i (\varepsilon_i - \mu) n_i + \frac{1}{2} \sum_{j \neq i} \frac{q^2}{\kappa r_{ij}} (n_i - \nu)(n_j - \nu) \\ &\quad - t \sum_{\langle ij \rangle} \left(\mathrm{e}^{\mathrm{i} \frac{q}{\hbar c} \int_{\mathbf{r}_j}^{\mathbf{r}_i} \mathbf{A} \mathbf{dr}} b_i^\dagger b_j + \mathrm{h.c} \right), \end{aligned} \tag{2.1}$$

where $b_i^\dagger$, b_i are the creation and annihilation operators of a hard-core boson of charge $q = 2e$ on site i, and $n_i = b_i^\dagger b_i$ is the local number operator. The hard core bosons represent strongly bound, preformed electron pairs. The chemical potential μ is adjusted such as to assure half-filling ($\nu = 1/2$) of

the lattice. The particles are subject to disordered onsite potentials ε_i being uniformly distributed in $\varepsilon_i \in [-W, W]$. They interact via long-range Coulomb interactions that decay as $1/r$, since the ambient space is 3d. κ denotes the dielectric constant of the film, which is typically fairly large in such nearly metallic structures [27, 78]. The Coulomb contribution from a neutralizing background charge of homogeneous density ν has been subtracted. The magnetic field enters via an Aharonov-Bohm phase factor multiplying the nearest-neighbor hopping amplitude t. The phase acquired on each link is the line integral of the vector potential $\mathbf{A}$, for which we choose the gauge $\mathbf{A} = Bx\mathbf{e_y}$. We measure the magnetic field B in terms of the fraction of flux quanta per plaquette, $f = B/B_0$, where $B_0 = hc/qS$, and $S = 3\sqrt{3}a^2/2$ is the area of the unit cell. The depairing Zeeman effect of the magnetic field on the electron pairs is neglected here. Its effect will be studied in forthcoming chapter.

The above model captures a rather generic situation in bosonic or spin-polarized fermionic insulators. Even though a given island i will in general host a rather large number of charges, in the insulating phase we may restrict ourselves to describing the two most relevant charge states, which differ by the absence or presence of a charge carrier (an electron pair in the case of the bosonic insulator). States differing by stronger charge fluctuations are not expected to modify the physical behavior of the insulator significantly, and thus we believe the above model to capture the gist of the experimental systems.

In the numerical studies carried out below, we study two-dimensional lattices and employ periodic boundary conditions. The Coulomb interaction between two sites is taken to be proportional to the inverse of the minimum distance on the torus. The Coulomb repulsion between nearest neighbor charges, $E_C = q^2/\kappa a$, is used as the unit of energy, while the lattice constant a serves as the unit of length.

2.2.1 Classical electron pair glass

It is impossible to solve the full Hamiltonian (2.1) exactly. Instead we approach the problem in an approximate way, which captures the main physical

effects. We consider the hopping as a perturbation and neglect it in a first step. That is, we first deal with a classical Hamiltonian describing a Coulomb glass of particles with charge $q = 2e$. Such a system is well-known to possess many metastable low-energy configurations which are stable with respect to the rearrangement of few particles. The Coulomb interactions with other particles strongly modify the distribution of the low-lying single-site excitation energies $\tilde{\varepsilon}_i$,

$$\tilde{\varepsilon}_i = \frac{dH}{dn_i} = \varepsilon_i - \mu + \sum_{j \neq i} \frac{q^2}{\kappa r_{ij}} (n_j - \nu). \tag{2.2}$$

In $d = 2$ the Coulomb interactions create a linear Coulomb gap in the density of single particle excitations at low energy, $\rho(\tilde{\varepsilon}) = C\tilde{\varepsilon}/E_C^2$, as predicted by Efros and Shklovskii [72]. Fig. 2.2 shows the corresponding single-particle density of states, $\rho(\tilde{\varepsilon})$ for various disorder strengths, as obtained numerically. The coefficient C is nearly independent of disorder (for $W \gtrsim 1$) and takes roughly the value $C \approx 0.61$, not far from theoretical predictions [79].

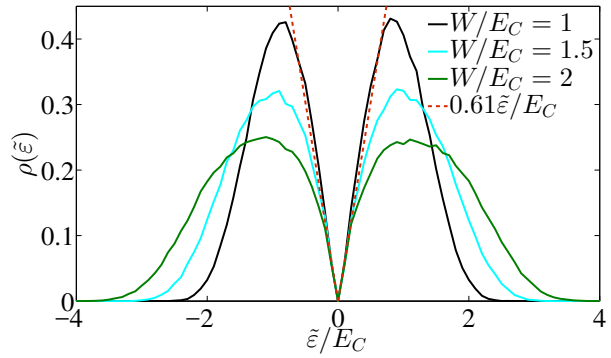

Figure 2.2: Single-particle density of states for various disorder strengths W in a two-dimensional Coulomb glass. A linear Coulomb gap forms, which ensures stability with respect to single particle transitions. Excitations are more strongly localized at low energies. An effective mobility edge may thus appear at higher energies within the Coulomb gap.

2.2.2 Localization on the background of a Coulomb gap

In the strongly insulating regime $t \ll W$, the hopping term can be treated as a perturbation. Here we study the localization properties of a single particle

excitation. It can be read off from the spatial dependence of the amplitude of poles of the Green's function. Following the formalism introduced in Ref. [60], the Green's function (in the $T \to 0$ limit) can be obtained in a perturbative expansion in the hopping using a locator expansion, whereby we treat the on-site potentials $\tilde{\varepsilon}_i$ as frozen-in static disorder which depends on the metastable state under consideration. In a given metastable state of the Coulomb glass (defined by a locally stable classical charge distribution), to leading order in the hopping, the Green's function at large distance is obtained as

$$\begin{aligned} \frac{G_{0,i}(\omega, B)}{G_{0,0}(\omega, B)} &= t^{r_{0i}} \sum_{\substack{\Gamma:0\to i \\ |\Gamma|=r_{0i}}} e^{i\Phi_\Gamma(B)} \prod_{k\in\Gamma\setminus\{0\}} \frac{\mathrm{sgn}(\tilde{\varepsilon}_k)}{\tilde{\varepsilon}_k - \omega} \\ &\equiv \left(\frac{t}{W}\right)^{r_{0i}} S_{0i}(\omega, B). \end{aligned} \tag{2.3}$$

Here the sum $S_{0i}(\omega, B)$ runs over all paths Γ of shortest length $|\Gamma| = r_{0i} \equiv \mathrm{dist}(0, i)$, defined as the minimal number of nearest neighbor hops necessary to connect the two sites. $\Phi_\Gamma(B)$ is the flux enclosed by the loop formed by path Γ and a fixed reference path connecting 0 and i. The latter merely fixes the gauge of the Green's function.

In Eq. (2.3), the only trace of quantum statistics is the residue $\mathrm{sgn}(\tilde{\varepsilon}_k)$ of the locator, which applies to hard core bosons. For non-interacting fermions, instead, this factor is absent. This forward scattering approximation, and especially its fermionic version, has been analyzed extensively in the literature [60, 62, 63, 64, 80, 81].

The localization length of excitations at energy ε_0 is defined as the inverse of the typical spatial decay rate of Green's function residues of poles at $\varepsilon = \varepsilon_0$,

$$\xi^{-1}(\varepsilon_0, B) = -\lim_{r_{0i}\to\infty} \frac{1}{r_{0i}} \overline{\ln \left| \frac{G_{0,i}(\omega, B)}{G_{0,0}(\omega, B)} \right|}_{\omega\to\varepsilon_0}. \tag{2.4}$$

The overbar denotes the disorder average. On a regular lattice, this definition depends on the direction in which the point i tends to infinite distance from 0, even though the relative variations will be very similar for different directions. Below we analyze the direction along a lattice base vector, as indicated in

Fig. 2.1.

From Eq. (2.3) it follows that at low excitation energies, $\omega \to 0$, in the absence of a magnetic field ($\Phi = 0$) all paths come with positive amplitudes and thus interfere constructively. A magnetic field destroys the perfect constructive interference by adding a phase factor to each path. In contrast, for fermions, the path amplitudes always have essentially random signs, whatever the magnetic field. However, for $B = 0$ the likelihood of occasional, strongly destructive interferences between two bunches of paths is bigger than in finite flux. This effect was first discovered by Nguyen, Spivak and Shklovskii. [63] It leads to a weak negative magnetoresistance for fermions, which contrasts with the strong positive response of bosons [62].

It is convenient to split the inverse localization length into a simple hopping part and a geometric part capturing interference,

$$\xi^{-1}(\varepsilon_0, B) = \ln\left(\frac{W}{t}\right) + \xi_g^{-1}(\varepsilon_0, B), \tag{2.5}$$

where

$$\xi_g^{-1}(\varepsilon_0, B) = -\lim_{r_{0i}\to\infty} \frac{1}{r_{0i}} \overline{\ln|S_{0i}(\omega, B)|}_{\omega\to\varepsilon_0}. \tag{2.6}$$

Definition of (effective) mobility edge

Due to the increase of the single particle density of states with energy ε, based on formula (2.3) one expects an increase of the localization length with increasing excitation energy $|\varepsilon - \mu|$. If the tunneling amplitude t is finite, the localization length of zero temperature excitations, as defined by (2.4), may diverge at sufficiently high energies. This is indeed expected to happen in dimensions $d > 2$ close enough to the transition to a conductor. This was analyzed in quite some detail for fermionic insulators in Refs. [74] and [75]. In such higher dimensional systems the energy

$$\epsilon_c = \inf\{E|\xi(E) = \infty\}. \tag{2.7}$$

sharply defines a mobility edge in the limit $T \to 0$.

However, in dimensions $d = 2$ (the case of interest to us here) at $T = 0$, one does not generally expect genuine delocalization at finite excitation energies. Rather, in close analogy with the well-known case of single particle excitations in the absence of anti-localizing spin-orbit interactions, one expects the proliferation of returns to the origin of any finite energy excitation to induce localization, albeit with a localization length that may become exponentially large upon varying a control parameter. In non-interacting fermionic problems the control parameter is given by $k\ell$, which is to be considered as a function of the energy E.

Nonetheless, even in $d = 2$ it is meaningful to identify a crossover energy ϵ_c at which strong localization (at lower energies) turns into exponentially weak localization (at higher energies). For most practical purposes, such a crossover scale ϵ_c acts like an *effective* mobility edge, above which the effects of localization become very weak. They will thus not show up down to very low temperatures. If the localization length is a strongly increasing function of excitation energy the effective mobility edge is expected to exhibit only a slow logarithmic increase with decreasing temperature. To illustrate this idea, let us briefly discuss the case of two-dimensional disordered insulators, where one expects that any finite energy excitation remains localized at strictly zero temperature. In other words, eigenstates with excitation energy $O(1)$ above the ground state are expected to differ only locally from the latter. One may in principle construct operators that create such "elementary" $T = 0$ excitations from the ground state. However, in general two such operators do not (anti-)commute with each other. As a consequence, eigenstates at finite energy density will not simply consist in a finite density of such localized excitations above the ground state, but hybridize various configurations with excitations in different locations. In particular the sufficiently weakly localized excitations at high energy will not commute (and thus collide) with many other elementary excitations. If the corresponding collision rate is bigger than the inverse of the level spacing in the localization volume of the high energy excitation, the localization of the latter should be irrelevant at that temperature, and one expects those excitations to be diffusive. This phenomenology

leads to a weakly temperature dependent effective mobility edge, as was discussed in Ref. [70]. At sufficiently low temperature, the collision rate with other elementary excitations will eventually become so infrequent that the finite system size becomes a more efficient cut-off for localization. In that case the effective mobility edge will become (weakly) size dependent [1].

A practical definition for an effective mobility edge can be obtained by identifying the energy ϵ_c where the perturbative locator expansion (2.4) ceases to decay with distance (while higher order loop corrections would most likely reinstate a weak exponential decay), i.e.,

$$\epsilon_c = \min\{E|\xi^{\mathrm{FSA}}(E) = \infty\}. \tag{2.8}$$

Here, the superscript FSA indicates the restriction to the leading order forward scattering approximation. For non-interacting fermions in $d \geq 3$ this criterion correctly selects an energy for which $k\ell(\epsilon_c) = O(1)$, a qualitative criterion which is also satisfied by the rigorously defined, sharp mobility edge (2.7). We stress that we are not so much interested in the absolute value of ϵ_c at a given set of parameters, but rather in its variations with magnetic field. We expect the qualitative features of such variations to be much less sensitive to the approximations involved in the restriction to forward scattering, than ϵ_c itself.

As mentioned before, in the absence of an efficient phonon or electron bath, the above defined ϵ_c will act like a mobility edge and may dominate transport in an intermediate temperature regime where activation to ϵ_c is less costly than weakly assisted variable range hopping passing through lower lying

[1] A simple example is given by single particle excitations in a non-interacting system with white-noise disorder in the continuum. The localization length $\xi(E)$ in the orthogonal universality class grows exponentially with energy, $\xi(E) \sim \exp[\gamma E]$. Transport th rough a finite system of size L then proceeds via levels of energy E that optimize the product $\exp[-E/T]\exp[-L/\xi(E)]$, which for no n-interacting 2d electrons leads to a quasi-activated conduction with an activation energy that grows logarithmically with system size. Inciden tally, activated transport with logarithmically growing activation energy was reported in insulating, bosonic systems in Ref. [82]. We caution though that the scenario we mention is just one out of many possible explanations for such a phenomenology; it could possibly apply only under the stringent condition that the coupling to phonons and the ensuing variable range hopping transport are too weak to provide a more efficient transport channel in the considered temperature window. Simpler scenarii yielding similar length dependent insulating transport have been discussed in Ref. [83].

energy states. Under such circumstances one may expect ϵ_c to appear as the activation energy in an Arrhenius-type resistance [27, 60].

2.3 Bosonic localization: Oscillations of localization length and mobility edge

2.3.1 Energy and field dependence of the localization length

Fig. 2.3 shows the numerically evaluated interference part of the inverse localization length as a function of excitation energy. At $\omega = 0$ all paths contribute positively to a maximally constructive interference sum, while at finite energy occasional negative locators occur. In the absence of interactions, i.e. without Coulomb gap in the density of states (data plotted in black), this leads to a slight increase of ξ_g^{-1} with increasing ω [60, 76]. A magnetic field frustrates the predominantly positive interference and leads to a shrinkage of the localization length (positive magnetoresistance). This effect is strongest for small ω where the field-free interference is maximal.

Adding Coulomb interactions has quite a dramatic effect on the localization. The presence of the Coulomb gap suppresses the low energy density of states and thus strongly enhances the localization tendency there. The localization length qualitatively traces the variation of the density of states. Hence, the enhancement of localization is the stronger the lower the energy. This overcompensates the effect of rarer and rarer negative locators as $\omega \to 0$. Within the forward approximation, the Coulomb gap indeed turns $\xi(\omega)$ into an increasing function of ω, even at $B = 0$, unlike in the limit of purely local hard core repulsions.

If the hopping is sufficiently strong, high energy excitations are essentially delocalized and there is an effective mobility edge, as defined in (2.7). A magnetic field frustrates the predominantly constructive interference. This makes the localization length at a given energy shrink and thus pushes up the effective mobility edge.

Fig. 2.4 presents the full flux dependence of the inverse localization length.

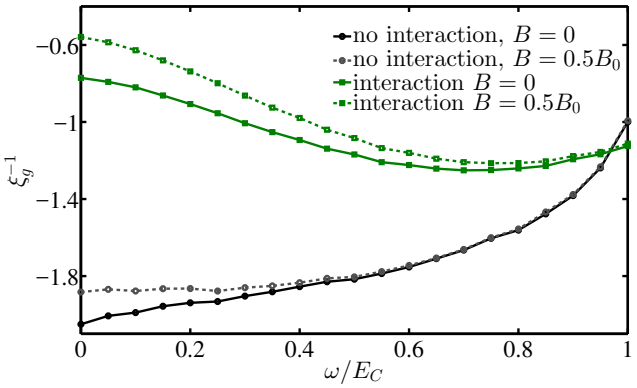

Figure 2.3: Geometric part of the inverse localization length of hard core bosons as a function of excitation energy ω. Without interactions and in the absence of a field, the localization length slightly decreases with increasing ω. The interaction-induced Coulomb gap enhances localization and reverses this trend, as localization becomes strongly enhanced at low energies. In either case the localization length shrinks with magnetic field (i.e., ξ_g^{-1} increases). The effect is strongest at low energies, where the zero field interference is maximally constructive.

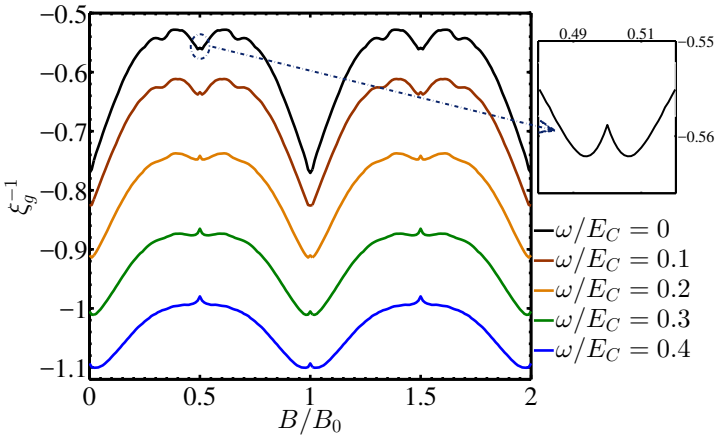

Figure 2.4: Geometric part of the inverse localization length of bosonic excitations as a function of magnetic field, at various excitation energies. ξ_g^{-1} tends toward a local minimum as the flux approaches integer values, or fractions with small denominators. There, for low energies, large subsets of paths interfere maximally positively. At finite energies, a tiny, non-analytic upward cusp of ξ_g^{-1} sits on top of this main feature. It reflects the destruction of negative interference at large scales, akin to the dominant mechanism of magnetoresistance in fermions. Similar cusps of the same origin appear at half integer fluxes, cf. the inset (for $\omega = 0$).

Its geometric part ξ_g^{-1} oscillates with the period of one flux quantum per plaquette, B_0. At $\omega = 0$ and for small fields, $B \ll B_0$, the localization length shrinks monotonically with increasing flux. However, at finite excitation en-

ergies the localization length is slightly non-monotonic very close to $B = 0$, even though this is hard to see in Fig. 2.4 except at larger $\omega \gtrsim 0.2$. Indeed, at non-zero energies locators occasionally have negative signs. At large scales the interference sum thus behaves like a fermionic problem, having a negative magnetoresistance at the smallest fields. This argument assumes the absence of the so-called sign transition, as discussed, e.g., in Refs. [80] or [84]. A small B-field then first reduces the destructive interference of paths with opposite signs, like in fermions, resulting in a very weak increase of ξ. A larger flux, however, has the main effect of suppressing the predominantly positive interference between shorter path segments. This then turns the magnetoresistance positive. This non-monotonicity in $\xi(B)$, which occurs for a small enough abundance of negative locators (i.e., not too large ω), was already observed and explained in Ref. [64] (cf. especially Fig. 3.2).

At half integer flux, $B = B_0/2$, further features appear in $\xi(B)$. At that flux all path amplitudes are real, but they fluctuate in sign. At exactly half-integer flux, the localization length is a local minimum of $\xi(B)$. This is reflected in a tiny upward cusp in ξ_g^{-1}, as illustrated by the inset of Fig. 2.4. It originates again from the elimination of occasional destructive interferences once the flux per plaquette deviates slightly from half integer. However, at larger deviations the dominant effect of B is the destruction of maximal interference between paths that differ by two unit cells; at least for sufficiently low energies ω where negative locators are rare. This results in an increase of ξ_g^{-1}. Similar local minima can be seen at the lowest ω for fluxes that are multiples of $B_0/3$.

The cusps at integer and half-integer flux are all non-analytic. This can be understood from a mapping to directed polymers. The mapping is truly faithful at $\omega = 0$, where all path weights are positive [62]. However, also negative weight problems exhibit the same type of scaling for the spatial roughness of paths (with wandering exponent $\zeta = 2/3$ in $d = 2$), and amplitude fluctuations governed by a Tracy-Widom distribution [65, 85]. From those, one predicts a change of the localization length which scales as $\delta\xi_g^{-1} \sim |\delta B|^{\psi}$ with the deviation δB from integer or half-integer flux, where the exponent has the

value $\psi = 2\zeta/(1+\zeta) = 4/5$ [62].

2.3.2 Magneto-oscillation of the effective mobility edge

For energies well inside the Coulomb gap, the localization length $\xi(\omega)$ is a monotonically growing function of ω. For sufficiently large hopping amplitude t, ξ diverges at the finite effective mobility edge ϵ_c, which is a periodic function of the flux. In Fig. 2.5 we plot $\epsilon_c(B)$ for a fixed value of the hopping amplitude, $t = 0.368E_C$, and disorder strength $W = E_C$. With these parameters, we find the amplitude of oscillations of ϵ_c to be about $\Delta\epsilon_c \approx 0.1E_C$. The qualitative features of the field dependence $\epsilon_c(B)$ are the same as those of $\xi_g^{-1}(B,\omega)$ (cf. Fig. 2.4) for an energy $\omega \approx 0.3E_C$ corresponding to the flux-averaged average mobility edge. Upon approaching criticality, as the average mobility edge decreases, we expect the function $\epsilon_c(B)$ to become non-monotonic in the range $B \in [0, B_0/2]$, exhibiting maxima slightly before and after $B_0/2$, in analogy to the field dependence of ξ_g^{-1} at low energies, cf. Fig. 2.4. However, we do not show corresponding results of the forward scattering analysis, since so close to criticality our approximation is for sure not reliable quantitatively; even though the discussed qualitative features presumably survive.

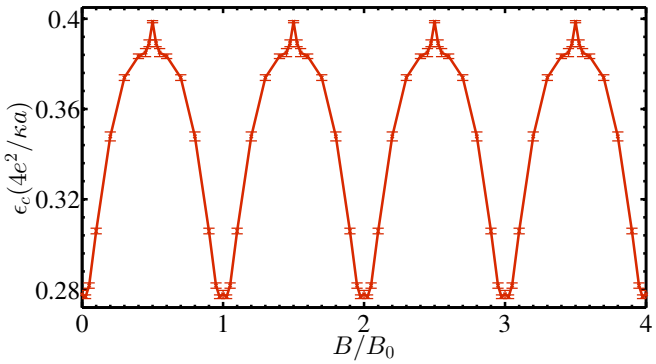

Figure 2.5: Flux dependence of the effective mobility edge of bosonic excitations. The upward cusps $\sim |\delta B|^{4/5}$ at half integer fluxes, and similar (but tiny) cusps at integer fluxes originate from the destruction of occasional negative interference among certain close pairs of paths with real amplitudes but opposite signs. The overall dome shape of the oscillation reflects the destruction of the predominantly positive interference by the Aharonov-Bohm phases introduced by incommensurate fluxes.

Qualitatively, $\epsilon_c(B)$ shows the same features as those of $\xi(B, \omega > 0)$. After a tiny, non-analytical decrease at $B \ll B_0$, the effective mobility edge increases as a consequence of the suppressed constructive interference in low energy bosonic excitations. At half flux per plaquette, $\epsilon_c(B)$ exhibits an upward cusp $|\delta B|^{4/5}$, like $\xi_g^{-1}(B)$. Its origin lies in the destruction of occasional, nearly complete negative interferences.

2.3.3 Increased relative oscillations upon approach to criticality

Note that as long as the effective mobility edge lies well within the Coulomb gap $\epsilon_c \lesssim E_{\rm gap} = E_C^2/(2CW)$ the disorder strength W plays a minor role, since the smallest locators have an abundance dictated by the pseudo-gapped part of the density of states, which is nearly disorder independent.

In contrast, the hopping amplitude t affects the location of the effective mobility edge directly, as illustrated in Fig. 2.6. That figure shows that, upon tuning the hopping between islands, the oscillation amplitude increases as the effective mobility edge decreases, i.e., as the transition to the superconductor is approached. The location of the transition can roughly be estimated from the criterion $\epsilon_c(B = 0) \approx 0$, but in its vicinity the forward scattering approximation should not be trusted quantitatively. For some range beyond the zero-field transition, the magnetic field is expected to be able to drive an SI transition.

It is interesting to compare these qualitative predictions with experimental data. To do so we interpret ϵ_c as the activation energy entering the Arrhenius-type resistance, and $\Delta\epsilon_c$ its field-induced variation. The experiments of Refs. [38] (Fig. 3) and [67] (Fig. 3(b)) show the same trends as we find from our theory: the further the system is from criticality, the smaller is the variation of the activation energy.

2.4 Relating theory to experiments

The experimental structured films [38, 39, 50] bear signatures of bosonic insulators, the small field magnetoresistance being positive, while the flux pe-

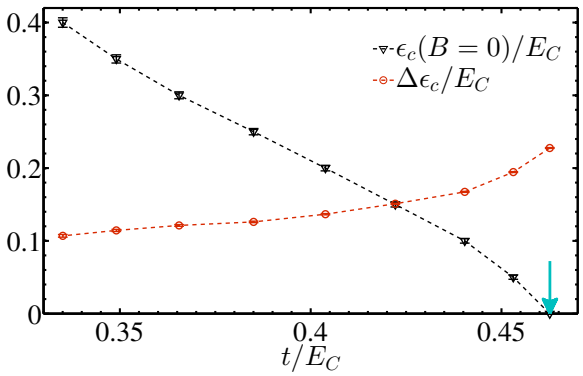

Figure 2.6: The zero-field effective mobility edge $\epsilon_c(B = 0)$ and the magneto-oscillation amplitude $\Delta\epsilon_c$, plotted as a function of the hopping amplitude t. The mobility edge ϵ_c can be tuned by the hopping t. It serves as a measure for the distance to criticality. As the mobility edge ϵ_c decreases and the transition is approached (approximately where $\epsilon_c(B = 0) \approx 0$, as marked by the arrow), the oscillation amplitude increases.

riodicity is that expected for charges $q = 2e$. We note that unpaired, non-interacting electrons of charge $q = 1e$ would exhibit the same flux periodicity as we recall in the next section; however, as we will discuss there, in the presence of interactions the period of single electrons is doubled and thus faithfully reflects the carrier's charge.

To relate our theoretical study to experimental systems, we need to discuss the relevant scale of Coulomb interactions, E_C. For an insulator of bosonic carriers of charge $q = 2e$, with a lattice spacing between islands $a \approx 50$nm and dielectric constant κ one obtains the Coulomb scale $E_C = q^2/\kappa a \approx 1334/\kappa\,\mathrm{K}$. The essential difficulty resides in determining the effective dielectric constant κ which governs the Coulomb interaction at and above the lattice scale a. This is nearly impossible to predict from first principles as the islands possess a large polarizability and have to be considered as nearly touching each other. Therefore they renormalize the dielectric constant of the medium surrounding the patterned film, such that values of $\kappa \sim 10^2 - 10^3$ are not unrealistic.

However, another consideration allows us to argue for an upper bound on E_C, simply on empirical grounds. The system essentially realizes an array of Josephson junctions. The proximity to the superconductor suggests that the charging energy ($\sim E_C$) is of the order of the Josephson energy, whose

role is played by the hopping t here. Deeply in the superconducting phase, the Josephson coupling determines the scale of the transition temperature T_c. These considerations imply that not too far from criticality E_C is of the order of typical T_c in well superconducting samples. Empirically, the latter never exceeds a few Kelvin, suggesting that $E_C \sim 2\text{K}$, and effectively $\kappa \sim 500$.

Our results in Fig. 2.6 show that typical magneto-oscillation amplitudes are of the order of one magnitude smaller than E_C. This is compatible with experimental oscillation amplitudes of activation energies of the order of $0.2K$, as extracted from resistance data that were fitted to an Arrhenius law [39].

Our theory predicts a non-analytic cusp of the effective mobility edge at half integer fluxes, and another cusp of much smaller size at integer flux. Interestingly, such cuspy features have been observed in measurements of the resistance as a function of B, cf. Ref. [38], Fig. 2A.

As we discussed in the previous section, we further expect that upon approaching criticality, when $\epsilon_c \lesssim 0.1E_C$, the resistance develops a double-hump within an oscillation period, akin to the low energy behavior of $\xi_g^{-1}(\omega)$. Unfortunately, in the experimental systems of Refs. [38] and [39] this corresponds to a rather small energy scale. Therefore very low temperatures will be requireed to reliably observe an activated behavior over a sufficient range of resistances and extract activation energies from it that would exhibit this double-hump feature.

2.5 Role of quantum statistics - Bosonic vs fermionic mobility edges

Apart from studying bosonic insulators per se, a central goal of this study is to investigate the role of quantum statistics in insulators. To this end we repeated the same type of analysis as above for a system of spinless fermions, subject to the same Coulomb interactions. The only difference with respect to the previously considered hard core bosons consists in the exchange statistics of the particles, while the Hilbert space and the terms in the Hamiltonian were left essentially identical. Data for the inverse localization lengths and

effective mobility edges of fermions are shown in Figs. 2.7 and 2.8. The effective mobility edge of fermions oscillates with magnetic flux similarly as ξ^{-1} at finite ω.

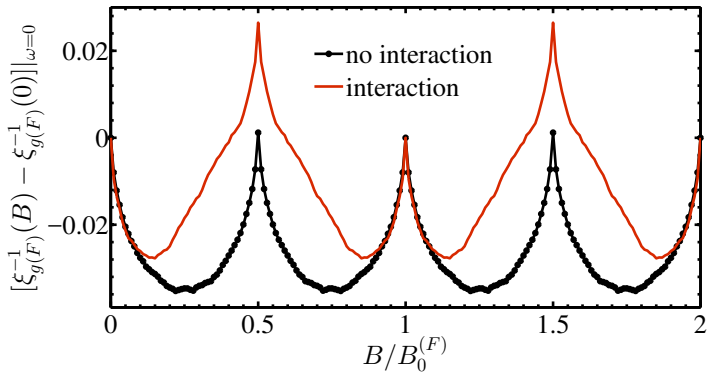

Figure 2.7: Variations of the inverse localization length $\xi^{-1}_{g,(F)}$ of fermionic excitations at $\omega = 0$ as a function of magnetic field - with and without interactions. In the non-interacting case, the symmetry in the distribution of the uncorrelated *disorder potential leads to a doubling of the oscillation period. In the presence of interactions, the effective disorder is correlated, which re-instates the flux periodicity expected for fermions, $B_0^{(F)} = hc/e$. The correlations due to Coulomb repulsion enhance the localization at half a flux per plaquette as compared to commensurate flux, as explained in the main text.*

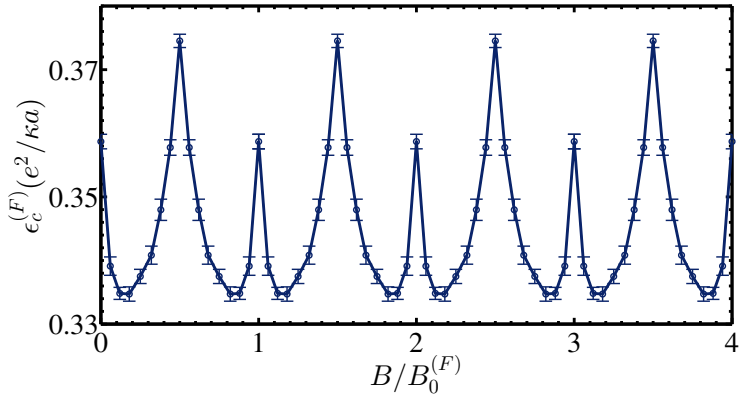

Figure 2.8: Magnetic field dependence of the fermionic effective mobility edge $\epsilon_C^{(F)}$. The qualitative features are similar to the variation of the inverse localization length in Fig. 2.7.

The comparison between Figs. 2.4 and 2.7 show three main effects of the opposite exchange statistics, some of which have been discussed previously in the literature [62, 64, 65]: (i) the magnetoresistance of fermions in small

fields is opposite to that of bosons at low energies; (ii) the amplitude of the field-induced variations are significantly smaller in fermions; (iii) the structure within an oscillation period is very different: bosons show one dome shaped oscillation, whereas fermions exhibit a pronounced double hump with a second local maximum in the localization length at half flux. As we discuss below the details of the latter reflect the nature of Coulomb correlations. Let us now explain these features in turn.

2.5.1 Negative magnetoresistance of fermions

The increase of the fermion's localization length at small fields, as opposed to the stronger decrease in low energy bosons, is due to the fact that at $B = 0$ fermionic paths already come with random signs, so that there is no dominant positive interference to be destroyed by an extra B-field. Instead it is the B-induced lifting of accidental negative interference between two bunches of paths of nearly equal amplitude, which dominates the magnetoresistance by occasionally enhancing the tunneling further away. Such negative interferences are not that abundant, however. Therefore the resulting negative magnetoresistance is significantly less strong than the suppression of maximally positive interference of all bosonic paths. This explains the smaller amplitude of the field-induced variations in fermions [62].

Fermionic path sums also obey the scaling of the Kardar-Parisi-Zhang universality class [85]. Probabilistic arguments on the occurrence of large, strongly interfering pairs of path bundles [62, 65] thus lead again to the prediction that ξ^{-1}, as well as the effective mobility edge, vary in a non-analytical fashion close to integer and half integer fluxes as $\delta\xi^{-1} \sim -|\delta B|^{4/5}$.

2.5.2 Approximate period doubling and traces of interaction correlations in fermionic magneto-oscillations

An interesting, hitherto little explored feature is the structure of the magneto-oscillation within a flux period. For fermions there are two local maxima of ξ^{-1} within one period. They occur at integer and half integer flux, where all path

amplitudes are real (albeit random in sign). This maximally favors negative interference. In fact, it has been known for a long time (cf., for example, Ref. [64], Fig. 3.2) that in non-interacting models, for an energy at the center of a symmetric impurity band, the magneto-oscillations of ξ have a shorter period, reduced from B_0 to $B_0/2$, with identical peaks at integer and half integer flux, as we reconfirm in Fig. 2.7. For completeness, the proof of this fact is given in App. A. It relies on the symmetry of the distribution of onsite-potentials, $\rho(\omega+\delta) = \rho(\omega-\delta)$, and, most importantly, on the independence of potentials from site to site.

The first assumption on the density of states is not that crucial. Indeed the deviations from perfect period doubling are not very significant as long as ω remains close to the band center of a featureless density of states. The assumption of independence of onsite potentials is much more important. Crucially, it breaks down in the presence of interactions that induce correlations between local energies of spatially close sites. Indeed, around a soft site with a low local potential, non-local repulsive interactions suppress other sites with small potentials of opposite sign. That is, low energy sites in the vicinity of an occupied low energy site will predominantly be occupied themselves, rather than empty. Otherwise the considered configuration would be unstable with respect to the transfer from the occupied to the nearby empty sites.

This bunching effect of low energy sites of the same kind has been described long ago in the literature of Coulomb glasses [86, 87]. For the locator expansion in the insulating phase, it has the following interesting implication. Consider a small loop of interfering paths. Paths with significant weight contain a lot of small denominators, that is, they tend to pass through low energy sites. The correlation effect implies that two small denominators occuring in the two branches of a small loop are more likely to be of the same sign, and thus to interfere positively in the absence of flux. At the level of such a loop, adding half a flux through the plaquette is equivalent to flipping the sign of one of the energies. This induces a bias towards negatively interfering path pairs and thus enhances the localization tendency. The bias introduced by correlations among nearby sites thus destroys the exact period doubling and

induces maximal localization of fermions at half-integer flux, as confirmed by Fig. 2.7.

Since this interaction effect is usually significantly stronger than the effect of a non-symmetric density of states, the deviation from period doubling in fermionic insulators can be used, qualitatively, as a measure and witness of Coulomb correlation effects.

2.6 Summary and conclusion

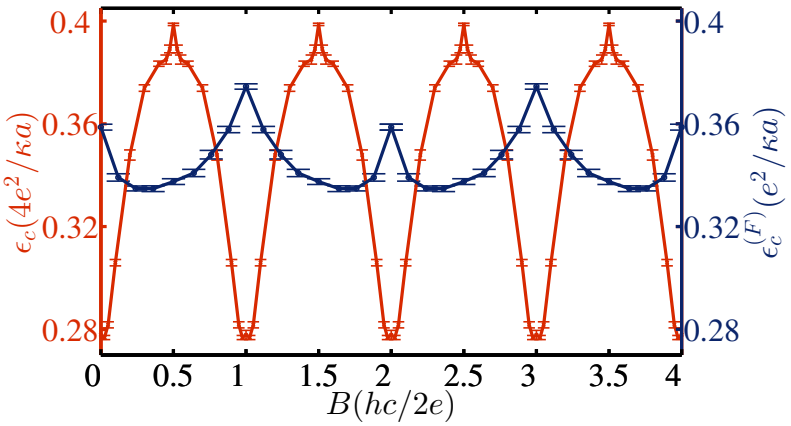

Figure 2.9: Oscillations of the effective mobility edge of hardcore bosons of charge $2e$ versus that of fermions of charge e. Each set of data is shown in units of the relevant Coulomb interaction between nearest neighbors. Due to the approximate period doubling for fermions, the flux interval between maxima is the same as for bosons, but the structure within the oscillation period is very different: Fermions start with negative magnetoresistance at small fields, exhibit a smaller oscillation amplitude and alternating peak heights.

In Fig. 2.9 we provide a direct comparison of the oscillations of the effective mobility edge as a function of magnetic field for fermions of charge e and those of hard core bosons (tightly bound electron pairs) of charge $2e$. Since these two systems share the same flux interval between peaks of enhanced localization, the latter cannot be used to determine the nature of the charge carriers. However, bosons and fermions are clearly distinguished by their opposite magnetoresistance close to integer fluxes: Bosons (at $\omega = 0$) have a minimum of localization tendency at those points, whereas fermions exhibit a (weaker) maximum; a cousin of that fermionic maximum also appears at

half integer flux. Note that the oscillation amplitude of the fermionic effective mobility edge is nearly one order of magnitude smaller than that of the bosons.

As we explained in the last section, the correlations induced by repulsive interactions render the two fermionic maxima within a flux period inequivalent and enhance localization at half integer fluxes. We hope that future experiments on patterned films of non-superconducting metals will reveal these qualitative features reflecting both fermionic statistics and correlations in the Coulomb glass.

Many aspects of our simple theoretical modelling are in reasonable semi-quantitative agreement with experimental data reported by J. Valles' group [38, 39, 67]: The overall sign and shape of the magneto-oscillations, their cuspy nature at half flux as well as the evolution of their relative size as one tunes the distance to criticality. It would be interesting to test further predictions of our model, such as the appearance of a double hump in the oscillation period, as one approaches criticality more closely.

Chapter 3

Giant magnetoresistance peak in a Cooper-pair insulator

3.1 Introduction

Due to the sensitivity of superconductivity to magnetic field, theories and experiments on magneto-transport shed light on the nature of the SIT and especially of its insulating side. As seen in the previous chapter, the magneto-oscillations of the resistance with an applied transverse field is one among those aspects that support the existence of localized electron pairs, on the insulating side of the transition. The oscillations dictated by the flux quantum $h/2e$ have been mostly reported in experiments on periodic lattice-like systems. More generally, in several amorphous superconducting films, patterned or non-patterned, field-driven or thickness-driven transitions, a giant nonmonotonic magnetoresistance peak has been reported on the insulating side in samples being nearly critical (in zero field) at very low temperature. The peak starts with a highly anisotropic (field orientation dependent) rise, showing positive magnetoresistance, and is followed by a dramatic drop in higher magnetic field. This remarkable nonmonotonicity of the magnetoresistance has attracted a considerable attention in the field. It implies that more than one mechanism is at play. Moreover, since negative magnetoresistance is usual, the giant negative part is particularly interesting. The appearance of the peak also suggests that superconductivity seems to enhance the insulating behavior.

Paalanen *et al.* [45] were the first to report the appearance of the peak on amorphous InO_x and suggested it to be a signature of a crossover or transition between a Bose insulator and a Fermi insulator. Very recently, on the experi-

mental side, to confirm and extend that work, there has been a large number of works carried out on amorphous InO_x [32, 33, 46, 88, 89], Bi [39, 47, 48], TiN [34], PbBi [49, 67], NbN[40]. A similar peak has also been reported in the high temperature superconductor $La_{2-x}Sr_xCuO_4$ implicating the existence of electron pairs in high magnetic fields [15].

Especially Shahar's group has performed a careful study of the field orientation dependence of the magnetoresistance peak presented in Refs [89, 90]. The main observations from those two experiments can be summarized as follows: (i) a strong anisotropic positive magnetoresistance is seen in the low field regime before the peak, the samples are more resistive as the field is out-of-plane; (ii) when the field direction changes from being parallel to being perpendicular to the film plane, the peak moves to lower fields and higher resistance values; (iii) beyond the peak, the degree of anisotropy decreases with the strength of the field; (iv) in the high field regime there is a temperature-dependent value B_{ISO} at which the magnetoresistance seems to be nearly independent of the field-orientation, and after which its anisotropy is reversed; as the temperature decreases, B_{ISO} moves closer to the peak position; (v) thinner, i.e., more disordered, samples, in which the superconducting state cannot be achieved, host much weaker anisotropy and no peak at all. Furthermore, the authors also suggested that there are at least two different mechanisms related to the magnetic field in their samples: an anisotropic one at low field is of orbital origin, and the other is isotropic and contributes significantly only at high field. Still it is not clear which mechanism is the "driving force" behind the peak. Adding to this picture, data on periodically patterned films of Bi [39] or PbBi [49] with a honeycomb array of holes shows a series of oscillations in the low field region before the peak.

On the theory side, several works attempted to tackle the underlying physics behind the magneto resistance peak [62, 91, 92, 93, 94, 95, 96, 97]. At a phenomenological level, a series of works based on the percolation description presented in Refs. [91, 92] proposed a qualitative explanation. Within that scheme, the SIT was considered as a percolation transition from a regime, in which transport is carried out by Cooper pairs tunneling through supercon-

ducting islands, to another regime, in which transport is carried by normal electrons due to a suppression of coherent superconducting clusters. Ref. [91] focused only on the orbital effect of the perpendicular field while Ref. [92] also took into account the Zeeman effect together with the orbital mechanism to describe the anisotropy observed in experiments. The approach reported in Ref. [93] gave an alternative view for the effect of the perpendicular field. It started with the boson picture of superconducting film in a perpendicular field and introduced fermionic degrees of freedom played by the vortices. Furthermore, recently, Pokrovsky *et al.* [94] have used a variational approach to explore the phase diagram of electron systems near the SIT and found a nonmonotonic tendency of the magnetoresistance when moving from a Bose to a Fermi insulating phase by increasing the magnetic field. Alternatively, based on the renormalization group for a nonlinear sigma model applicable in the weak disorder regime, Burmistrov *et al.* [95] predicted a nonmonotonic magnetoresistance when a perpendicular field is applied, which is stronger than the case with a parallel field. Within that framework, they also observed a considerable increase of magnetoresistance with field in the high parallel field regime that is in contrast with the perpendicular field case and has not been reported experimentally.

Despite a significant theoretical effort devoted to this subject and the fact that the magnetoresistance peak is often interpreted as a crossover from bosonic to fermionic transport, its underlying microscopic origin and possible magnetic field-related mechanisms affecting it have not been resolved yet. It is a main goal of this part of the thesis to understand the magnetic field effects, their associated physical mechanisms and implications about the magnetoresistance peak in an insulator close to the SIT.

The orbital effect of a magnetic field, or in other words, its frustration on quantum interference, has been studied in detail [60, 62, 64, 65]. It has strongly opposite impacts on bosonic and fermionic systems due to their quantum statistical nature. A strong positive magnetoresistance for bosons, and in contrast, a much weaker negative magnetoresistance have been discussed. However, in this work, we explore more carefully the Zeeman effect that com-

petes with pairing attraction causing the depairing of electron pairs. We will show that it is the main driving force leading to the magnetoresistance peak. The above interference effect enhances that effect further due to its field orientation dependence.

As mentioned previously, in experiments close to the SIT, at low fields below the peak where magnetoresistance is positive, most of the systems exhibit activated transport behavior. On the other hand, in the high field regime beyond the peak, single-electron Mott's variable-range hopping has been reported at low temperatures [98]. Therefore, in the present chapter, to capture the magneto-transport in a wide range of the magnetic field, we consider that the transport is to follow Mott's variable range hopping [99] in which the Mott's characteristic temperature T_M governs the growth of the resistance with a stretched power: $R(T) \propto \exp(T_M/T)^{1/3}$ for two dimensional systems. This is a well-known model of transport in disordered insulators where the hopping conduction is carried out by carriers that hop between localized electronic states. At low temperature, the length of the hops grows to optimize the conductivity. In principle, in disordered superconducting films, electronic conduction can occur through hopping of either single electrons or electron pairs. Depending on system parameters, the transport can be dominated by only one of the two, and as we will see below, it is interesting to study the crossover between two transport regimes dominated by different carrier types. At first, we neglect Coulomb interactions among charges so as to provide a clear and simple, but adequate picture of the physics behind the magnetoresistance peak. Nevertheless, after discussing the main obtained results, we will comment on the case involving Coulomb interactions.

The remainder of this chapter is organized as follows. In Sec. 3.2 we introduce the microscopic model in detail. The effect of Zeeman depairing on the single-site density of states (DOS) is analyzed in Sec. 3.3. Sec. 3.4 presents the total impact of a magnetic field, both Zeeman depairing and orbital effects, on the localization lengths of the zero energy excitations. The resulting crossover in the characteristic Mott's temperature representing the appearance of magnetoresistance peak and its properties varying with the field

and other model parameters are shown in Sec. 3.5. Sec. 3.6 is devoted to a discussion of the case in which Coulomb interactions are present. The main results are summarized in Sec. 3.7.

3.2 Model

Here we propose a microscopic model that incorporates key ingredients that seem essential to describe the strongly insulating side of the SIT in the presence of a magnetic field. Electrons on a square lattice are subject to strong onsite disorder, local attraction that facilitates electron pairing and thus are ultimately responsible for superconductivity, a Zeeman field promoting unpaired electrons, and quantum transport characterized by hopping amplitudes whose phases are modified by the orbital effect of the magnetic field. The Hamiltonian of such a minimal model reads

$$\begin{aligned} H &= \sum_{i,s}(\varepsilon_i - \mu)n_{is} - \sum_i \left(\lambda_i n_{i\uparrow}n_{i\downarrow} - B(n_{i\uparrow} - n_{i\downarrow})\right) \\ &\quad - \sum_{\langle i,j\rangle}\left(\sum_s t_1 e^{\mathrm{i}\gamma\phi^g_{ij}B\sin\alpha}c^\dagger_{is}c_{js} + t_2 e^{\mathrm{i}2\gamma\phi^g_{ij}B\sin\alpha}c^\dagger_{i\uparrow}c^\dagger_{i\downarrow}c_{j\downarrow}c_{j\uparrow} + \text{h.c.}\right), \end{aligned} \tag{3.1}$$

where $c^\dagger_{is}, c_{is}$ are the creation and annihilation of an electron with spin $s = \{\downarrow,\uparrow\}$ on site i. $n_{is} = c^\dagger_{is}c_{is}$ is the local occupation number operator, and each site can have at most two particles, $n_i = 0, 1, 2$. The chemical potential μ is adjusted to assure half filling. The disordered onsite potentials ε_i are uniformly distributed

$$P(\varepsilon) = \frac{1}{2W}\Theta(W - |\varepsilon|). \tag{3.2}$$

λ_i describes the local bias towards attraction between two opposite spins to form a singlet. It varies from site to site, and a Gaussian distribution with mean λ_0 and variance σ^2 is chosen to describe them,

$$P(\lambda) = \frac{1}{\sigma\sqrt{2\pi}}\exp\left(-\frac{(\lambda - \lambda_0)^2}{2\sigma^2}\right). \tag{3.3}$$

In granular superconductors, the variation of local attraction arises naturally with varying local grain size and concentration. The presence of an attractive interaction inducing local pairing representing superconductivity has been assumed in other theoretical models [27, 54, 94, 100].

In the presence of a magnetic field, the Zeeman effect suppresses superconducting states, diminishes the attraction-induced local pairing. B is the Zeeman energy that measures how much the magnetic field B_0 is applied to the system, $B = \frac{1}{2} g \mu_B B_0$, where g denotes the g-factor, and μ_B is the Bohr magneton. The orbital component of the field is proportional to $\sin\alpha$, where α is the angle between the magnetic field and the plane of the film. It enters via an Aharonov-Bohm phase factor. Each hop of an electron with the charge e or a pair with the charge $2e$ between two nearest neighbor sites i and j comes with the hopping amplitude $t_{1,2}$, respectively, and a corresponding phase factor. To evaluate the Aharonov-Bohm phase as

$$\frac{e}{\hbar c} \int_{\mathbf{r}_i}^{\mathbf{r}_j} \mathbf{A} \mathrm{d}\mathbf{r} = \gamma \phi_{ij}^g B \sin\alpha, \tag{3.4}$$

we have chosen the gauge such that the in-plane component of the vector potential $\mathbf{A}$ is given by $\mathbf{A}_\parallel = B_0 \sin\alpha x \mathbf{e_y}$. ϕ_{ij}^g is the geometric part of the phase, $\phi_{ij}^g = \frac{1}{a^2} \int_{\mathbf{r}_i}^{\mathbf{r}_j} x \mathbf{e_y} \mathrm{d}\mathbf{r}$, where a is the lattice constant. In the constant $\gamma = 2\pi/E_Z$, E_Z is the Zeeman energy induced by a magnetic field corresponding to a flux quantum of an electron per unit cell, $E_Z = \frac{1}{2} g \mu_B \frac{hc}{ea^2}$.

In conventional systems, it is expected that the pair hopping is generated as a second order process in the single particle hopping amplitude, i.e. much weaker than and dependent on the latter. However, in realistic superconducting materials, the relation between the two might be more complicated due to the local electronic structure that is responsible for local attraction and enhances pair hopping. Therefore, in the present model, we have chosen to work with two independent parameters, namely t_1 and t_2 for the electron and pair hopping amplitudes. Later, to characterize the distance to the superconductor transition, we consider the pair hopping amplitude as a control parameter while the single electron hopping remains untouched.

3.3 Classical ground state: DOS effect induced by Zeeman depairing

Solving the full Hamiltonian is an ambitious goal. Instead, we tackle the problem step by step as in the previous chapter. First the hoppings are neglected for a moment, and we focus on describing the effect of Zeeman depairing on the density of states. In the next step, quantum transport on the background of the classical ground state configuration is discussed by bringing back the hoppings in a perturbative way.

3.3.1 Single-site density of states

In this section, we analyze the single-site DOS's for single electron and pair excitations corresponding to the classical part of the Hamiltonian. A classical ground state configuration is defined by a set of occupation numbers $\{n_{is}\}$. The chemical potential μ is the value such that the total particle number is $N_e = \sum_i n_i = N_{sites}$. Once μ is determined, we have the following ground state configuration: on any site i, the occupation is given by the following rules

$$\begin{aligned} \varepsilon_D \equiv \varepsilon_i - \mu - \min(\lambda_i/2, \lambda_i - B) < 0 \;\; &\rightarrow \;\; n_{i,\downarrow} = n_{i,\uparrow} = 1, \\ \varepsilon_{S1} \equiv \varepsilon_i - \mu - \lambda_i + B > 0; \quad \varepsilon_{S2} \equiv \varepsilon_i - \mu - B < 0 \;\; &\rightarrow \;\; n_{i,\downarrow} = 1, n_{i,\uparrow} = 0, \\ \varepsilon_E \equiv \varepsilon_i - \mu - \max(B, \lambda_i/2) > 0 \;\; &\rightarrow \;\; n_{i,\downarrow} = n_{i,\uparrow} = 0. \end{aligned} \quad (3.5)$$

Thus the local occupation number n_i on each site i in a given random realization is

$$n_i(\varepsilon_i, \lambda_i, B, \mu) = 2\Theta(-\varepsilon_D) + 1\Theta(\varepsilon_{S1})\Theta(-\varepsilon_{S2}). \quad (3.6)$$

The chemical potential μ has to be found as the unique root of the equation $\bar{n}(\mu, B) = 1$ where the average particle density reads

$$\bar{n}(\mu, B) = \int_{-\infty}^{\infty} \mathrm{d}\lambda P(\lambda) \int_{-W}^{W} \mathrm{d}\varepsilon P(\varepsilon) n_i(\varepsilon, \lambda, B, \mu). \quad (3.7)$$

The relation among onsite disorder, attraction, and magnetic field determines the location of the chemical potential in the energy spectrum.

The excitation energies $E^{m\pm}_{n_i,s}$ corresponding to adding or removing $m \in \{1,2\}$ charges on site i occupied by $n_i = 0,1,2$ particles are, respectively,

for $n_i = 2$:

$$E^{1-}_{2,\downarrow} = (\varepsilon_i - \mu) - \lambda_i - B, \tag{3.8}$$

$$E^{1-}_{2,\uparrow} = (\varepsilon_i - \mu) - \lambda_i + B, \tag{3.9}$$

$$E^{2-}_{2} = 2(\varepsilon_i - \mu) - \lambda_i, \tag{3.10}$$

for $n_i = 1$:

$$E^{1+}_{1,\uparrow} = (\varepsilon_i - \mu) - \lambda_i + B, \tag{3.11}$$

$$E^{1-}_{1,\downarrow} = (\varepsilon_i - \mu) - B, \tag{3.12}$$

for $n_i = 0$:

$$E^{1+}_{0,\downarrow} = (\varepsilon_i - \mu) - B, \tag{3.13}$$

$$E^{1+}_{0,\uparrow} = (\varepsilon_i - \mu) + B, \tag{3.14}$$

$$E^{2+}_{0} = 2(\varepsilon_i - \mu) - \lambda_i. \tag{3.15}$$

As those excitations are excited from a classical ground state configuration, they obviously obey $E^{m+}_n > 0$ and $E^{m-}_n < 0$. The single-site DOS for spin $\downarrow$ electron excitations is averaged over the distributions of the disorder ε_i and the attraction λ_i, and receives contribution from all types of occupancies

$$\rho_{S\downarrow}(E) = \rho^{0+}_{\downarrow}(E) + \rho^{1-}_{\downarrow}(E) + \rho^{2-}_{\downarrow}(E). \tag{3.16}$$

Each element in the above sum coming from an empty, singly occupied, or doubly occupied site is given by, respectively,

$$\begin{aligned}\rho^{0+}_{\downarrow}(E) &= \int_{-\infty}^{\infty} \mathrm{d}\lambda P(\lambda) \int_{-W}^{W} \mathrm{d}\varepsilon P(\varepsilon) \delta(E - E^{1+}_{0,\downarrow}) \Theta(\varepsilon_E) \\ &= \frac{1}{4W}\left[\mathrm{erf}\left(\frac{2(E+B)-\lambda_0}{\sigma\sqrt{2}}\right)+1\right]\Theta(E)\Theta(W-|E+B+\mu|),\end{aligned} \tag{3.17}$$

$$\begin{aligned}\rho^{1-}_{\downarrow}(E) &= \int_{-\infty}^{\infty} \mathrm{d}\lambda P(\lambda) \int_{-W}^{W} \mathrm{d}\varepsilon P(\varepsilon) \delta(E - E^{1-}_{1,\downarrow}) \Theta(\varepsilon_{S1}) \Theta(-\varepsilon_{S2}) \\ &= \frac{1}{4W}\left[\mathrm{erf}\left(\frac{E+2B-\lambda_0}{\sigma\sqrt{2}}\right)+1\right]\Theta(-E)\Theta(W-|E+B+\mu|),\end{aligned} \tag{3.18}$$

$$\rho_{\downarrow}^{2-}(E) = \int_{-\infty}^{\infty} \mathrm{d}\lambda P(\lambda) \int_{-W}^{W} \mathrm{d}\varepsilon P(\varepsilon)\delta(E - E_{2,\downarrow}^{1-})\Theta(-\varepsilon_D) \tag{3.19}$$

$$= \frac{1}{4W}\Big[\mathrm{erf}\left(\frac{\min\{W - E - \mu - B, -2(E+B)\} - \lambda_0}{\sigma\sqrt{2}}\right) - \mathrm{erf}\left(\frac{-W - E - \mu - B - \lambda_0}{\sigma\sqrt{2}}\right)\Big]\Theta(-E-2B)\Theta(W - E - B + \mu).$$

The same procedure is applied to find the single-site DOS for spin $\uparrow$ electron excitations

$$\rho_{S\uparrow}(E) = \rho_{\uparrow}^{0+}(E) + \rho_{\uparrow}^{1+}(E) + \rho_{\uparrow}^{2-}(E), \tag{3.20}$$

where

$$\rho_{\uparrow}^{0+}(E) = \int_{-\infty}^{\infty} \mathrm{d}\lambda P(\lambda) \int_{-W}^{W} \mathrm{d}\varepsilon P(\varepsilon)\delta(E - E_{0,\uparrow}^{1+})\Theta(\varepsilon_E) \tag{3.21}$$

$$= \frac{1}{4W}\left[\mathrm{erf}\left(\frac{2(E-B) - \lambda_0}{\sigma\sqrt{2}}\right) + 1\right]\Theta(E-2B)\Theta(W - |E - B + \mu|),$$

$$\rho_{\uparrow}^{1+}(E) = \int_{-\infty}^{\infty} \mathrm{d}\lambda P(\lambda) \int_{-W}^{W} \mathrm{d}\varepsilon P(\varepsilon)\delta(E - E_{1,\uparrow}^{1+})\Theta(\varepsilon_{S1})\Theta(-\varepsilon_{S2}) \tag{3.22}$$

$$= \frac{1}{4W}\Big[\mathrm{erf}\left(\frac{\min\{W - E + B - \mu, -E + 2B\} - \lambda_0}{\sigma\sqrt{2}}\right) - \mathrm{erf}\left(\frac{-W - E + B - \mu - \lambda_0}{\sigma\sqrt{2}}\right)\Big]\Theta(E)\Theta(W + B + \mu),$$

$$\rho_{\uparrow}^{2-}(E) = \int_{-\infty}^{\infty} \mathrm{d}\lambda P(\lambda) \int_{-W}^{W} \mathrm{d}\varepsilon P(\varepsilon)\delta(E - E_{2,\uparrow}^{1-})\Theta(-\varepsilon_D) \tag{3.23}$$

$$= \frac{1}{4W}\Big[\mathrm{erf}\left(\frac{\min\{W - E + B - \mu, 2(B-E)\} - \lambda_0}{\sigma\sqrt{2}}\right) - \mathrm{erf}\left(\frac{-W - E + B - \mu - \lambda_0}{\sigma\sqrt{2}}\right)\Big]\Theta(-E)\Theta(W - E + B + \mu), \tag{3.24}$$

Finally, the pair DOS gets contributions only from empty and doubly occupied sites

$$\rho_P(E) = \rho_P^{0+}(E) + \rho_P^{2-}(E), \tag{3.25}$$

where

$$\begin{aligned}\rho_P^{0+}(E) &= \int_{-\infty}^{\infty} \mathrm{d}\lambda P(\lambda) \int_{-W}^{W} \mathrm{d}\varepsilon P(\varepsilon)\delta(E - E_0^{2+})\Theta(\varepsilon_E) \qquad (3.26)\\ &= \frac{1}{8W}\Big[\mathrm{erf}\left(\frac{2(W-\mu) - E - \lambda_0}{\sigma\sqrt{2}}\right)\\ &\quad -\mathrm{erf}\left(\frac{\max\{2(-W-\mu) - E, 2B - E\} - \lambda_0}{\sigma\sqrt{2}}\right)\Big]\Theta(E)\Theta(W - B - \mu),\end{aligned}$$

$$\begin{aligned}\rho_P^{2-}(E) &= \int_{-\infty}^{\infty} \mathrm{d}\lambda P(\lambda) \int_{-W}^{W} \mathrm{d}\varepsilon P(\varepsilon)\delta(E - E_2^{2-})\Theta(-\varepsilon_D) \qquad (3.27)\\ &= \frac{1}{8W}\Big[\mathrm{erf}\left(\frac{2(W-\mu) - E - \lambda_0}{\sigma\sqrt{2}}\right)\\ &\quad -\mathrm{erf}\left(\frac{\max\{2(-W-\mu) - E, 2B + E\} - \lambda_0}{\sigma\sqrt{2}}\right)\Big]\Theta(-E)\Theta(W - E - B - \mu).\end{aligned}$$

Figs. 3.1 and 3.2 show the above DOS functions and their evolution with the applied magnetic field in the two cases of a constant attraction and a distributed one.

Without magnetic field, the distribution of occupancies through out a half-filled system is governed by the on-site disorder and attraction profiles. Even though it is unrealistic to have constant attraction in real materials, we first discuss this case in detail to emphasize later the case with non-trivially distributed attraction. In that limit $\sigma = 0$, at low fields $B < \lambda_0/2$, since the local attraction wins over the depairing Zeeman effect, all electrons are paired in the lowest potential wells, i.e all sites are either empty or doubly occupied. Therefore, adding or removing one particle at a given site requires a minimal energy of order $\lambda_0/2 - B$ creating a hard gap in the single DOS, see Fig. 3.1. When the field becomes moderately larger, some sites change their occupants from a pair to unpaired electrons. This happens for sites whose energies are close to the Fermi energy μ while sites with energies lying deep in the spectrum remain unchanged. The appearance of low energy electron excitations leads to an exchange of gap in the electron and pair DOS: the hard gap in

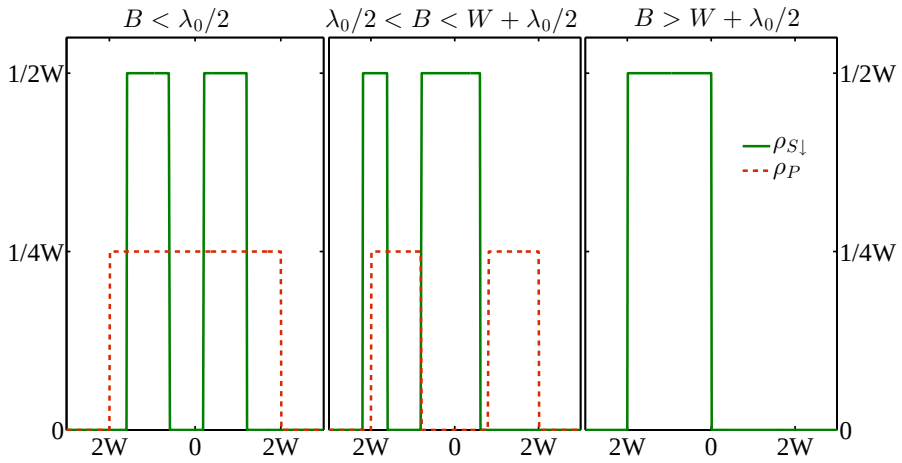

Figure 3.1: The single-site DOS's for single electron and pair excitations for a constant attraction. For a whole range of the magnetic field, the regime in which both the electron and pair DOS's are ungapped does not exist. When $B < \lambda_0/2$, all sites in the system are doubly occupied; it requires a minimal energy of order $\lambda_0/2 - B$ to add or remove an electron from a given site leading to a hard gap in the electron DOS while the pair DOS is simply flat. As B field is moderately larger than $\lambda_0/2$, the picture is reversed since some unpaired electrons appear, whose energies are close to the Fermi energy, resulting in the hard gap in pair DOS of order $2B - \lambda_0$ and the closing of the other one in electron DOS. At a certain value of $B > W + \lambda_0/2$, all electrons are singly occupied all sites in the system, and the pair DOS vanishes.

the former is closed while simultaneously a gap opens up in the pair DOS. As $B > W + \lambda_0/2$, all electrons are unpaired and all sites are singly occupied, the pair DOS disappears. The overall picture follows that there is no regime for a genuine mixture of pair and single electron transport since the excitations of one of the two carrier types are always gapped. At low temperature, transport is carried out by ungapped species.

On the other hand, as shown in Fig. 3.2, the situation is more interesting in the presence of a distributed attraction since a regime for pair-electron mixture emerges in transport. At low fields, the previous sharp gap in the electron DOS is smeared out by an amount corresponding to the standard deviation of the attraction distribution. In this case, even at zero field, a slight negative tail of the Gaussian distribution of λ_i induces a small number of soft sites occupied by unpaired electrons whose energies are close to the Fermi energy. They add more weight to the low energy single particle excitation sector and simultaneously reduce the weight of pair excitations. Their presence is felt

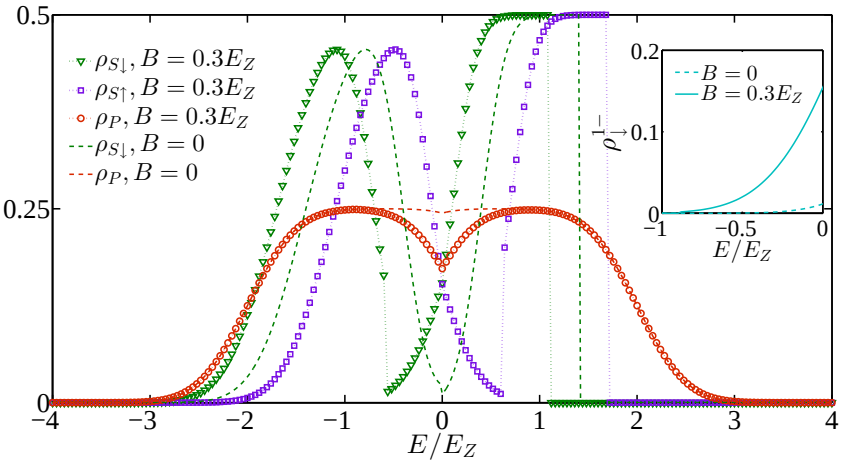

Figure 3.2: The single-site DOS's for single electron and pair excitations for a Gaussian distributed attraction. At zero magnetic field, the presence of a small number of unpaired electrons in the system is marked by a discontinuity and a slight dip at zero energy in the electron, pair DOS's, respectively. As the field increases, the more those electrons grow in number, the significantly higher the density of low energy states contributed by them becomes, e.g see in the inset presenting the contribution of singly occupied sites to the electron DOS. The total effect is to quickly fill up the low energy part of the electron DOS's and simultaneously suppress the same sector for pair excitations.

in both the single electron and pair DOS's: a tiny jump in the former and a slight dip in the latter at the zero excitation energy. This is so because all the occupancies contribute to the single-site DOS's for single electron excitations in Eqs. (3.16, 3.20) while only the empty or double occupancies contribute to the pair DOS. Consequently, the area covered by the pair DOS relates to the number of unpaired electrons in the system and will reduce if that number increases.

When a magnetic field is applied to the system, it modifies dramatically the low excitation energy sector. Due to the Zeeman effect, the magnetic field competes with the local pairing tendency on each site i supported by the attraction λ_i. As a result, there are more and more unpaired electrons in the system as the magnetic field is strengthened. The degenerate energy levels close to the chemical potential, which were previously occupied by pairs of electrons, now are replaced by single electron levels. Therefore, the low excitation energy sector provided by those unpaired electrons in the single

electron DOS's grows quickly with the applied field as seen in the inset of Fig. 3.2, while the low energy pair excitation sector falls off further. In other parts of the electron DOS's coming from empty and double occupancies, if the change in the magnetic field is ΔB, the value of the DOS is just a simple shift in the possible energy of the order of ΔB, e.g. $\rho_{\downarrow}^{0+}(E, B + \Delta B) = \rho_{\downarrow}^{0+}(E - \Delta B, B)\Theta(E - \Delta B)$. For the pair DOS, outside the growing deeper dip at low energy $E \leq 2B$ with increasing B, it remains untouched reflecting the fact that the B field changes only those degenerate levels close to the Fermi energy, but not the ones deep inside the spectrum. Furthermore, due to the possibility of multiple occupancies, the electron DOS is highly asymmetric.

As the above picture emerges with an increasing magnetic field, the unpaired electrons actively contribute to the transport and eventually overtake the pairs in the role as the main carriers in transport. Moreover, comparing the low excitation energy sector corresponding to spin $\downarrow$ in (3.16) and spin $\uparrow$ in (3.20), we can see that the former has higher weight than the latter. This observation suggests that the single electron transport is dominated by spin $\downarrow$.

3.3.2 The evolution of the DOS's at zero energy with a magnetic field

For transport at the lowest temperatures, obviously the low energy excitations matter the most. In this subsection, we focus on analyzing the DOS at zero energy. It can be extracted from the above given general Eqs. (3.16, 3.20, 3.25). A zero energy excitation of a spin $\downarrow$ ($\uparrow$) electron can be created by adding one to an empty (singly occupied) site or removing one from a singly (doubly) occupied site; a similar procedure for other zero energy pair excitation is applied. Following either way, one comes up with the following expressions for those DOS's at zero energy

$$\rho_{S\downarrow}^{0} = \frac{1}{4W}\left[\mathrm{erf}\left(\frac{2B - \lambda_0}{\sigma\sqrt{2}}\right) + 1\right]\Theta(W - |B + \mu|), \tag{3.28}$$

$$\rho^0_{S\uparrow} = \frac{1}{4W}\left[\mathrm{erf}\left(\frac{\min\{W+B-\mu,2B\}-\lambda_0}{\sigma\sqrt{2}}\right)-\mathrm{erf}\left(\frac{-W+B-\mu-\lambda_0}{\sigma\sqrt{2}}\right)\right] \Theta(W+B+\mu), \tag{3.29}$$

$$\rho^0_{P} = \frac{1}{8W}\left[\mathrm{erf}\left(\frac{2(W-\mu)-\lambda_0}{\sigma\sqrt{2}}\right)-\mathrm{erf}\left(\frac{\max\{2(-W-\mu),2B\}-\lambda_0}{\sigma\sqrt{2}}\right)\right] \Theta(W-B-\mu). \tag{3.30}$$

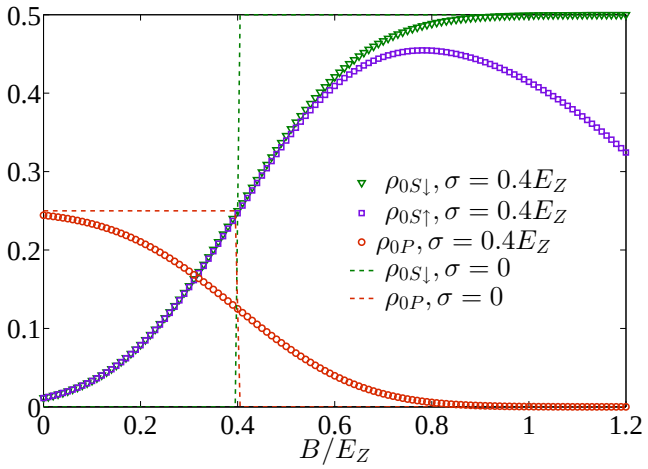

Figure 3.3: The DOS for zero excitation energy as a function of the Zeeman energy. The calculated result is shown for $W = 1$, $\lambda_0 = 0.8$. As the field is strengthened, a decrease in the pair DOS at that energy transfers into a strong rise of the electron DOS. It reflects the appearance of more and more unpaired electrons in the system, which possess energies close to the Fermi energy. For a constant attraction case, at $B = \lambda_0/2$ the gap is swapped between the two DOS's.

We are interested in the parameter regime $|\mu + B| < W$ in which both pairs and unpaired electrons occur in the ground state simultaneously. The above formulae for the DOS's can be rewritten as follows

$$\rho^0_{S\downarrow} = \frac{1}{4W}\left[\mathrm{erf}\left(\frac{2B-\lambda_0}{\sigma\sqrt{2}}\right)+1\right], \tag{3.31}$$

$$\rho^0_{S\uparrow} = \frac{1}{4W}\left[\mathrm{erf}\left(\frac{2B-\lambda_0}{\sigma\sqrt{2}}\right)-\mathrm{erf}\left(\frac{-W+B-\mu-\lambda_0}{\sigma\sqrt{2}}\right)\right], \tag{3.32}$$

$$\rho^0_{P} = \frac{1}{8W}\left[\mathrm{erf}\left(\frac{2(W-\mu)-\lambda_0}{\sigma\sqrt{2}}\right)-\mathrm{erf}\left(\frac{2B-\lambda_0}{\sigma\sqrt{2}}\right)\right]. \tag{3.33}$$

Those quantities reflect the evolution of the low excitation energy sector with an increasing magnetic field. Due to the conservation of the total particle number, a growing in the number of unpaired electrons occupying low energy sector is accompanied by a reduction of the one for pairs. This leads to a depletion of zero energy pair DOS with an enhancement of B field by an amount represented by the last term in Eq. (3.33). Concurrently, a corresponding amount cast by the first term in Eq. (3.31) is added to the zero energy DOS for the spin $\downarrow$ electrons. Moreover, it is worth to mention that the DOS at zero energy of a spin $\uparrow$ excitation is never smaller than the one of a spin $\downarrow$. It follows from the fact that on a singly occupied site, it is always more costly to add one more particle to that site than to empty it. Therefore, below we consider only spin $\downarrow$ type in term of electron excitation.

To demonstrate more how quickly the B field changes the DOS's, we examine their logarithmic derivatives

$$L_1(B) = \frac{\mathrm{d}\ln\rho^0_{\mathrm{S}\downarrow}}{\mathrm{d}\ln \mathrm{B}} = \frac{4B}{\sigma\sqrt{2\pi}} \frac{\exp\left[-\left(\frac{2B-\lambda_0}{\sigma\sqrt{2}}\right)^2\right]}{\mathrm{erf}\left(\frac{2B-\lambda_0}{\sigma\sqrt{2}}\right)+1}, \tag{3.34}$$

$$L_2(B) = \frac{\mathrm{d}\ln\rho^0_{\mathrm{P}}}{\mathrm{d}\ln \mathrm{B}} = -\frac{4B}{\sigma\sqrt{2\pi}} \frac{\exp\left[-\left(\frac{2B-\lambda_0}{\sigma\sqrt{2}}\right)^2\right]}{\mathrm{erf}\left(\frac{2(W-\mu)-\lambda_0}{\sigma\sqrt{2}}\right)-\mathrm{erf}\left(\frac{2B-\lambda_0}{\sigma\sqrt{2}}\right)}. \tag{3.35}$$

The signs of those functions confirm the tendencies of the relevant DOS's with B: a positive slope for an increasing of the single particle DOS and a negative one for a decreasing pair DOS. Besides that, at low field the amplitude with a convex feature accompanied with the former is bigger than the one with a concave tendency associated with the latter. It says how strong the depairing effect endorses the single particle transport by creating quickly more and more low energy excitations as a magnetic field is applied. At the field value at which $\rho^0_{S\downarrow}$ and ρ^0_P are equal, the magnitude of the derivative of the first one is twice bigger than the one of the second. That ratio comes purely from the difference in the number of particles in a given state they represent. At fields that are higher than the DOS meeting field, the dramatic rise of the electron

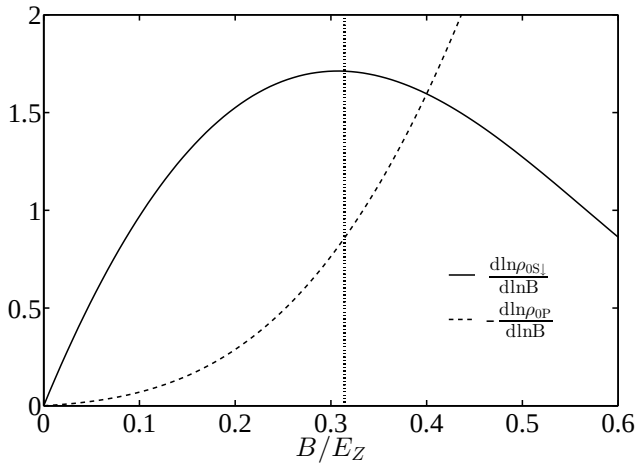

Figure 3.4: The variations of the DOS's with magnetic field for a set of parameters: $W = 1$, $\lambda_0 = 0.8$, and $\sigma = 0.4$. The vertical dotted line marks the value where $\rho^0_{S\downarrow} = \rho^0_P$. From low B, ρ^0_P approaches that value with a negative slope while $\rho^0_{S\downarrow}$ does with a much steeper positive slope showing a rapid increase of $\rho^0_{S\downarrow}$ with B. Comparing the variation of the pair DOS before and the visibly higher one of the electron DOS after the crossing field, it signals a possible asymmetry in quantities characterized transport in those regimes.

DOS is replaced by a slower trend with the slope becoming to decrease.

3.4 Quantum transport: localization properties

3.4.1 Formalism

In the strongly insulating regime $t_{1,2} \ll W$, the quantum hopping can be considered as a perturbation on a background of the classical ground state configurations. Following the formalism proposed in Ref. [60] and used in previous chapter, we study the localization properties of the system by examining the localization lengths of electron and pair excitations. The localization length measures the spatial decay rate of the relevant Green's function. The single electron and pair propagators are defined as follows, respectively,

$$G^R_{i0,\sigma}(t) = -\mathrm{i}\Theta(t)\left\langle\{c_{i\sigma}(t), c^\dagger_{0\sigma}(0)\}\right\rangle, \tag{3.36}$$

$$F^R_{ii,0}(t) = -\mathrm{i}\Theta(t)\left\langle\left[c_{i\downarrow}(t)c_{i\uparrow}(t), c^\dagger_{0\uparrow}(0)c^\dagger_{0\downarrow}(0)\right]\right\rangle. \tag{3.37}$$

Those functions are the probabilities of finding an electron or a pair at time $t > 0$ on a site i after being inserted into the system at time 0 on a given site of the lattice, denoted by 0. The notation $\langle \ldots \rangle$ indicates an expectation value with respect to the ground state of the Hamiltonian.

The equations of motion for the creation and annihilation of an electron read

$$\mathrm{i}\frac{\mathrm{d}c_{i\downarrow}(t)}{\mathrm{d}t} = (\varepsilon_i - \mu - \lambda_i n_{i\uparrow}(t) - B)\, c_{i\downarrow}(t) - \sum_{j\in\partial i}\left(t_1^{(ij)} c_{j\downarrow}(t) - t_2^{(ij)} c_{i\uparrow}^{\dagger}(t) c_{j\downarrow}(t) c_{j\uparrow}(t)\right), \tag{3.38}$$

$$\mathrm{i}\frac{\mathrm{d}c_{i\uparrow}(t)}{\mathrm{d}t} = (\varepsilon_i - \mu - \lambda_i n_{i\downarrow}(t) + B)\, c_{i\uparrow}(t) - \sum_{j\in\partial i}\left(t_1^{(ij)} c_{j\uparrow}(t) + t_2^{(ij)} c_{i\downarrow}^{\dagger}(t) c_{j\downarrow}(t) c_{j\uparrow}(t)\right). \tag{3.39}$$

In the above expressions, $t_q^{(ij)} = t_q e^{\mathrm{i}q\gamma\phi_{ij}^g B\sin\alpha}$ denotes the effective amplitude of a hop from site j to site i of an electron with $q = 1$ or a pair with $q = 2$. The sum runs over all sites j that belong to the group of nearest neighbors of site i, denoted as ∂i. We obtain the Green's functions in the frequency space:

$$G_{i0,\downarrow}^R(\omega) = \frac{1}{\varepsilon_i - \mu - \lambda_i \bar{n}_{i\uparrow} - B - \omega}\left(-\delta_{i,0} + \sum_{j\in\partial i} t_1^{(ij)} G_{j0,\downarrow}^R(\omega)\right), \tag{3.40}$$

$$G_{i0,\uparrow}^R(\omega) = \frac{1}{\varepsilon_i - \mu - \lambda_i \bar{n}_{i\downarrow} + B - \omega}\left(-\delta_{i,0} + \sum_{j\in\partial i} t_1^{(ij)} G_{j0,\uparrow}^R(\omega)\right), \tag{3.41}$$

$$F_{ii,0}^R(\omega) = \frac{1}{2(\varepsilon_i - \mu) - \lambda_i - \omega}\Bigg\{ -\delta_{i,0}\,(1 - \bar{n}_{0\uparrow} - \bar{n}_{0\downarrow}) + \sum_{j\in\partial i} t_1^{(ij)}\left[F_{ji,0}^R(\omega) + F_{ij,0}^R(\omega)\right] + \sum_{j\in\partial i} t_2^{(ij)}\,(1 - \bar{n}_{i\uparrow} - \bar{n}_{i\downarrow})\, F_{jj,0}^R(\omega)\Bigg\}, \tag{3.42}$$

where

$$F_{ij,0}^R(\omega) = \frac{1}{\varepsilon_i + \varepsilon_j - \lambda_i \bar{n}_{i\uparrow} - \lambda_j \bar{n}_{j\downarrow} - \omega}\left(\sum_{k\in\partial i} t_1^{(ik)} F_{kj,0}^R(\omega) + \sum_{k\in\partial j} t_1^{(jk)} F_{ik,0}^R(\omega)\right). \tag{3.43}$$

In the strongly insulating regime $t_{1,2} \ll W$, one can take the number operator $n_{i\sigma}$ outside the brackets $\langle \ldots \rangle$ by its eigenvalue $\bar{n}_{i\sigma}$ with respect to the classical ground state of the classical Hamiltonian. To get to Eqs. (3.40, 3.41), the same argument is applied, i.e. to the leading order in the hoppings, the expectation value of the type $\left\langle c^{\dagger}_{i\uparrow}(t), c_{j\downarrow}(t) \right\rangle$ can be approximately replaced by its value at the time $t = 0$ in the classical ground state, and thus gets zero value.

In the expression (3.42), there are two sources contributing to the pair propagator. The first accompanied by the single electron hopping amplitude t_1 comes from pair disintegration/formation processes while hopping through the lattice. In the second with the pair hopping t_2, a pair travels from an initial site to a final site as a rigid boson without being broken into its constituents. In the next step, we assume that in intermediate states the pair remains intact allowing us to neglect the contribution of all the processes containing the travel of single particle to the pair propagator. This is the case when the energy required to break a pair is large so that a pair would choose to stay intact and make a hop with t_2 rather than to be disintegrated and then hop paying an energy t_1 for a hop of each electron. The pair Green's function (3.42) is simplified as

$$F^{R}_{ii,0}(\omega) = \frac{1}{2(\varepsilon_i - \mu) - \lambda_i - \omega} \left\{ -\delta_{i,0} \left(1 - \bar{n}_{0\uparrow} - \bar{n}_{0\downarrow}\right) + \sum_{j \in \partial i} t_2^{(ij)} \left(1 - \bar{n}_{i\uparrow} - \bar{n}_{i\downarrow}\right) F^{R}_{jj,0}(\omega) \right\}. \tag{3.44}$$

In the course of the forward scattering approximation, which is reasonable in the strongly insulating regime, one is only allowed to take recursion steps that approach the final point. With that, the Green's function can be cast as a sum over only shortest paths $\{\Gamma\}$ connecting the initial site 0 to the final one i. It leads to the final expressions for the Green's functions in the expansion in the hoppings:

$$\frac{F^{R}_{ii,0}(\omega)}{F^{R}_{00,0}(\omega)} = t_2^{r_{0i}} \sum_{\substack{\Gamma: 0 \to i \\ |\Gamma| = r_{0i}}} e^{\mathrm{i}2\gamma\phi_\Gamma B \sin\alpha} \prod_{k \in \Gamma \setminus \{0\}} \frac{1 - \bar{n}_{k\uparrow} - \bar{n}_{k\downarrow}}{2(\varepsilon_k - \mu) - \lambda_k - \omega} \tag{3.45}$$

$$\frac{G^R_{i0,\downarrow}(\omega)}{G^R_{00,\downarrow}(\omega)} = t_1^{r_{0i}} \sum_{\substack{\Gamma:0\to i \\ |\Gamma|=r_{0i}}} e^{\mathrm{i}\gamma\phi_\Gamma B\sin\alpha} \prod_{k\in\Gamma\setminus\{0\}} \frac{1}{\varepsilon_k-\mu-\lambda_k\bar{n}_{k\uparrow}-B-\omega} \quad (3.46)$$

$$\frac{G^R_{i0,\uparrow}(\omega)}{G^R_{00,\uparrow}(\omega)} = t_1^{r_{0i}} \sum_{\substack{\Gamma:0\to i \\ |\Gamma|=r_{0i}}} e^{\mathrm{i}\gamma\phi_\Gamma B\sin\alpha} \prod_{k\in\Gamma\setminus\{0\}} \frac{1}{\varepsilon_k-\mu-\lambda_k\bar{n}_{k\downarrow}+B-\omega} \quad (3.47)$$

Here the shortest length $|\Gamma| = r_{0i}$ is defined as the minimal number of nearest neighbor hops needed to connect 0 and i. ϕ_Γ is the geometric part of the flux enclosed by the loop formed by a path Γ and a reference path connecting those two sites.

In the above expressions, the amplitude of each shortest path is a product of all locators that a site belonging to that path contributes. The appearance of the factor $1-\bar{n}_{k\uparrow}-\bar{n}_{k\downarrow}$ in the pair locator indicates the weakening of the pair propagator if there are more singly occupied sites blocking on the way since in this case the locator picks its zero value.

The localization length of an excitation of energy ω can be read off from the typical spatial decay rate of the Green's function. Having the variable range hopping transport at lowest temperature in mind, we are interested in the lowest excitation energy $\omega = 0$ whose localization lengths for eletrons and pairs are given by, respectively,

$$\xi^{-1}_{0S\downarrow,\uparrow} \equiv \xi^{-1}_{S\downarrow,\uparrow}(\omega=0) = -\lim_{r_{0i}\to\infty} \frac{1}{r_{0i}} \overline{\ln\left|\frac{G^R_{i0,\downarrow,\uparrow}(\omega')}{G^R_{00,\downarrow,\uparrow}(\omega')}\right|}_{\omega'\to\omega}, \quad (3.48)$$

$$\xi^{-1}_{0P} \equiv \xi^{-1}_{P}(\omega=0) = -\lim_{r_{0i}\to\infty} \frac{1}{r_{0i}} \overline{\ln\left|\frac{F^R_{ii,0}(\omega')}{F^R_{00,0}(\omega')}\right|}_{\omega'\to\omega}. \quad (3.49)$$

The overbar denotes the average over different disorder and attraction realizations. On a square lattice we carry the simulation out below, the localization length is calculated by choosing a fixed distance which is the largest one on that lattice to evaluate the sum over paths.

The calculated localization lengths reflect both the DOS effect via the distribution of amplitudes of locators and the orbital field effect via the Aharonov-Bohm phase factors. The former affects the amplitude of each possible path

by changing the value of its belonging locators. That is the place where the importance of the growth of the low energy electron excitation sector shows up as one varies the field strength.

Separately, the field orientation affects the interference of paths. At zero frequency, a non-zero pair locator (if $n_i \neq 1$) always comes with a positive sign, and thus all paths have positive amplitudes no matter what the field amplitude or orientation are. In the absence of a magnetic field or in the case the field is parallel to the system, that fact results in a positive interference among paths. An out-of plane field introduces a complex phase for each path, destroys that constructive interference, and therefore narrows the pair localization length. On the other hand, the opposite effect holds for the electron propagation. Its locators and so the paths come with random signs. Hence, an out-of plane field frustrates the negative interference of random sign paths pushing farther the localization length of an electron excitation.

As seen previously, the low energy sector of electron excitation with spin $\uparrow$ has lighter weight than the one with spin $\downarrow$. With that being transformed into a more frequent appearance of costly denominators of the locators, the propagation of a spin $\uparrow$ excitation is cut shorter than its counter part. In other words, its localization length is smaller, and the corresponding resistance is always higher than for spin $\downarrow$. Consequently, in term of the single electron transport, the main contribution comes from spin $\downarrow$ electron excitations. Therefore, from now on to the rest of this chapter, we refer to only that excitation type whenever discussing about the transport of single electron excitations, i.e. we omit the spin index.

Below we carry out a numerical study to understand the localization and transport properties of a system governed by the Hamiltonian (3.1). We choose a half-filled regular square lattice of 24×24 sites. First step is to find the classical ground state configuration of the Hamiltonian. The chemical potential is chosen to be the average of the minimal energy to add and remove an electron from a given classical ground state. Single electron excitation energies are counted from μ while pair excitation energies are measured from the reference energy 2μ. On the classical configuration background, to

obtain the localization length, we perform the sum over shortest paths enclosed in a diamond-shape region illustrated in Fig. (3.5). All energies are measured in the units of E_Z that is the Zeeman energy given by a magnetic field corresponding to one flux quantum per unit cell from an electron. The lattice constant a is chosen as the unit of length. All below observables are obtained by averaging over 500 random configurations.

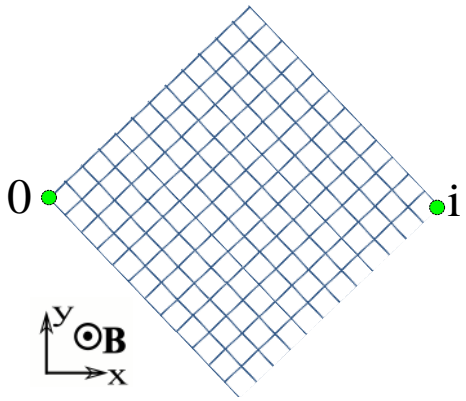

Figure 3.5: The diamond-shape region enclosing all the shortest paths between two chosen sites 0 and i to perform the numerical evaluation of the propagators.

3.4.2 Field and field-orientation dependence of the localization length: DOS and orbital effects

Fig. (3.6) presents the field dependence of the inverse localization lengths of pair and electron excitations at zero-energy for various values of the angle between the field direction and the system plane. When a parallel field is applied to the system, the Aharonov-Bohm phase factor has not yet entered into play, the only effect of the field is presented in the Zeeman term, or in other words the DOS effect. As the field increases, in the system there are more unpaired electrons whose energies are close to the Fermi energy. The low energy sector occupied by those single electrons grows and contributes significantly to the transport, while the low energy sector of pair excitations shrinks considerably. In the sum over paths, the small denominators connected to the former amplify the electron propagator, and thus make the electron localization length bigger. On the other hand, for pairs, the reduction of

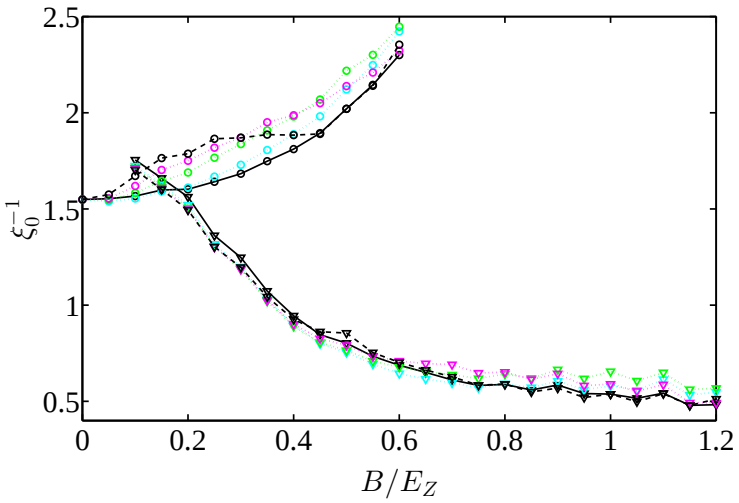

Figure 3.6: The inverse localization lengths of pair (∘) and electron (▽) zero-energy excitations as a function of Zeeman field for various angles: $\alpha = 0°$ (solid black) (parallel field), $15°$ (cyan), $30°$ (green), $45°$ (magenta), $90°$ (dashed black) (perpendicular field). Other parameters are taken to be: $W = E_Z$, $\lambda_0 = 0.8E_Z$, $\sigma = 0.4E_Z$, $t_1 = 0.06E_Z$, $t_2 = 0.04E_Z$. For a parallel field, there is only the DOS effect which promotes more low energy electron excitations, therefore, enhances the electron localization length and also reduces the pair one. For an out-of-plane field, the orbital effect is taken into account on top of the DOS effect. It frustrates the interference of paths and suppresses the maximally positive one among pair paths and the accidentally negative one among electron ones. This leads to a significantly additional increase of the single electron localization length at low field, and oppositely a weak extra decrease of the pair one. The effect reaches its maximum as the field is perpendicular to the system. Here only data corresponding to electron with spin ↓ is shown since it is the most important to the transport between two spin orientations.

small denominators and also the rise in the number of paths being blocked by singly occupied sites shorten the propagation of a pair excitation resulting in a shrinkage of the pair localization length.

When the field direction is out-of-plane, on top of the DOS effect, the interference effect starts adding its contribution to the localization properties. An out-of-plane field affects the localization lengths for pair and electron excitations in two opposite ways as discussed above. For a zero-energy pair excitation, the fact that the field suppresses the positive interference of paths all having positive sign leads to a decrease of the pair localization length. In contrast, the field reduces the negative interference of paths in case of single

electron giving rise for a broadening of the localization length. At zero energy, the field-free interference for pairs is strongest. Therefore, at low field, the more out-of-plane the field is, the stronger is the orbital effect; the maximal effect is reached when the field direction is perpendicular to that system. The suppression of the perfectly positive interference of all pair paths reduces the pair localization length much stronger comparing to a weak enhancement of the electron localization length. The latter is weak due to the reduction of an accidental cancellation of two bunches of electron paths that are close in the amplitude, but have opposite signs.

At very large B, upon approaching the point where all the electrons are unpaired and singly occupy all the sites, the average of the sum over electron paths slowly saturates to a certain value. In that regime, increasing the field hardly changes the electron localization length and also the resistance.

On a strictly periodic lattice, if only the orbital effect is taken into account while neglecting the Zeeman depairing term in the Hamiltonian, the data of the inverse localization lengths at different angles would collapse onto each other after an appropriate scaling related to factor $\sin\alpha$ revealing magneto oscillations with a fixed periodicity. For pairs, the period of oscillations comes naturally as a flux quantum per unit cell of a particle with charge $2e$, $\frac{h}{2e}$. For electrons, due to the asymmetry of the DOS, it cannot be the same period $\frac{h}{2e}$ for the electron localization length at zero energy. Nonetheless, the quasi doubling structure with two minima in one period $\frac{h}{e}$ discussed in the previous chapter still holds. Now taking into account the DOS effect, the rapid change of the amplitudes of the locators changes significantly the path amplitudes with increasing field, and thus destroys the perfect magneto-oscillations. In real materials, some have small Zeeman energy, e.g. in the one of high atomic number substrate with strong spin-orbit coupling, one might observe a remnant of those oscillations. However, for others or in the context of granular superconductors, the case where there are multiple fluxes is hardly realistic.

As discussed earlier for the case of a constant attraction λ_0, $B = \lambda_0/2$ is the value of the field at which the hard gap in the electron DOS is closed while the one in pair DOS is opened up. For the distributed attraction, we examine how

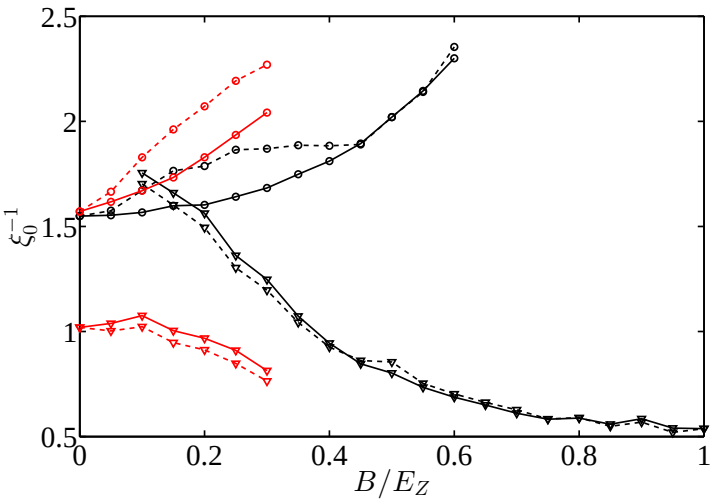

Figure 3.7: The field dependence of the inverse localization length for pair (∘) and electron (▽) zero-energy excitations for two values of the mean of the attraction: $\lambda_0 = 0.8E_Z$ (black) and $0.4E_Z$ (red) while keeping other parameters the same $W = E_Z$, $\sigma = 0.4E_Z$, $t_1 = 0.06E_Z$, $t_2 = 0.04E_Z$. Data is presented for parallel (solid), perpendicular (dashed) fields. The impact of DOS effect shows up: at the same field strength in low B regime, there are more and more low energy single particle excitations for a system that has smaller attraction. Therefore, the localization length of those excitations increases enormously as the attraction decreases.

the field dependence of the localization lengths changes due to the DOS effect as varying the mean attraction value. In the Fig. (3.7), we show the inverse localization lengths of pair and electron zero energy excitations for two values of the attraction: $\lambda_0 = 0.8E_Z$ and $\lambda_0 = 0.4E_Z$. At the smaller attraction, a weaker field strength is needed to free electrons from being paired. Because of that, at the same field strength, there are more low energy electron excitations contributing to transport for a system that has smaller attraction value. It substantially reinforces the single electron transport by a drastic rise of the electron localization length. At the same time, the pair localization length is suppressed further for a smaller attraction. Less importantly, a tiny initial decrease of the electron localization length at small field in case $\lambda_0 = 0.4E_Z$ comes from the asymmetry of the electron DOS.

In Eqs. (3.48, 3.49), the dependence of the localization length on the hopping amplitude is trivial. When the hopping changes by a factor n, the relevant inverse localization length is varied by an amount $-\ln(n)$. Therefore,

it is natural to expect a shrinkage of the localization length as the associated hopping is weakened.

3.5 Transport properties: Pair-to-single crossover

3.5.1 The crossover and its field orientation dependence

In the course of variable range hopping transport, there are two parallel channels for transport, by pairs of electrons and by single electrons themselves. Each of them can be characterized by the Mott's characteristic temperature

$$T_{M\beta}^{(0)} = \frac{1}{\rho_{0\beta}\xi_{0\beta}^2}, \tag{3.50}$$

where the subscript $\beta = P, S$ denotes the type of carriers, pairs and singles, respectively. As long as one of the two temperatures is smaller, the transport will be dominated by the carrier corresponding to that lower characteristic temperature. Based on that fact, a crossover in transport regimes dominated by different types of carriers happens when one of the two Mott's temperatures takes over the other to be the lower. Therefore, at lowest temperature, the pair-to-single crossover in transport is driven by the crossover in the Mott's temperature for pairs and electrons.

Despite its unrealistic nature, it is worth to mention the case of a constant attraction. At a zero field, the DOS of electron excitations possesses a hard gap up to an energy of the order of a half attraction value, and all electrons are paired. It means, for a field below that value, the transport is carried purely by pairs. A higher B field closes that gap in the electron DOS and opens a gap in the pair DOS. After that switch, the low energy transport is dominated by electrons forming a sort of crossover in transport.

With the same spirit is the picture in our case of interest with a distributed attraction. At a zero field, almost all electrons in the system are paired in local minima, only few unpaired ones are present due to a negative tail of the distributed attraction. In the low field regime, which is still overshadowed by the strong attraction, the pair transport is dominated as long as nearlly all

sites are doubly occupied, and there is a soft gap in the electron DOS. This is seen in Fig. (3.8) showing that the Mott's temperature for electrons are completely out of scale compared to the one for pairs at very low field.

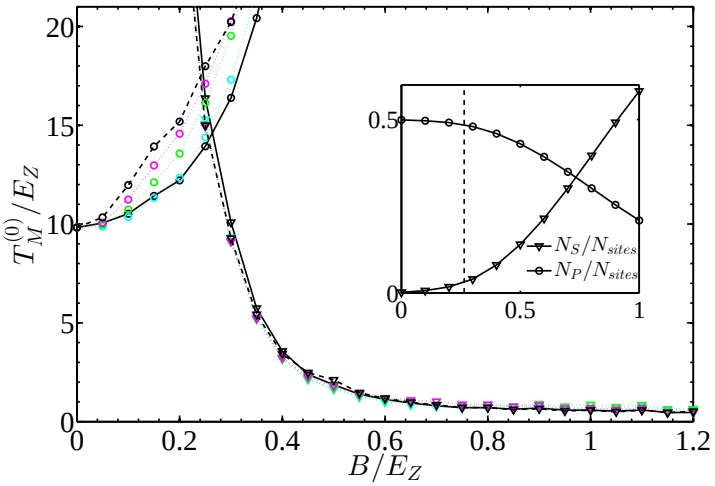

Figure 3.8: The field dependence of the Mott's temperature for pair ($\circ$) and electron ($\triangledown$) zero-energy excitations for various angles: $\alpha = 0^\circ$ (black, solid) (parallel field), 15° (cyan), 30° (green), 45° (magenta), 90° (black, dashed) (perpendicular field). Other parameters are: $W = E_Z$, $\lambda_0 = 0.8E_Z$, $\sigma = 0.4E_Z$, $t_1 = 0.06E_Z$, $t_2 = 0.04E_Z$. A crossover in Mott's temperature happens at any field orientation. It is a result of Zeeman depairing solely for a parallel field. The interference effect on the localization lengths accelerates it in case of out-of-plane field leading to a strong field orientation dependence of the MR peak: a considerable anisotropy on its pair side compared to its electron side. In high B regime, the Mott's temperature for electron transport slowly reaches its typical value when all electron are depaired, which is much smaller than the value for pair at $B = 0$. Inset: the average fraction of pairs, N_P/N_{sites}, and electrons, N_S/N_{sites}, evolving with the applied magnetic field; at the field where the crossover to electron dominated transport happens, pairs are still outnumbered by single electrons.

Gradually increasing the field fills up the gap in the low energy electron excitation sector by driving previously paired electrons into unpaired electron whose energies are close to the Fermi level. It, on one hand, gives rise to an increase of both the DOS of zero-energy electron excitation and its localization length, and on the other hand, decreases the ones for pair. That reflects into a gradual rise of Mott's temperature for pairs and a rapid downturn of the temperature for electrons. As the field is strong enough, the latter takes over the former to be the lower characteristic temperature. That is a signature

when transport changes from pair to electron dominated regimes resulting in a giant magnetoresistance peak seen in experiments. And that transport crossover and its associated resistance peak happen regardless of the field orientation because it is purely from the DOS effect.

Notice that at the value of B where the crossover in transport takes place, in the system, still a majority of electrons is paired, see the inset in Fig. (3.8). It tells us how robust is the contribution to transport of the unpaired electrons freed by an increasing field even though there are just few of them. Those electrons become an important source of transport since they hold the low energy excitation sector. In contrast, most of paired electrons possess very deep energy levels far from the chemical potential, and thus do not actively contribute to the low energy transport.

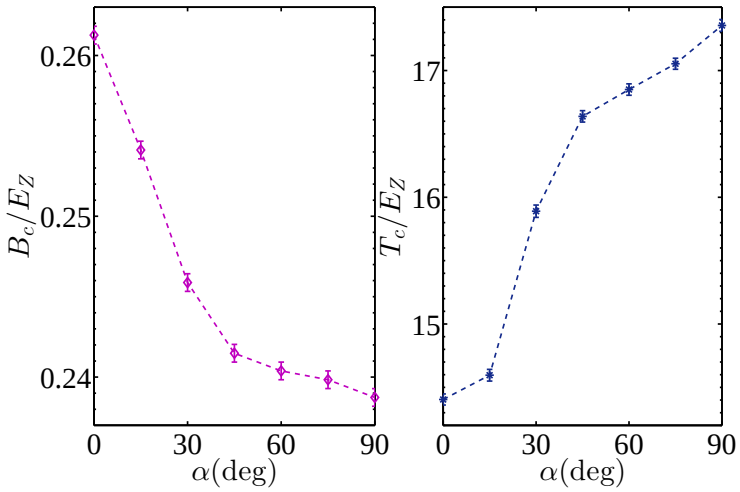

Figure 3.9: The crossing field B_c and corresponding Mott's temperature T_c as a function of the angle between the field orientation and the system plane. Toward a perpendicular direction at which the orbital effect has its maximum impact, the crossover happens at a smaller field and a higher temperature.

Now what the field orientation does in this context is to add the interference effect, when the field is out-of-plane, on top of the pair-breaking DOS effect. That affects only the localization lengths leaving the zero-energy DOS's untouched. Therefore, qualitatively, Mott's temperatures follow the trend of the inverse localization length seen in Fig. (3.6). Fig. (3.8) plots those temperatures for pairs and electrons for various degrees of the angle α between

the field and the system plane. On the low (high) field side of the crossover, the bigger the angle is toward a perpendicular direction, the more frustration due to an Aharonov-Bohm phase is added to reduce the maximal constructive (occasional destructive) interference of pair (electron) paths at $\alpha = 0$; and thus, the higher (lower) the Mott's temperature is for pair (electron). The overall picture is that the magnetoresistance peak moves to a lower field, a higher characteristic temperature as the field direction changes from being parallel to being perpendicular to the system plane, which is presented in Fig. (3.9). Moreover, the variation of magnetoresistance with the field orientation is much stronger on the pair side of the peak than on the electron side. These results are in agreement with the anisotropy and its exhibition on two sides of the peak observed in Fig. 3 in Ref. [89] and Fig. 2 in Ref. [90].

In the very high B regime, after a strong drop after the peak, while the pair Mott's temperature is out of scale (not shown in the figure), the electron one varies slowly and reaches its saturated value. That is when nearly all electrons are unpaired and singly occupy most of lattice sites. The DOS of the zero-energy electron excitation gets to its peak, and increasing field no longer changes the setting. The typical value of the Mott's temperature (and so the resistance) in this electron dominated regime is much smaller than the temperature for pairs at $B = 0$.

3.5.2 Magnetoresistance peak and various model parameters

In this subsection, we analyze the dependence of the pair-to-single crossover on the model parameters. Putting together the DOS's in Eqs. (3.31, 3.33) in the expression for Mott's temperature at lowest temperature, Eq. (3.50), one obtains a condition for the field B_c and the corresponding characteristic temperature T_c at which the crossover or the magnetoresistance peak happens

$$B_c = \frac{\lambda_0}{2} + \frac{\sigma}{\sqrt{2}}\mathrm{erf}^{-1}\left[\frac{\frac{u^2}{2}\mathrm{erf}\left(\frac{2(W-\mu)-\lambda_0}{\sigma\sqrt{2}}\right)-1}{\frac{u^2}{2}+1}\right] \overset{\lambda_0 \gg \sigma}{\approx} \frac{\lambda_0}{2} + \frac{\sigma}{\sqrt{2}}\mathrm{erf}^{-1}\left(\frac{u^2-2}{u^2+2}\right), \tag{3.51}$$

$$T_c = \frac{8W}{\xi_{0,P}^2(B_c)} \frac{\frac{u^2}{2}+1}{\frac{u^2}{2}\mathrm{erf}\left(\frac{2(W-\mu)-\lambda_0}{\sigma\sqrt{2}}\right)+1} \overset{\lambda_0 \gg \sigma}{\approx} W\left(\frac{1}{\xi_{0P}^2(B_c)} + \frac{2}{\xi_{0S}^2(B_c)}\right), \quad (3.52)$$

where $u \equiv \xi_{0P}(B_c)/\xi_{0S}(B_c)$.

As seen above, in the limit when the attraction is sharply distributed around its mean value, $\lambda_0 \gg \sigma$, the peak position pinpoints closely a half of that value. This result is independent of the on-site disorder profile. It is so because the transport is sensitive the most to the soft gap in the electron DOS and the gap closing process itself, which depend nearly only on the attraction mean value and the Zeeman field, but not on the on-site disorder distribution. It also says in that expression that, besides the main component coming from the attraction, other contributions through the localization length, e.g. the hoppings and B orientation, are counted in the ratio between the two localization lengths. If that ratio exceeds $\sqrt{2}$, or $\sqrt[d]{2}$ in a d dimension, in which 2 stands for the charge ratio between a pair and an electron, the transport crossover takes place at a higher field than a half of the attraction mean value. Despite an obvious attraction dependence of the peak position, for its height, everything is encoded into the two localization lengths that are heavily relied on not only the DOS effect, but also the interference one, and so the hopping amplitudes.

In our model, the most important parameters to the magnetoresistance peak are the Zeeman field, the attraction, and the hoppings, especially the pair hopping in the context of the superconductor-to-insulator transition. Examining the dependence of the current picture of the crossover as one varies the attraction and the pair hopping is shown in Figs. (3.10) and (3.11), respectively. In the former, reducing the mean attraction value by a half while keeping other parameters the same accelerates the crossover to happens at much smaller B. Due to a fatter tail of the attraction distribution in the negative value regime, the presence of a greater number of unpaired electrons even at zero field promotes this escalation. The peak position moves disproportionately comparing to the change of the mean attraction value. Moreover, a strong enhancement of the electron localization length, in contrast to a slight decrease of the pair one, makes the peak happens at a smaller characteristic

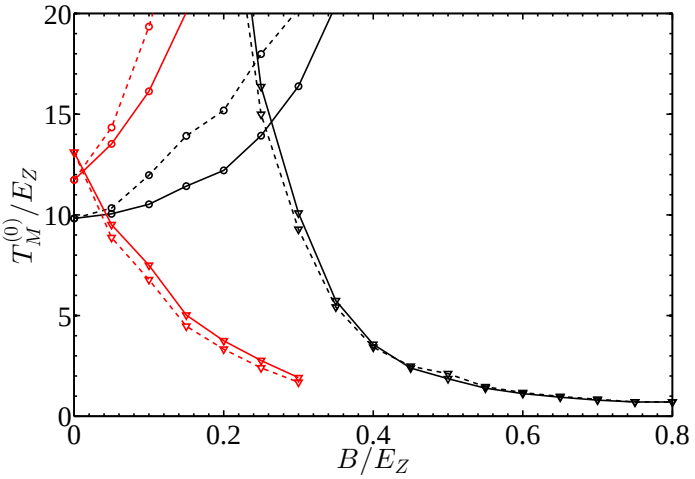

Figure 3.10: The Mott's temperature for pair (∘) and electron (▽) zero-energy excitations for two values of the mean of the attraction: $\lambda_0 = 0.8E_Z$ (black) and $0.4E_Z$ (red) while keeping other parameters the same $W = E_Z$, $\sigma = 0.4E_Z$, $t_1 = 0.06E_Z$, $t_2 = 0.04E_Z$. Data is presented for parallel (solid), perpendicular (dashed) fields. The peak moves to a lower field as the attraction is reduced due to the a strong rise of low energy single particle DOS and a suppression of pair DOS at smaller field.

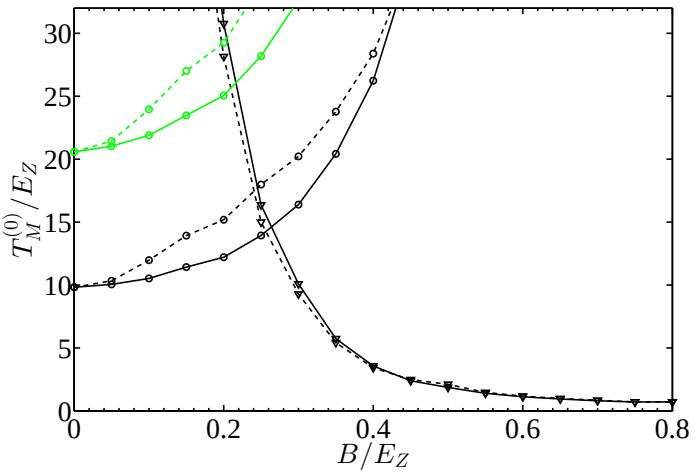

Figure 3.11: The Mott's temperature for pair (∘) and electron (▽) zero-energy excitations for two values of pair hopping: $t_2 = 0.04E_Z$ (black) and $0.02E_Z$ (green) and for perpendicular (dashed) and parallel (solid) fields while keeping other parameters the same $W = E_Z$, $\lambda_0 = 0.8E_Z$, $\sigma = 0.4E_Z$, $t_1 = 0.06E_Z$. The peak height increases significantly as the pair hopping decreases resulting in a profound reduction of the localization length for pair excitations.

temperature in this case. On the other hand, in Fig. (3.11), reducing the pair hopping to its half value significantly raises of the peak height due to an

additional shift of ln(2) to the inverse pair localization length while the DOS's at zero energy remain unchanged.

The above two parameters, the mean attraction value and the pair hopping are important in the granular superconductor context as they reflect the distance to the superconductor transition. The further the system is away from criticality, the smaller both values are. The combined effect will lead to the following picture: as the distance to criticality increases, the magnetoresistance peak occurs at smaller field. Eventually, the electron part of the peak is already dominant even at zero field exhibiting all the corresponding behavior, a negative magnetoresistance with a very weak field orientation dependence, the magnetoresistance peak is no longer seen. This explains the disappearance of the peak and also its strong anisotropy at low field as the sample gets deeper into the insulating regime seen in experiments [49, 90].

3.6 What could Coulomb interactions do?

In previous sections, one can see how dominantly the DOS effect determines the whole magnetoresistance peak picture. A natural question to ask is how that picture changes if Coulomb interactions are taken into account. One may expect that the well-known Coulomb gap created in both the pair and electron DOS's modifies the DOS effect. Here we discuss some preliminary results about the DOS's. A more complete picture for MR will be reported elsewhere.

Here we briefly describe the procedure to include the Coulomb interaction term into the Hamiltonian in (3.1). The classical part of the full Hamiltonian becomes

$$H_{Coulomb} = \sum_{i,s}(\varepsilon_i - \mu)n_{is} + \frac{1}{2}\sum_{j\neq i}\frac{e^2}{\kappa r_{ij}}(n_i - \nu)(n_j - \nu) - \sum_i \left(\lambda_i n_{i\uparrow}n_{i\downarrow} - B(n_{i\uparrow} - n_{i\downarrow})\right), \tag{3.53}$$

where κ denotes the dielectric constant of the film, r_{ij} is the distance between those two sites, and $\nu = \frac{1}{2}$ is the filling of the lattice due to which the Coulomb contribution of the positive background is subtracted to assure the neutrality

condition. We employ the same procedure that has been used in various works, eg. Refs. [96, 97]. It is to consider the DOS's within typical metastable states that are energetically stable with respect to moves of single electrons, pairs, or to disintegration/formation of pairs. Numerically, on a finite size system, a simulation is carried out by looping over all pairs of sites (i, j) and attempting to move either one or two electrons. The proposed move is accepted if it lowers the total energy, otherwise it is rejected. A metastable configuration is found if there is no longer any pair/single electron move that lowers the total system energy. It is equivalent with the requirement that the following stability conditions are fulfilled

$$E_i^{1+} - E_j^{1-} - \frac{e^2}{\kappa r_{ij}} > 0, \tag{3.54}$$

$$E_i^{2+} - E_j^{2-} - \frac{4e^2}{\kappa r_{ij}} > 0, \tag{3.55}$$

where $E_i^{m\pm}$ are the excitation energies to add or remove $m = 1, 2$ particles from a given site i. Those excitation energies can be obtained from Eqs. (3.8)-(3.15) by replacing

$$\varepsilon_i \to \varepsilon_i + \sum_{j \neq i} \frac{e^2}{\kappa r_{ij}} (n_j - \nu) \tag{3.56}$$

Below is the numerical result obtained on a 30×30 square lattice with the periodic boundary condition. The Coulomb interaction between nearest neighbor electrons, $E_C = e^2/\kappa a$, is taken to be equal to the energy unit E_Z. The numerically evaluated DOS's shown in Fig. (3.12) are the histograms of the electron/pair excitation energies and are averaged over 200 initial random configurations. Energies are defined relatively to the chemical potential at which $E_i^{m+} > 0$ and $E_i^{m-} < 0$.

In the case of a constant attraction, there is a sharp gap of order of $\lambda_0/2 - B$ around the Fermi energy in the electron DOS at zero field due to the fact that all electrons are paired. The well-known mechanism for Coulomb gap is active only for those energy states outside that gap. Increasing the field shortens the

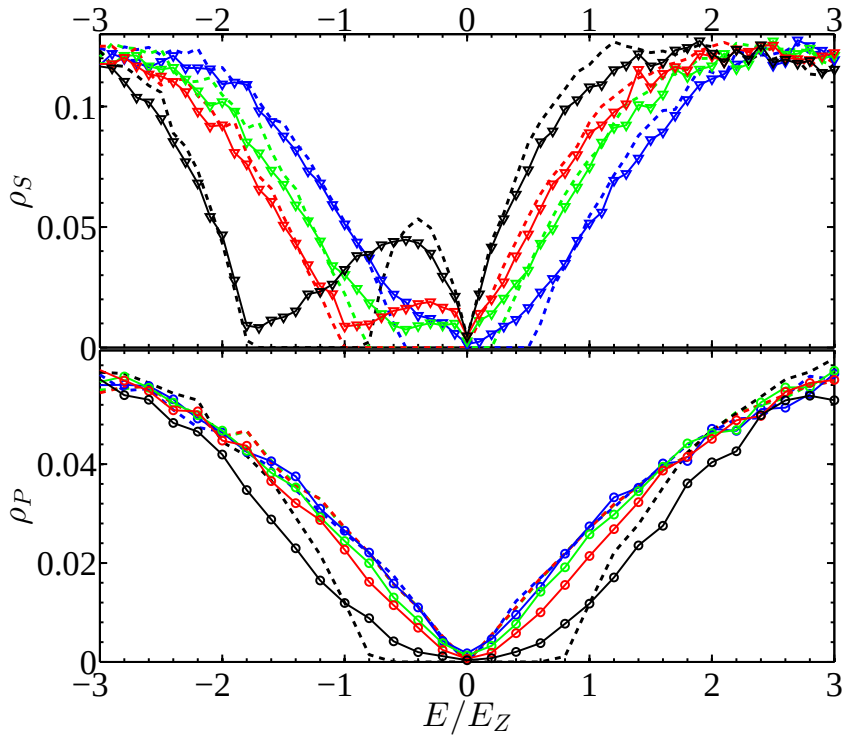

Figure 3.12: The electron (▽), pair (○) DOS's, ρ_S and ρ_P, in the presence of Coulomb interactions with a constant (dashed), $\lambda_0 = 1$, $\sigma = 0$, and a Gaussian distributed attraction (solid), $\lambda_0 = 1$, $\sigma = 0.4$ for various values of the field: $B = 0$ (blue), 0.3 (green), 0.5 (red), 0.9 (black). The on-site disorder strength is chosen to be $W = 4E_Z$, and $E_C = E_Z$. In the constant attraction case, when $B < \lambda_0/2$, Coulomb interactions only modify the energies outside the hard gap of order of $\lambda_0/2 - B$ in ρ_S while a linear Coulomb gap is created at low energy pair excitations. The reverse is seen for higher B field. As the attraction is distributed, all sharp features are smeared out due to the presence of unpaired electrons in the system. The low energy electron excitations contributed by those electrons leak into the λ_0 hard gap, and are subject to be depleted by the Coulomb interaction. But the overall picture of the DOS's evolving with the field seems unaffected.

gap. After $B = \lambda_0/2$, that hard gap disappears and is replaced by a Coulomb gap: lowest energy excitations come from unpaired electrons and are subject to the Coulomb gap. On the other hand, the same analogy acts in a reverse way for the pair DOS. In the regime $B < \lambda_0/2$, the pair DOS changes from being a flat, featureless form when without Coulomb interactions to possessing a linear gap at low excitation energy in the presence of those repulsive long-range interactions. Out side that regime of the field, a hard, flat gap of order $2B - \lambda_0$ appears at low energy. This is entirely due to the depairing effect of

the Zeeman field. For higher excitation energies, a combination of Coulomb interaction and depairing effect smoothly governs the density of those states.

Comparing to the above picture, a Gaussian distributed attraction changes mostly the low energy sectors of both electron and pair DOS's. While the latter is smeared out just a little bit for small field, a much stronger impact is seen for the former due to the presence of the unpaired electrons already at zero field in the absence of the Coulomb interactions. They provide a finite amount of low energy electron excitations around the Fermi energy that, in turn, becomes the subject to be depleted by the long-range repulsion creating a Coulomb Gap. In this case, the Coulomb gap in the electron or pair DOS's is always there for any small to mediate value of the field.

Within this scope, we are not interested in the question whether the Coulomb gap in this setting is universal or not. That question would require much more resources to answer, but provide not much insight into the problem we try to address here. Instead, we focus only on the magnetoresistance peak, trying to answer the question of any possibility for the Coulomb interactions to alter the explained above picture. The next (pending) step would be to calculate the electron and pair resistances and see how they evolve with the field. Despite the presence of the Coulomb gap in both the pair and electron DOS's, the prominent role of the B field to lift off low electron excitation energies shows up. One of its representative is a steeper and steeper Coulomb gap in the electron DOS, while a weaker reverse trend is seen in the pair DOS, when the field gets stronger. This suggests the current explanation for magnetoresistance peak should hold even in the presence of Coulomb interactions.

3.7 Summary and conclusion

In this part of the thesis, we have proposed a microscopic model that captures the underlying physics behind the MR peak reflecting the crossover from pair to single electron dominated transport. It is the interplay between the isotropic DOS and the anisotropic interference effects. The former is the main driving force toward the crossover. It represents the process of an increasing

Zeeman field that releases unpaired electrons from being paired to contribute greater impact to the transport. This happens by filling the low energy sector with electron excitations coming from those unpaired electrons. This effect occurs regardless of the orientation of the field.

The interference effect of an out-of-plane field highlights the role of quantum statistics that emphasizes the difference in dominant carrier type on either side of magnetoresistance peak. The more out-of-plane the field, the stronger the orbital effect. The maximal effect is reached as B field is perpendicular to the system. As the angle α increases from 0° to 90°, in the pair dominated transport, the magnetoresistance is significantly enhanced while, in contrast, a much weaker opposite impact is seen in the electron dominated one. As a result, the magnetoresistance peak occurs at a lower field and a higher characteristic Mott's temperature in perpendicular field as compared to parallel field.

Further into the insulating regime, due to a strong suppression of both the local attraction and the pair hopping, the electron dominated transport takes over at lower fields. At strong enough disorder or distance to the SIT, it already occurs even at zero field. In this case, the peak disappears leaving only (strong) negative magnetoresistance which arises from the destruction of local superconducting regions that do not participate in the electronic transport.

Our theory captures qualitatively many key features observed in the experiments in Refs. [89, 90]: the relative magnitudes and opposite tendencies of the anisotropy of MR before and after the peak, the evolution of the peak field and height with the field orientation, its disappearance when the system gets deeper into the insulating regime. The current picture is expected to hold at lowest temperature even down to zero temperature. The Coulomb interactions can be present as a part of a more realistic model. However, we believe that the essential nature of the pair-to-single crossover in the transport remains intact.

Chapter 4

Interaction-induced delocalization in 2D interacting systems

4.1 Introduction

In this chapter, we leave the superconductivity aside. Instead we discuss the role of the long-range electron-electron interactions on the localization properties of a two-dimensional system with multiple electron flavors that can be pocket or band or spin indices.

After the discovery of Anderson localization [3] and the later scaling theory of localization [9], it was generally believed that no true metallic state exists in one- and two- dimensional (2D) non-interacting disordered systems while a metal-insulator transition (MIT) is predicted in three dimensional systems. With the exclusion of electron-electron interaction, the original scaling theory by Abraham *et al.* [9] implies that an infinite 2D system is always an insulator due to the localization of electronic wavefunctions, no matter how weak the disorder is. In that work, the main assumption was that the scaling function $\beta(g) \equiv \mathrm{d}\ln g/\mathrm{d}\ln L$ is a function of the conductance g itself but not an explicit function of the length scale L. The behavior of $\beta(g)$ is shown in Fig. (4.1). In 2D, $\beta(g)$ is always negative meaning that the conductance decreases monotonically upon increasing the length scale, or decreasing the temperature. In contrast, in 3D there is an unstable fixed point, i.e. moving away from it, the scaling trajectory goes either towards small g for a negative $\beta(g)$ (insulating behavior) or towards large g for a positive $\beta(g)$ (metallic behavior) as the length scale increases.

On the other hand, in the limit of strong electron-electron interaction

without disorder, the 2D electronic system forms a Wigner crystal, and the conductivity reduces to zero due to collective trapping and weak collective pinning of the crystal [101].

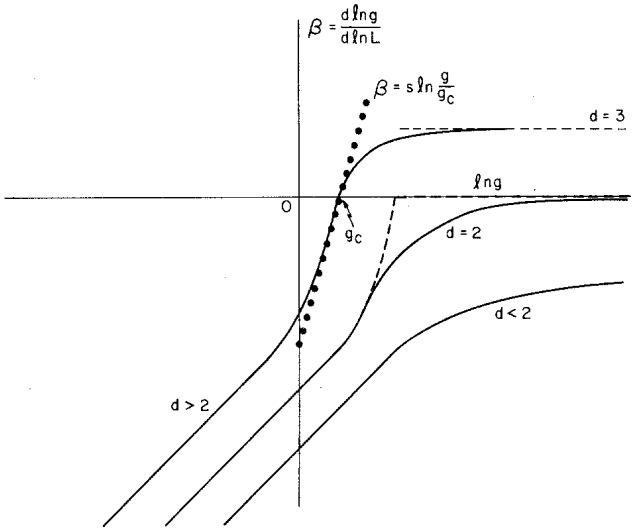

Figure 4.1: The scaling function $\beta(g)$ versus the logarithmic of the conductance g, taken from Ref. [9].

In the 1990s, a series of experimental works in high-mobility silicon metal-oxide-semiconductor field-effect transistors (Si MOSFETs) [10, 102, 103, 104, 105], and also in other materials [106, 107, 108, 109, 110], reported metallic behavior in 2D samples. This observation suggested the scaling theory for non-interacting systems might not hold for interacting cases. In these experiments, at low carrier density the resistivity diverged with lowering temperature as expected for an insulator. At higher carrier density, however, above a certain critical value $n_c \sim 0.8 \times 10^{11}$ cm^{-1}, it showed metallic behavior, and the resistivity dropped to a finite constant upon lowering temperature. This raised a fundamental question about localization, namely, whether a genuine metal-insulator transition might exist in 2D systems.

There has been an extensive number of theoretical works over the last decades proposing different scenarios about the 2D MIT. However, a final answer to the above question has not been reached. On the numerical side, a significant effort has been devoted to this issue, including different methods

and techniques, for example quantum Monte Carlo, Hartree-Fock, or dynamical mean field theory [111, 112, 113, 114, 115]. On the analytical side, in the 1980s, there were perturbative calculations performed in the weak disorder regime attempting to include electron-electron interactions in 2D disordered systems, first by Altshuler *et al.* [116] and later by Finkel'stein [117] and Castellani *et al.* [118]. In the breakthrough work [116], Altshuler *et al.* showed the weak-localization (logarithmic) corrections to the conductivity for 2D systems at low temperature. Within a perturbative renormalization group approach, Finkel'stein [117] suggested a mechanism of delocalization due to the spin-spin interaction. Unfortunately, this perturbative treatment is invalid at zero temperature. Those above mentioned works were focused on the diffusive limit. Interestingly, the work by Zala *et al.* [119] on the systems in the ballistic regime found the correction to the conductivity to be linear in temperature, and this correction changes its sign depending on the strength of the interaction.

Later, Punnoose and Finkel'stein [11, 52] re-summed over the most divergent terms that caused the breakdown of the previous perturbation theory upon approaching zero-temperature. Their work emphasized the crucial role of spin and valley (degenerate regions in the conduction band of semiconductors) degeneracy. They considered $2n_\nu$ flavors of electrons, where n_ν is the number of valleys, and the extra factor two refers to the two possible spin states of an electron. The existence of a quantum critical point separating a metallic and an insulating phase has been argued. Below we review only the most relevant approaches to our work, for reviews on this subject see for example [120, 121].

The essence of Punnoose and Finkel'stein's work is summarized by the following renormalization group equations for two parameters, the dimensionless resistance ρ and the electron-electron scattering amplitude γ_2, reflecting the interplay between disorder and interaction,

$$\frac{\mathrm{d}\ln\rho}{\rho \mathrm{d}l} = \left[n_\nu + 1 - (4n_\nu^2 - 1)\left(\frac{1+\gamma_2}{\gamma_2}\ln(1+\gamma_2) - 1\right)\right], \tag{4.1}$$

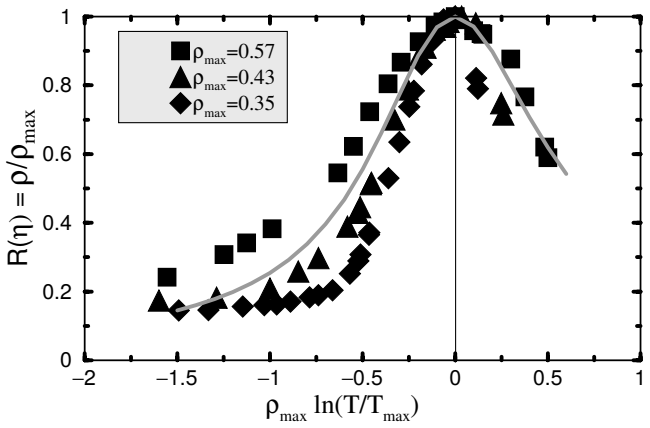

Figure 4.2: ρ/ρ_{max} as a function of $\rho_{max}\ln(T/T_{max})$. The solid line presents the solution of Eq. 4.1 with $n_\nu = 2$ showing the non-monotonic scale dependence of the resistivity. The symbols correspond to different values of the electron density, 0.83 (square), 0.88 (triangle), and 0.94 (diamond) $\times 10^{11}$ cm^{-2}. The plot is taken from Ref. [11].

$$\frac{\mathrm{d}\gamma_2}{\rho \mathrm{d}l} = \frac{(1+\gamma_2)^2}{2}. \tag{4.2}$$

In the above, $l = -\ln(T\tau)$ is a relevant scale of those two quantities, where τ is the elastic scattering time, T is the temperature, and $T\tau \ll 1$ is in the diffusive regime. In Eq. (4.1), the first term is the usual Anderson localization without interactions. This term corresponds to the quantum interference leading to weak localization in non-interacting systems with n_ν valleys. The second term is a contribution of a singlet mode of interaction in the charge channel, discovered in Ref. [116]. It is independent of n_ν as the singlet mode is unique no matter how many flavors. Moreover, the effective constant of the interaction in front of this term is unity due to the (over) screening of the long-range Coulomb interaction (leading to a universal constant of the interaction in the singlet channel). Finally, the last term represents the multiplet modes with the total number of those modes $4n_\nu^2 - 1$. Note that this term includes a function of the effective interaction γ_2 as the corresponding interaction is not screened. γ_2 and thus the value of that function are small at small scale l, but grow monotonically with increasing the scale l, or lowering the temperature T. This effect is described in Eq. (4.2) as the right hand side is always positive.

In Eq. (4.1), the first two terms favorable to localization come with a positive sign whereas the last term has a negative sign supporting anti-localization. Due to the presence of the factor $4n_\nu^2 - 1$, the anti-localization tendency gets enhanced dramatically in the case of multi-valleys while the total contribution from terms favorable to localization increases much slower. That enhancement together with the gradual increase of γ_2 upon a larger scale can give a non-monotonic scale dependence to the resistance, a growth (an insulating behavior $\mathrm{d}\rho/\mathrm{d}l > 0$) at small scale and a decrease (a metallic trend $\mathrm{d}\rho/\mathrm{d}l < 0$) at larger scale. Therefore, for a large number of flavors, at large scale, eventually, the net effect is in favor of delocalization.

With $n_\nu = 2$, Fig. (4.2), taken from Ref. [11], plots the rescaled resistivity ρ/ρ_{max} as a function of $\rho_{max}\ln(T/T_{max})$, where the maximum value ρ_{max} is reached when the temperature T gets to a certain value T_{max}. Experiment data are provided for comparison also. In this case, if one starts from a temperature above T_{max}, upon decreasing the temperature, γ_2 increases but is still small, and thus the first two terms dominate the right hand side of Eq. (4.1) leading to an enhancement of the resistivity. At $T \sim T_{max}$, γ_2 is big enough so that the contribution from the last term favoring antilocalization is of the order of the one from the above two terms. From this point on, with lowering the temperature further, the antilocalization term is dominant and strengthened, resulting in a reduction of the resistivity.

Motivated by the above theory we carry out below a numerical study using Hartree-Fock treatment aiming at addressing the role of electron-electron interactions in a 2D disordered system with multiple electron species. As we will discuss later, at the Hartree-Fock approximation level, a correspondence with the Finkel'stein's renormalization group equation can emerge.

Although the Hartree-Fock Hamiltonian is effectively a single-particle one, it has been shown in Ref. [74] that the treatment in 3D systems is capable of demonstrating such subtle wavefunction correlations in the presence of Coulomb interactions. In that work, the correlation fractal dimension reflecting the multifractality of the Hartree-Fock wavefunctions is determined. The fractality is a characteristic of critical states, but also exhibits in off-critical

states within the localized region of the wavefunction.

4.2 Model and method

On a regular square lattice of size $N = L \times L$, we consider a system of $N_e = pfL^2$ electrons, where $p \equiv 2n_\nu$ is the number of electron species, and f denotes the filling per species. The electrons in a random potential are subject to Coulomb interactions and can hop between nearest neighbor sites with the hopping amplitude t. The Hamiltonian describing this system reads

$$H = \sum_{i,\alpha} (\varepsilon_{i\alpha} - \mu)\, c^\dagger_{i\alpha} c_{i\alpha} + \frac{1}{2} \sum_{\substack{i \neq j \\ \alpha\alpha'}} V_{ij}\, (n_{i\alpha} - f)(n_{j\alpha'} - f) - \sum_{\langle i,j \rangle, \alpha} t \left(c^\dagger_{i\alpha} c_{j\alpha} + h.c \right). \tag{4.3}$$

$c^\dagger_{i\alpha}$, $c_{i\alpha}$ are the creation and annihilation operators of an electron of flavor $\alpha = 1, 2, \ldots, p$ on site i, and $n_{i\alpha} = c^\dagger_{i\alpha} c_{i\alpha}$ is the local occupation number operator. The onsite disorder ε_i is uniformly distributed between $[-W/2, W/2]$. $V_{ij} = U/r_{ij}$ represents the Coulomb interaction between charges at two sites i and j. To ensure the charge neutrality, each site of the lattice carries a compensating background positive charge of fe per flavor. The chemical potential is determined self-consistently according to the filling f. We set $t = 1$ to be the unit of energies and the lattice spacing a to be the unit of length.

Within the Hartree-Fock approximation, the Coulomb interaction term can be decoupled, and we obtain the following Hartree-Fock Hamiltonian

$$H = \sum_{i,\alpha} \tilde{\varepsilon}_{i\alpha} c^\dagger_{i\alpha} c_{i\alpha} - \sum_{i \neq j, \alpha, \alpha'} V_{ij} \langle c^\dagger_{i\alpha} c_{j\alpha'} \rangle c^\dagger_{j\alpha'} c_{i\alpha} - \sum_{\langle i,j \rangle, \alpha} t \left(c^\dagger_{i\alpha} c_{j\alpha} + h.c \right). \tag{4.4}$$

The second term is the long-range Fock exchange interaction while the Hartree energy is included in the effective onsite energy

$$\tilde{\varepsilon}_{i\alpha} = \varepsilon_{i\alpha} - \mu + \sum_{j \neq i, \alpha'} V_{ij} \langle c^\dagger_{j\alpha'} c_{j\alpha'} \rangle. \tag{4.5}$$

The $\langle \ldots \rangle$ denotes the expectation value with respect to the Hartree-Fock

ground state which has to be determined self-consistently. By using the Hartree-Fock approximation, the interacting many-body Hamiltonian is reduced to an effective single-particle one.

As seen above, on one hand, the presence of the onsite energy Hartree shift enlarges the fluctuation amplitude of the effective onsite disorder energies. This effect somehow favors localization. On the other hand, due to the interaction-induced deterministic energy added, the effective onsite disorder energies are no longer uncorrelated. The effective correlation indeed prefers to delocalize an excitation. Adding to this picture, also there is a long-range hopping due to the nature of long-range Coulomb interaction via the presence of the exchange Fock term. The interplay between opposite tendencies favoring anti-localization and localization can lead to a rather complex behavior of the system.

To simplify the problem such that the computational cost can be reduced, from Eq. (4.3) to Eq. (4.4), we have chosen to retain only the terms that obey the flavor symmetry. Since it is diagonal in electron flavor space, the practical Hilbert space is now reduced to $N \times N$ instead of a full size $pN \times pN$. In general, the flavor symmetry can be kept or broken.

To numerically determine the Hartree-Fock solutions of the above Hamiltonian for a given set of random realization of the onsite energies $\{\varepsilon_i\}$, we follow a standard set of steps which are briefly summarized as follows. First the program creates randomly an initial input set for the density matrix $n_{ij} = \langle c_i^\dagger c_j \rangle$, and then forms a $N \times N$ Hamiltonian matrix given by Eq. (4.4) from that input set. The Hamiltonian matrix is diagonalized to obtain the eigenvalues $\{E_m\}$ and eigenvectors $\{\psi_m\}$, based on which one can calculate the output density matrix

$$n_{ii} = \sum_m |\psi_m(\mathbf{r}_i)|^2 f(E_m), \tag{4.6}$$

$$n_{ij} = \sum_m \psi_m^*(\mathbf{r}_i)\psi_m(\mathbf{r}_j) f(E_m), \tag{4.7}$$

where $f(E)$ is the Fermi distribution function. The chemical potential μ is

adjusted by choosing randomly a value between the highest occupied energy E_{N_e} and the lowest empty one E_{N_e+1}. This choice helps to prevent an artificial hard gap in the density of states. After this step, all eigenenergies are counted from that chosen chemical potential, $E_m \equiv E_m - \mu$. The iteration procedure stops if the convergence criterion is satisfied. This is the difference between the density matrices $n_{ij}^{(k),in}$, $n_{ij}^{(k),out}$ going in to and out from an iteration loop k is smaller than a small error value $\delta = 10^{-4}$:

$$|n_{ij}^{(k),in} - n_{ij}^{(k),out}| \leq \delta. \tag{4.8}$$

Otherwise, a new iteration $p+1$ is to start with an update from the previous density matrices

$$n_{ij}^{(k+1),in} = (1-\lambda) n_{ij}^{(k),in} + \lambda n_{ij}^{(k),out}. \tag{4.9}$$

The parameter λ is chosen in the interval $[0,1]$ such that the iteration procedure is stable and converges. Once the converged solutions are obtained, one can compute the physical quantities that are expressed in terms of the eigenvalues $\{E_m\}$ and eigenvectors $\{\psi_m\}$. The numerical procedure is repeated for other random realizations to finally attain the disorder averaged quantities.

Following the formalism used in Refs. [74, 122] that focuses on the multifractality of the electronic wavefunctions, we are interested in the autocorrelation of the local density of states, or the spatial correlation of the Hartree-Fock wavefunctions, in a normalized form

$$K(R;E) = \frac{\overline{\sum_{m,E_m\in\Omega(E)} \sum_{\mathbf{r}} |\psi_m(\mathbf{r})|^2 |\psi_m(\mathbf{r}+\mathbf{R})|^2}}{\overline{\sum_{m,E_m\in\Omega(E)} \sum_{\mathbf{r}} |\psi_m(\mathbf{r})|^4}}. \tag{4.10}$$

The overbar denotes the average over random configurations of the disorder. $\Omega(E) = [E-\Delta, E+\Delta]$ is the interval energy centered at a given energy E with the width of the order of the mean level spacing $\Delta = W/L^2$.

The above correlation function can be used as an indicator to distinguish between an insulating and a metallic behavior since it is related to the overlapping the wavefunctions centered away from each other by a distance $R = |\mathbf{R}|$, see for example for 3D systems in Ref. [74]. Apart from being suppressed

initially at short distance that is smaller than the correlation length ξ in both cases, the larger distance behavior of the correlator is totally different. In the insulating regime, the correlator decays exponentially to zero at the distance $R \gg \xi$ demonstrating the zero overlap of the electronic wavefunctions. In contrast, in the metallic regime, it saturates to a constant value reflecting the minimal correlation of electrons even at large distance in this regime.

4.3 Density-density correlation function

In this section we report our numerical results for the correlation function. Starting with a non-interacting system of single flavor electrons, we then increase both the number of flavors and the interaction strength to detect any signal of delocalization. For all results presented below for interacting systems we have chosen a moderate disorder strength $W = 12t$ for a lattice with $L = 28$ at the filling $f = 0.1$ and at a fixed distance to the Fermi energy $E = 0.1t$. For the non-interacting case we are able to perform simulations for a system of size $L = 40$ with various values of disorder strength. The disorder average is done over 2000 realizations.

4.3.1 Non-interacting case

Without interaction, since this is a 2D system, it shows insulating behavior for any disorder strength regardless of the number of electron flavor. The correlator is suppressed further, and the localization length is reduced as the interaction gets stronger.

As for this case and also in 3D case [74], the correlation function is expected to obey a scaling behavior. This means the correlator should have a form $K(R; E) \sim A(\xi)F(R/\xi)$, where the prefactor $A(\xi)$ depends on the disorder strength while $F(x)$ is an universal function of $x = R/\xi$. After rescaling the correlator by the factor A and the distance R by the disorder-dependent localization length ξ, all the curves corresponding to different values of the disorder strength should collapse to a single curve.

Fig. (4.3) presents the data collapse after a proper rescaling with the uni-

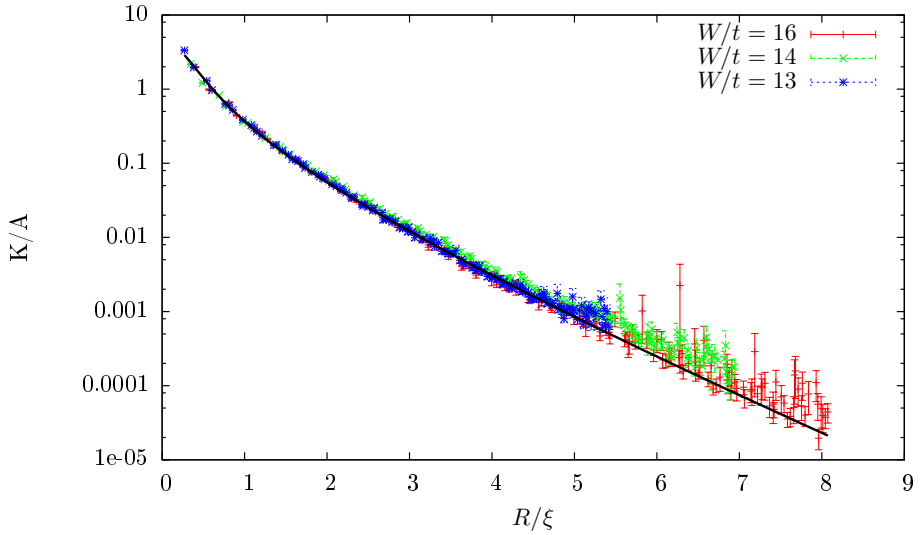

Figure 4.3: Data collapse of the correlation function for different values of disorder strength to a single scaling function $F(R/\xi)$ (solid line) for non-interacting systems. The disorder-dependent localization length is larger for a weaker disorder strength.

versal form of the scaling function found as follows. Given the localization or correlation length ξ, for $R > \xi$, the correlation function decreases exponentially with increasing distance while a weaker suppression is expected for $R < \xi$ since there is the overlapping of the wavefunctions within the localization volume. Therefore, the following form has been suggested for the scaling function:

$$F(x) \equiv K/A = x^{-\eta} e^{-x}. \tag{4.11}$$

The exponent $\eta \equiv \eta(x)$ is chosen such that it correctly obeys asymptotic behaviors.

For small distance $R < \xi$, the localization property of the wavefunction is related to its multifractal nature expressed in terms of the fractal dimension d_2, and $d_2 < d$, where $d = 2$ is the dimension of the space. The multifractal statistic of a single eigenstate corresponding to d_2 is characterized by the second moment of a single eigenstate at a given energy (i.e. the inverse participation ratio). Due to the multifractality, the typical amplitude of the local probability density is not just the inverse localization volume, but has the

following form $|\psi_m(\mathbf{r})|^2 \propto 1/\xi^{d_2}$. Therefore, we have

$$\overline{\sum_{\mathbf{r}} |\psi_m(\mathbf{r})|^4} \sim \frac{a^{d_2-d}}{\xi^{d_2}}, \tag{4.12}$$

and

$$\overline{\sum_{\mathbf{r}} |\psi_m(\mathbf{r})|^2 |\psi_m(\mathbf{r}+\mathbf{R})|^2} \sim \frac{R^{d_2-d}}{\xi^{d_2}}. \tag{4.13}$$

Putting altogether one obtains the asymptotic form for the correlation function

$$K(R) \propto \left(\frac{\xi}{R}\right)^{d-d_2}. \tag{4.14}$$

(Here the ξ-dependent constant has been absorbed into the proportional prefactor.) Therefore, the exponent in (4.11) is $\eta(x) = 2 - d_2$ for 2D.

On the other hand, in the limit $R < \xi$, it is expected that the scaling function follows the scaling theory of localization for non-interacting systems. Namely, $\eta(x) = 2 - d_2$ is a function of the dimensionless conductance g which obeys the renormalization group equation $\beta(g)$ for $g \gg 1$. This leads to $\eta(x) = 2 - d_2 \overset{R\ll\xi}{=} 2/g(x) \overset{g\gg1}{=} 2/[1 - \ln(x)]$ [123, 124].

For large distance $R > \xi$, the wavefunctions centered far away from each other by distance R just overlap via their exponential tails as it is equivalent to the case in the strongly insulating regime. The fractal dimension is thus expected to approximately be zero [125], resulting in a asymptotic value two for η, $\eta(x) \overset{R\gg\xi}{\to} 2$. Taking both the above limits into account, we have employed the following function

$$\eta(x) = \frac{2}{c_1^{-1} \ln(x^{-c_1} + c_2) e^{-x/c_3} + c_4}, \tag{4.15}$$

where $c_{1,2,3,4} \sim O(1)$.

4.3.2 Interacting case

Figs. (4.4), (4.5), (4.6) plot the normalized correlation function for various values of the interaction strength and for three values of the electron flavor number $p = 1, 2, 4$, respectively. For the single flavor case $p = 1$, the corre-

lation function is suppressed more with distance as the interaction gradually gets enhanced.

However, the picture changes when there is more than one electron species in the system. At small interaction strength, $U/t < 0.8$ for $p = 2$ in Fig. (4.5) and $U/t \leq 0.4$ for $p = 4$ in Fig. (4.6), the behavior of the correlation function is almost similar to the single species case. In contrast, for larger interaction strengths, after a drastic drop at small distance, the correlator slowly varies with larger distance, even seems to saturate in the case $p = 4$. Upon increasing the number of electron flavors, the above two-stage behavior of the correlator with increasing distance occurs at smaller interaction strength and gets more significant.

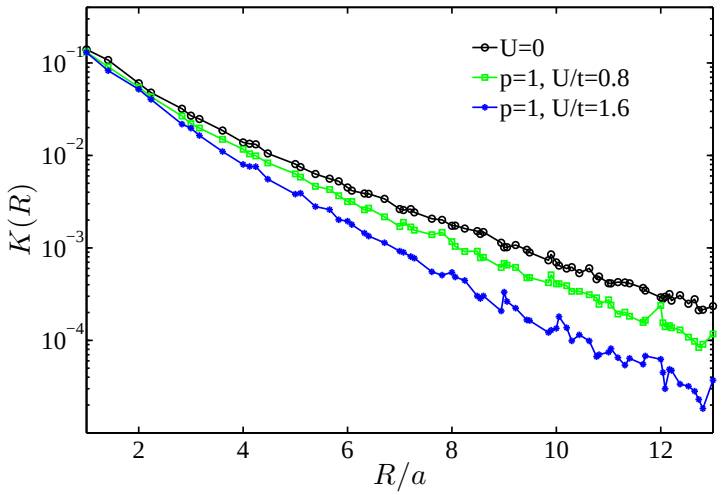

Figure 4.4: The normalized correlation function for different values of interaction strength for the single flavor case.

Our first attempt is to employ the same scaling ansatz presented above for the insulating behavior that has been shown to work well for the non-interacting case. However, it turns out that the one-parameter scaling function is applicable to the current data only for the case with a single electron species, $p = 1$, for any value of the interaction. The complex behavior apparently does not allow the correlation function in the multiple electron flavor case to follow the same simple ansatz as in the single flavor case.

Indeed, it seems counterintuitive that upon increasing the electron flavor number, the Hartree term is strengthened, one sees a stronger drop of the cor-

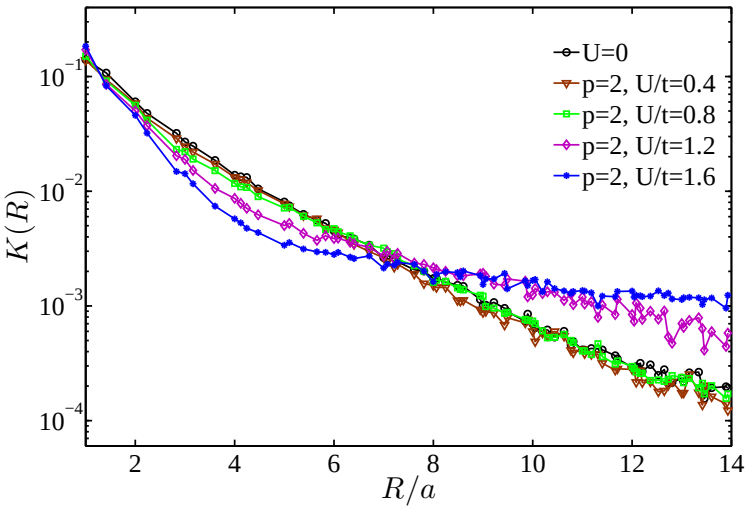

Figure 4.5: The normalized correlation function for different values of interaction strength for the flavor number $p = 2$.

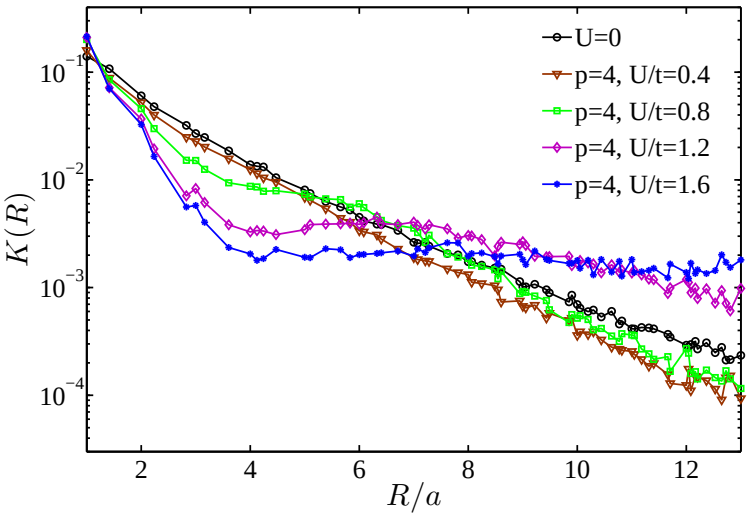

Figure 4.6: The normalized correlation function for different values of interaction strength for the flavor number $p = 4$.

relation function at short distance. However, this initial strong drop and the following slow variation at larger distance of the function might correspond to the non-monotonicity of the scale-dependent resistance predicted in Punnoose and Finkel'stein's renormalization group equations due to a complex interplay of terms favorable to anti-localization and localization. In the case with $p = 2, 4$, a drastic change happens, a steep derivative at small distance is replaced by a much flatter one at large distance.

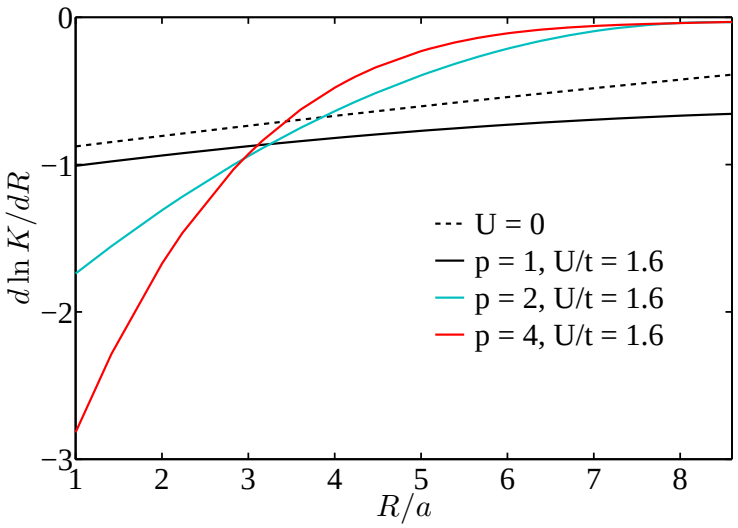

Figure 4.7: The rough approximation for the logarithmic derivatives of the correlation function as a function of distance R.

The possible scale l in our current problem is the minimum among $\ln L$, $-\ln(T\tau)$, and $\ln R$. However, since the system we study is at zero temperature $T = 0$ and initially is localized, the most relevant length scale is the distance R. In Fig. (4.7), we demonstrate better the two-stage behavior of the correlator in cases with multiple flavors by sketching its logarithmic derivative for a given interaction strength $U/t = 1.6$. There is a similar tendency, gradually slightly increasing, of the logarithmic derivative in the non-interacting and interacting case with single flavor, although the amplitude of the derivative in the latter is larger reflecting an enhancement of localization. (Note that the employed Hartree-Fock treatment does not include the (random phase approximation) screening, and thus the interaction strength may enter.)

4.4 Discussion and summary

At this primary stage, our message here is that at the Hartree-Fock level there is a clear difference in the localization property between cases with single and multiple flavors of electrons. In the single flavor case where the Hartree and Fock terms are on an equal footing, only localization tendency is observed as the interaction increases as expected. In contrast, in the case with

multiple flavors that emphasizes the Hartree term, a complex behavior of the correlation function has emerged: a strong suppression at short distance and a very slow variation at larger distance for a moderate or large interaction strength.

It is worth to notice that the above two-stage characteristic of the correlation function may reflect the non-monotonic scale-dependent resistance obtained in Punnoose and Finkel'stein's theory. It all comes from the striking competition between opposite tendencies that support localization or anti-localization in two dimensional systems.

Our unsuccessful attempt to employ the one-parameter scaling that has worked well in 3D case for the correlation functions in the current setting raises some related questions. Firstly, does it mean that the scaling with one-parameter is not adequate to detect the effect here? One could also suspect that the correlation length is also scale-dependent, and thus, requires a different approach for the scaling function.

As for next step, one could try to work out a suitable interpolating function for the correlation function to obtain the characteristic length of the system. Or there might be other quantities that describe better the non-monotonicity of the resistance. On the numerical side, a further implementation of the Hartree-Fock procedure is needed in order to incorporate better the correlation and the many-body physics in the study. For example, to take into account a proper screening treatment via the random phase approximation is certainly relevant for a better result.

Appendix A

Period doubling in the magnetoresistance of non-interacting fermions

This appendix recalls the period-doubling in the magnetoresistance of non-interacting fermions on regular lattices, as evaluated within the forward scattering approximation. If the disordered onsite energies are uncorrelated and symmetrically distributed around $\omega = 0$, one can prove that the localization length as a function of flux, $\xi(B)$, is a periodic function of B with the reduced period $B_0/2$, B_0 corresponding to one flux quantum threading a unit cell of the lattice. We show this for the cases of square and honeycomb lattices, see Fig. A.1. In both lattices we marked a fraction of the sites with blue spots.

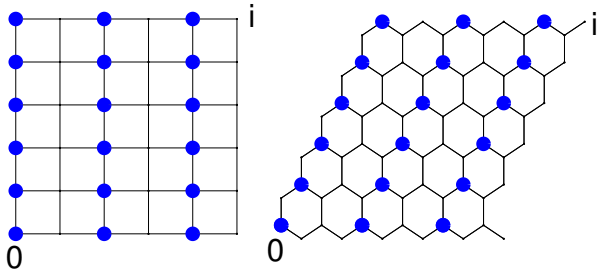

Figure A.1: Analyzing fermionic localization on two different lattices. For localization at energy $\omega = 0$, adding half a flux quantum per unit cell is equivalent to having no flux and changing the sign of onsite disorder on the subset of sites marked by circles, which yields a statistically equiprobable disorder configuration. For a symmetric disorder distribution, this property implies a period doubling of the magnetoresistance for non-interacting fermions, when evaluated in forward scattering approximation.

Consider the sum over shortest paths Γ connecting site 0 to site i, in the presence of a magnetic field B. Adding half a flux quantum per plaquette, one easily checks that the extra Aharonov-Bohm phase between two paths Γ and Γ' is given by $(-1)^{N_s}$, where N_s is the number of marked sites that are not shared by both paths. One can verify that the same relative phase is obtained if the signs of all locators on the marked sites is reversed. This implies that up to a global sign the sum over paths at $\omega = 0$ is equivalent to a sum in a field $B + B_0/2$, but with reversed sign of the onsite energy on marked sites. This change of sign leaves the measure of uncorrelated random energies invariant, provided the disorder distribution is symmetric around $\omega = 0$, $\rho(\epsilon) = \rho(-\epsilon)$. From this, one concludes that $\xi(B) = \xi(B + B_0/2)$ is periodic with period $B_0/2$ for a symmetric disorder distribution and for $\omega = 0$.

For featureless densities of states and energies in the bulk of the spectrum the doubling of the periodicity is not exact, but nevertheless holds to a very good approximation.

Note that time reversal symmetry further implies the symmetry $\xi(B) = \xi(-B)$.

As we discuss in the main text, the above proof breaks down when the onsite energies are correlated, even if the density of states remains symmetric.

Bibliography

[1] H. Kamerlingh-Onnes. On the sudden change in the rate at which the resistance of mercury disappears. *Comm. Phys. Lab. Univ. Leiden*, page 124, 1911. (Cited on page 5.)

[2] J. Bardeen, L. N. Cooper, and J. R. Schrieffer. Theory of superconductivity. *Phys. Rev.*, 108:1175–1204, 1957. (Cited on page 5.)

[3] P. W. Anderson. Absence of diffusion in certain random lattices. *Phys. Rev.*, 109:1492–1505, 1958. (Cited on pages 5 and 73.)

[4] L. N. Cooper. Bound electron pairs in a degenerate Fermi gas. *Phys. Rev.*, 104:1189–1190, 1956. (Cited on page 5.)

[5] P. Monthoux, D. Pines, and G. G. Lonzarich. Superconductivity without phonons. *Nature*, 450(7173):1177–1183, 2007. (Cited on page 5.)

[6] P. W. Anderson. Theory of dirty superconductors. *J. Phys. Chem. Solids*, 11(1-2):26–30, 1959. (Cited on page 5.)

[7] A. A. Abrikosov and L. P. Gor'kov. Superconducting alloys at finite temperatures. *Sov. Phys.-JETP (Engl. Transl.);(United States)*, 9(1), 1959. (Cited on page 5.)

[8] M. Ma and P. A. Lee. Localized superconductors. *Phys. Rev. B*, 32:5658–5667, 1985. (Cited on pages 6, 13 and 17.)

[9] E. Abrahams, P. W. Anderson, D. C. Licciardello, and T. V. Ramakrishnan. Scaling theory of localization: Absence of quantum diffusion in two dimensions. *Phys. Rev. Lett.*, 42:673–676, 1979. (Cited on pages 6, 73 and 74.)

[10] S. V. Kravchenko, G. V. Kravchenko, J. E. Furneaux, V. M. Pudalov, and M. D'Iorio. Possible metal-insulator transition at B =0 in two dimensions. *Phys. Rev. B*, 50:8039–8042, 1994. (Cited on pages 6 and 74.)

[11] A. Punnoose and A. M. Finkel'stein. Dilute electron gas near the metal-insulator transition: Role of valleys in silicon inversion layers. *Phys. Rev. Lett.*, 88:016802, 2001. (Cited on pages 6, 12, 75, 76 and 77.)

[12] Sachdev S. *Quantum Phase Transitions:*. Cambridge University Press, Cambridge, 2 edition, 2011. (Cited on page 6.)

[13] C. Bruder, R. Fazio, and G. Schön. The Bose-Hubbard model: from Josephson junction arrays to optical lattices. *Ann. Phys. (Leipzig)*, 14(9-10):566–577, 2005. (Cited on page 6.)

[14] L. Sanchez-Palencia and M. Lewenstein. Disordered quantum gases under control. *Nat. Phys.*, 6(2):87–95, 2010. (Cited on page 6.)

[15] M. A. Steiner, G. Boebinger, and A. Kapitulnik. Possible field-tuned superconductor-insulator transition in high-T_c superconductors: Implications for pairing at high magnetic fields. *Phys. Rev. Lett.*, 94:107008, 2005. (Cited on pages 7 and 38.)

[16] Y. Dubi, Y. Meir, and Y. Avishai. Nature of the superconductor–insulator transition in disordered superconductors. *Nature*, 449(7164):876–880, 2007. (Cited on pages 7 and 8.)

[17] D. M. Basko, I. L. Aleiner, and B. L. Altshuler. Metal–insulator transition in a weakly interacting many-electron system with localized single-particle states. *Ann. Phys. (N.Y.)*, 321(5):1126–1205, 2006. (Cited on page 7.)

[18] I. V. Gornyi, A. D. Mirlin, and D. G. Polyakov. Interacting electrons in disordered wires: Anderson localization and low-T transport. *Phys. Rev. Lett.*, 95:206603, 2005. (Cited on page 7.)

[19] A. M. Finkel'stein. Suppression of superconductivity in homogeneously disordered systems. *Physica B*, 197(1-4):636–648, 1994. (Cited on page 7.)

[20] A. M. Finkel'stein. Superconducting transition temperature in amorphous films. *JETP Lett.*, 45:46, 1987. (Cited on pages 7 and 13.)

[21] K. B. Efetov. Phase transition in granulated superconductors. *Sov. Phys.-JETP (Engl. Transl.);(United States)*, 51(5), 1980. (Cited on page 8.)

[22] A. Larkin. Superconductor-insulator transitions in films and bulk materials. *Ann. Phys. (Leipzig)*, 8(7-9):785–794, 1999. (Cited on page 8.)

[23] Y. M. Strelniker, A. Frydman, and S. Havlin. Percolation model for the superconductor-insulator transition in granular films. *Phys. Rev. B*, 76:224528, 2007. (Cited on page 8.)

[24] Y. Dubi, Y. Meir, and Y. Avishai. Quantum hall criticality, superconductor-insulator transition, and quantum percolation. *Phys. Rev. B*, 71:125311, 2005. (Cited on page 8.)

[25] M. P. A. Fisher. Quantum phase transitions in disordered two-dimensional superconductors. *Phys. Rev. Lett.*, 65:923–926, 1990. (Cited on pages 8 and 13.)

[26] M. V. Feigel'man, L. B. Ioffe, V. E. Kravtsov, and E. A. Yuzbashyan. Eigenfunction fractality and pseudogap state near the superconductor-insulator transition. *Phys. Rev. Lett.*, 98(2):027001, 2007. (Cited on pages 8 and 13.)

[27] M. V. Feigel'man, L. B. Ioffe, V. E. Kravtsov, and E. Cuevas. Fractal superconductivity near localization threshold. *Ann. Phys. (N.Y.)*, 325:1390–1478, 2010. (Cited on pages 8, 13, 18, 24 and 42.)

[28] I. S. Burmistrov, I. V. Gornyi, and A. D. Mirlin. Enhancement of the critical temperature of superconductors by Anderson localization. *Phys. Rev. Lett.*, 108(1):017002, 2012. (Cited on pages 8 and 13.)

[29] V. F. Gantmakher and V. T. Dolgopolov. Superconductor-insulator quantum phase transition. *Phys. Usp.*, 53(1):1–49, 2010. (Cited on page 8.)

[30] A. M. Goldman. Superconductor-insulator transitions. *Int. J. Mod Phys B*, 24(20n21):4081–4101, 2010. (Cited on page 8.)

[31] A. F. Hebard and M. A. Paalanen. Magnetic-field-tuned superconductor-insulator transition in two-dimensional films. *Phys. Rev. Lett.*, 65(7):927, 1990. (Cited on pages 8 and 13.)

[32] G. Sambandamurthy, L. W. Engel, A. Johansson, and D. Shahar. Superconductivity-related insulating behavior. *Phys. Rev. Lett.*, 92(10):107005, 2004. (Cited on pages 8, 9, 14 and 38.)

[33] M. Steiner and A. Kapitulnik. Superconductivity in the insulating phase above the field-tuned superconductor–insulator transition in disordered indium oxide films. *Physica C*, 422(1):16–26, 2005. (Cited on pages 8, 9, 14 and 38.)

[34] T. I. Baturina, A. Yu. Mironov, V. M. Vinokur, M. R. Baklanov, and C. Strunk. Localized superconductivity in the quantum-critical region of the disorder-driven superconductor-insulator transition in tin thin films. *Phys. Rev. Lett.*, 99(25):257003, 2007. (Cited on pages 8, 9, 14 and 38.)

[35] T. I. Baturina, S. V. Postolova, A. Yu. Mironov, A. Glatz, M. R. Baklanov, and V. M. Vinokur. Superconducting phase transitions in ultrathin tin films. *Europhys. Lett.*, 97(1):17012, 2012. (Cited on page 8.)

[36] D. B. Haviland, Y. Liu, and A. M. Goldman. Onset of superconductivity in the two-dimensional limit. *Phys. Rev. Lett.*, 62:2180–2183, 1989. (Cited on page 8.)

[37] Kevin A. Parendo, K. H. Sarwa B. Tan, A. Bhattacharya, M. Eblen-Zayas, N. E. Staley, and A. M. Goldman. Electrostatic tuning of the superconductor-insulator transition in two dimensions. *Phys. Rev. Lett.*, 94:197004, 2005. (Cited on page 8.)

[38] M. D. Stewart, A. Yin, J. M. Xu, and J. M. Valles. Superconducting pair correlations in an amorphous insulating nanohoneycomb film. *Science*, 318:1273, 2007. (Cited on pages 8, 10, 14, 17, 28, 30 and 35.)

[39] H. Q. Nguyen, S. M. Hollen, M. D. Stewart, Jr., J. Shainline, A. Yin, J. M. Xu, and J. M. Valles, Jr. Observation of giant positive magnetore-

sistance in a Cooper pair insulator. *Phys. Rev. Lett.*, 103(15):157001, 2009. (Cited on pages 8, 9, 10, 14, 17, 28, 30, 35 and 38.)

[40] M. Chand, G. Saraswat, A. Kamlapure, M. Mondal, S. Kumar, J. Jesudasan, V. Bagwe, L. Benfatto, V. Tripathi, and P. Raychaudhuri. Phase diagram of the strongly disordered *s*-wave superconductor NbN close to the metal-insulator transition. *Phys. Rev. B*, 85:014508, 2012. (Cited on pages 8, 9 and 38.)

[41] A. Yazdani and A. Kapitulnik. Superconducting-insulating transition in two-dimensional *a*-MoGe thin films. *Phys. Rev. Lett.*, 74:3037–3040, 1995. (Cited on page 8.)

[42] A. D. Caviglia, S. Gariglio, N. Reyren, D. Jaccard, T. Schneider, M. Gabay, S. Thiel, G. Hammerl, J. Mannhart, and J.-M. Triscone. Electric field control of the LaAlO3/SrTiO3 interface ground state. *Nature*, 456(7222):624–627, 2008. (Cited on page 8.)

[43] M. Kim, Y. Kozuka, C. Bell, Y. Hikita, and H. Y. Hwang. Intrinsic spin-orbit coupling in superconducting δ-doped $SrTiO_3$ heterostructures. *Phys. Rev. B*, 86:085121, 2012. (Cited on page 9.)

[44] J. T. Ye, Y. J. Zhang, R. Akashi, M. S. Bahramy, R. Arita, and Y. Iwasa. Superconducting dome in a gate-tuned band insulator. *Science*, 338(6111):1193–1196, 2012. (Cited on page 9.)

[45] M. A. Paalanen, A. F. Hebard, and R. R. Ruel. Low-temperature insulating phases of uniformly disordered two-dimensional superconductors. *Phys. Rev. Lett.*, 69(10):1604, 1992. (Cited on pages 9, 13 and 37.)

[46] V. F. Gantmakher, M. V. Golubkov, V. T. Dolgopolov, G. E. Tsydynzhapov, and A. A. Shashkin. Destruction of localized electron pairs above the magnetic-field-driven superconductor-insulator transition in amorphous In-O films. *JETP Lett.*, 68(4):363–369, 1998. (Cited on pages 9 and 38.)

[47] N. Marković, A. M. Mack, G. Martinez-Arizala, C. Christiansen, and A. M. Goldman. Evidence of vortices on the insulating side of the superconductor-insulator transition. *Phys. Rev. Lett.*, 81:701–704, 1998. (Cited on pages 9 and 38.)

[48] Y.-H. Lin and A. M. Goldman. Magnetic-field-tuned quantum phase transition in the insulating regime of ultrathin amorphous Bi films. *Phys. Rev. Lett.*, 106:127003, 2011. (Cited on pages 9 and 38.)

[49] S. M. Hollen, J. Shainline, J. M. Xu, and J. M. Valles. Cooper pair insulator phase induced in amorphous $Pb_{0.9}Bi_{0.1}$ thin films. *Physica C*, 486:23–25, 2013. (Cited on pages 9, 38 and 67.)

[50] G. Kopnov, O. Cohen, M. Ovadia, K. H. Lee, C. C. Wong, and D. Shahar. Little-Parks oscillations in an insulator. *Phys. Rev. Lett.*, 109(16):167002, 2012. (Cited on pages 9, 14 and 28.)

[51] Thuong T. Nguyen and M. Müller. Magneto-oscillations of the mobility edge in coulomb frustrated bosons and fermions. *arXiv:1606.07747*, 2016. (Cited on page 11.)

[52] A. Punnoose and A. M. Finkel'stein. Metal-insulator transition in disordered two-dimensional electron systems. *Science*, 310(5746):289–291, 2005. (Cited on pages 12 and 75.)

[53] A. Kapitulnik and G. Kotliar. Anderson localization and the theory of dirty superconductors. *Phys. Rev. Lett.*, 54:473–476, 1985. (Cited on page 13.)

[54] A. Ghosal, M. Randeria, and N. Trivedi. Role of spatial amplitude fluctuations in highly disordered s-wave superconductors. *Phys. Rev. Lett.*, 81:3940–3943, 1998. (Cited on pages 13 and 42.)

[55] V. E. Kravtsov. Wonderful life at weak Coulomb interaction: increasing of superconducting/superfluid transition temperature by disorder. *J. Phys.: Conf. Ser.*, 376(1):012003, 2012. (Cited on page 13.)

[56] A. Ghosal, M. Randeria, and N. Trivedi. Inhomogeneous pairing in highly disordered s-wave superconductors. *Phys. Rev. B*, 65(1):014501, 2002. (Cited on page 13.)

[57] M. V. Feigel'man, L. B. Ioffe, and M. Mézard. Superconductor-insulator transition and energy localization. *Phys. Rev. B*, 82(18):184534, 2010. (Cited on page 13.)

[58] P. Reunchan, X. Zhou, S. Limpijumnong, A. Janotti, and C. G. Van de Walle. Vacancy defects in indium oxide: An ab-initio study. *Curr. Appl. Phys.*, 11(3):S296–S300, 2011. (Cited on page 13.)

[59] M. Dzero and J. Schmalian. Superconductivity in charge Kondo systems. *Phys. Rev. Lett.*, 94(15):157003, 2005. (Cited on page 13.)

[60] M. Müller. Magnetoresistance and localization in bosonic insulators. *Europhys. Lett.*, 102:67008, 2013. (Cited on pages 14, 15, 16, 20, 24, 39 and 52.)

[61] S. V. Syzranov, A. Moor, and K. B. Efetov. Strong quantum interference in strongly disordered bosonic insulators. *Phys. Rev. Lett.*, 108(25):256601, 2012. (Cited on page 14.)

[62] A. Gangopadhyay, V. Galitski, and M. Müller. Magnetoresistance of an Anderson insulator of bosons. *Phys. Rev. Lett.*, 111(2):026801, 2013. (Cited on pages 14, 20, 21, 26, 27, 31, 32, 38 and 39.)

[63] V. L. Nguyen, B. Z. Spivak, and B. I. Shklovskii. Jetp lett. 41 (1985) 42. *Pisma Zh. ÉEksp. Teor. Fiz*, 41:35, 1985. (Cited on pages 14, 20 and 21.)

[64] B. I. Shklovskii, B. Z. Spivak, M. Pollak, and B. I. Shklovskii. Hopping transport in solids. *Modern Problems in Condensed Matter Physics, North Holland, Amsterdam*, 28:271, 1991. (Cited on pages 14, 20, 26, 31, 33 and 39.)

[65] L. B. Ioffe and B. Z. Spivak. Giant magnetoresistance in the variable-range hopping regime. *J. Exp. Theor. Phys.*, 117:551–569, 2013. (Cited on pages 14, 26, 31, 32 and 39.)

[66] Y.-H. Lin, J. Nelson, and A. M. Goldman. The role of mesoscopic disorder in determining the character of the field-induced insulating regime of amorphous ultrathin films. *Physica C (Amsterdam, Neth.)*, 497:102–109, 2014. (Cited on page 14.)

[67] S. M. Hollen, G. E. Fernandes, J. M. Xu, and J. M. Valles Jr. Fate of the Bose insulator in the limit of strong localization and low Cooper-pair density in ultrathin films. *Phys. Rev. B*, 90(14):140506, 2014. (Cited on pages 14, 28, 35 and 38.)

[68] D. Gurovich, K. S. Tikhonov, D. Mahalu, and D. Shahar. Little-Parks oscillations in a single ring in the vicinity of the superconductor-insulator transition. *Phys. Rev. B*, 91(17):174505, 2015. (Cited on page 14.)

[69] S. Mitra, G. C. Tewari, D. Mahalu, and D. Shahar. Finite-size effects in amorphous indium oxide. *Phys. Rev. B*, 93(15):155408, 2016. (Cited on page 14.)

[70] M. Müller. Purely electronic transport and localization in the Bose glass. *Ann. Phys. (Leipzig)*, 521:849–855, 2009. (Cited on pages 14, 15 and 23.)

[71] L. B. Ioffe and M. Mézard. Disorder-driven quantum phase transitions in superconductors and magnets. *Phys. Rev. Lett.*, 105(3):037001, 2010. (Cited on page 15.)

[72] A. L. Efros and B. I. Shklovskii. Coulomb gap and low temperature conductivity of disordered systems. *J. Phys. C: Solid State Phys.*, 8:L49–L51, 1975. (Cited on pages 15 and 19.)

[73] F. Epperlein, M. Schreiber, and T. Vojta. Quantum Coulomb glass within a Hartree-Fock approximation. *Phys. Rev. B*, 56(10):5890, 1997. (Cited on page 15.)

[74] M. Amini, V. E. Kravtsov, and M. Müller. Multifractality and quantum-to-classical crossover in the Coulomb anomaly at the Mott-Anderson metal-insulator transition. *New J. Phys.*, 16(1):015022, 2014. (Cited on pages 15, 21, 77, 80 and 81.)

[75] I. S. Burmistrov, I. V. Gornyi, and A. D. Mirlin. Multifractality at Anderson transitions with Coulomb interaction. *Phys. Rev. Lett.*, 111(6):066601, 2013. (Cited on pages 15 and 21.)

[76] X. Yu and M. Müller. Localization of disordered bosons and magnets in random fields. *Ann. Phys. (N.Y.)*, 337:55–93, 2013. (Cited on pages 16 and 24.)

[77] E. Cuevas, M. Feigel'man, L. Ioffe, and M. Mezard. Level statistics of disordered spin-1/2 systems and materials with localized Cooper pairs. *Nat. Commun.*, 3:1128, 2012. (Cited on page 16.)

[78] B. I. Shklovskii. Variable range hopping in thin film with large dielectric constant. *ArXiv e-prints*, 2008. (Cited on page 18.)

[79] S. D. Baranovskii, A. L. Efros, B. L. Gelmont, and B. I. Shklovskii. Coulomb gap in disordered systems: computer simulation. *J. Phys. C: Solid State Phys.*, 12:1023–1034, 1979. (Cited on page 19.)

[80] E. Medina and M. Kardar. Quantum interference effects for strongly localized electrons. *Phys. Rev. B*, 46:9984–10006, 1992. (Cited on pages 20 and 26.)

[81] M. Kardar. *Statistical Physics of Fields*. 2007. (Cited on page 20.)

[82] M. V. Fistul, V. M. Vinokur, and T. I. Baturina. Collective Cooper-pair transport in the insulating state of Josephson-junction arrays. *Phys. Rev. Lett.*, 100(8):086805, 2008. (Cited on page 23.)

[83] D. Kowal and Z. Ovadyahu. Scale dependent superconductor insulator transition. *Physica C*, 468:322–325, 2008. (Cited on page 23.)

[84] H. Kim and D. A. Huse. Interfering directed paths and the sign phase transition. *Phys. Rev. B*, 83(5):052405, 2011. (Cited on page 26.)

[85] J. Prior, A. M. Somoza, and M. Ortuño. Conductance distribution in two-dimensional localized systems with and without magnetic fields. *Eur. Phys. J. B*, 70:513–521, 2009. (Cited on pages 26 and 32.)

[86] J. H. Davies, P. A. Lee, and T. M. Rice. Properties of the electron glass. *Phys. Rev. B*, 29:4260–4271, 1984. (Cited on page 33.)

[87] S. A. Basylko, V. A. Onischouk, and A. Rosengren. Coulomb glass in the random phase approximation. *Phys. Rev. B*, 65(2):024206, 2001. (Cited on page 33.)

[88] V. F. Gantmakher, M. V. Golubkov, V. T. Dolgopolov, G. E. Tsydynzhapov, and A. A. Shashkin. Superconductor–insulator transition in amorphous In–O films. *Physica B*, 284:649–650, 2000. (Cited on page 38.)

[89] A. Johansson, I. Shammass, N. Stander, E. Peled, G. Sambandamurthy, and D. Shahar. Angular dependence of the magnetic-field driven superconductor–insulator transition in thin films of amorphous indium-oxide. *Solid State Commun.*, 151(9):743–746, 2011. (Cited on pages 38, 64 and 71.)

[90] I. Shammass, O. Cohen, M. Ovadia, I. Gutman, and D. Shahar. Superconducting correlations in thin films of amorphous indium oxide on the insulating side of the disorder-tuned superconductor-insulator transition. *Phys. Rev. B*, 85:140507, 2012. (Cited on pages 38, 64, 67 and 71.)

[91] Y. Dubi, Y. Meir, and Y. Avishai. Theory of the magnetoresistance of disordered superconducting films. *Phys. Rev. B*, 73:054509, 2006. (Cited on pages 38 and 39.)

[92] E. Porat and Y. Meir. Magnetoresistance anisotropy in amorphous superconducting thin films: Site-bond percolation approach. *Phys. Rev. B*, 92:024509, 2015. (Cited on pages 38 and 39.)

[93] Victor M. Galitski, G. Refael, Matthew P. A. Fisher, and T. Senthil. Vortices and quasiparticles near the superconductor-insulator transition in thin films. *Phys. Rev. Lett.*, 95:077002, 2005. (Cited on pages 38 and 39.)

[94] V. L. Pokrovsky, G. M. Falco, and T. Nattermann. Phase diagram of electron systems near the superconductor-insulator transition. *Phys. Rev. Lett.*, 105:267001, 2010. (Cited on pages 38, 39 and 42.)

[95] I. S. Burmistrov, I. V. Gornyi, and A. D. Mirlin. Superconductor-insulator transitions: Phase diagram and magnetoresistance. *Phys. Rev. B*, 92:014506, 2015. (Cited on pages 38 and 39.)

[96] T. Chen, B. Skinner, and B. I. Shklovskii. Coulomb gap triptychs, $\sqrt{2}$ effective charge, and hopping transport in periodic arrays of superconductor grains. *Phys. Rev. B*, 86:045135, 2012. (Cited on pages 38 and 68.)

[97] J. Mitchell, A. Gangopadhyay, V. Galitski, and M. Müller. Two-component coulomb glass in insulators with a local attraction. *Phys. Rev. B*, 85:195141, 2012. (Cited on pages 38 and 68.)

[98] B. Sacépé, J. Seidemann, M. Ovadia, I. Tamir, D. Shahar, C. Chapelier, C. Strunk, and B. A. Piot. High-field termination of a cooper-pair insulator. *Phys. Rev. B*, 91:220508, 2015. (Cited on page 40.)

[99] N. F. Mott. Conduction in non-crystalline materials: Iii. localized states in a pseudogap and near extremities of conduction and valence bands. *Philosophical Magazine*, 19(160):835–852, 1969. (Cited on page 40.)

[100] K. Bouadim, Y. L. Loh, M. Randeria, and N. Trivedi. Single-and two-particle energy gaps across the disorder-driven superconductor-insulator transition. *Nat. Phys.*, 7(11):884–889, 2011. (Cited on page 42.)

[101] B. Tanatar and D. M. Ceperley. Ground state of the two-dimensional electron gas. *Phys. Rev. B*, 39:5005–5016, 1989. (Cited on page 74.)

[102] S. V. Kravchenko, Whitney E. Mason, G. E. Bowker, J. E. Furneaux, V. M. Pudalov, and M. D'Iorio. Scaling of an anomalous metal-insulator transition in a two-dimensional system in silicon at B =0. *Phys. Rev. B*, 51:7038–7045, 1995. (Cited on page 74.)

[103] K. M. Mertes, D. Simonian, M. P. Sarachik, S. V. Kravchenko, and T. M. Klapwijk. Response to parallel magnetic field of a dilute two-dimensional electron system across the metal-insulator transition. *Phys. Rev. B*, 60:R5093–R5096, 1999. (Cited on page 74.)

[104] D. Popović, A. B. Fowler, and S. Washburn. Metal-insulator transition in two dimensions: Effects of disorder and magnetic field. *Phys. Rev. Lett.*, 79:1543–1546, 1997. (Cited on page 74.)

[105] S. V. Kravchenko and T. M. Klapwijk. Metallic low-temperature resistivity in a 2D electron system over an extended temperature range. *Phys. Rev. Lett.*, 84:2909–2912, 2000. (Cited on page 74.)

[106] Y. Hanein, U. Meirav, D. Shahar, C. C. Li, D. C. Tsui, and H. Shtrikman. The metallic-like conductivity of a two-dimensional hole system. *Phys. Rev. Lett.*, 80:1288–1291, 1998. (Cited on page 74.)

[107] E. Ribeiro, R. D. Jäggi, T. Heinzel, K. Ensslin, G. Medeiros-Ribeiro, and P. M. Petroff. Metal-insulator transition in a disordered two-dimensional electron gas in GaAs-AlGaAs at zero magnetic field. *Phys. Rev. Lett.*, 82:996–999, 1999. (Cited on page 74.)

[108] A. P. Mills, A. P. Ramirez, L. N. Pfeiffer, and K. W. West. Nonmonotonic temperature-dependent resistance in low density 2D hole gases. *Phys. Rev. Lett.*, 83:2805–2808, 1999. (Cited on page 74.)

[109] M. Y. Simmons, A. R. Hamilton, M. Pepper, E. H. Linfield, P. D. Rose, D. A. Ritchie, A. K. Savchenko, and T. G. Griffiths. Metal-insulator transition at $B = 0$ in a dilute two dimensional GaAs-AlGaAs hole gas. *Phys. Rev. Lett.*, 80:1292–1295, 1998. (Cited on page 74.)

[110] K. Lai, W. Pan, D. C. Tsui, S. A. Lyon, M. Mühlberger, and F. Schäffler. Two-dimensional metal-insulator transition and in-plane magnetoresistance in a high-mobility strained Si quantum well. *Phys. Rev. B*, 72:081313, 2005. (Cited on page 74.)

[111] G. Benenti, X. Waintal, and J.-L. Pichard. New quantum phase between the Fermi glass and the Wigner crystal in two dimensions. *Phys. Rev. Lett.*, 83:1826–1829, 1999. (Cited on page 75.)

[112] R. Kotlyar and S. Das Sarma. Disorder and interaction in 2D: Exact diagonalization study of the Anderson-Hubbard-Mott model. *Phys. Rev. Lett.*, 86:2388–2391, 2001. (Cited on page 75.)

[113] G. Fleury and X. Waintal. Many-body localization study in low-density electron gases: Do metals exist in two dimensions? *Phys. Rev. Lett.*, 101:226803, 2008. (Cited on page 75.)

[114] P. J. H. Denteneer, R. T. Scalettar, and N. Trivedi. Conducting phase in the two-dimensional disordered Hubbard model. *Phys. Rev. Lett.*, 83:4610–4613, 1999. (Cited on page 75.)

[115] B. Srinivasan, G. Benenti, and D. L. Shepelyansky. Delocalizing effect of the Hubbard repulsion for electrons on a two-dimensional disordered lattice. *Phys. Rev. B*, 67:205112, 2003. (Cited on page 75.)

[116] B. L. Altshuler, A. G. Aronov, and P. A. Lee. Interaction effects in disordered Fermi systems in two dimensions. *Phys. Rev. Lett.*, 44:1288–1291, 1980. (Cited on pages 75 and 76.)

[117] A. M. Finkel'stein. Influence of Coulomb interaction on the properties of disordered metals. *Sov. Phys. JETP*, 57(1):97–108, 1983. (Cited on page 75.)

[118] C. Castellani, C. Di Castro, P. A. Lee, and M. Ma. Interaction-driven metal-insulator transitions in disordered fermion systems. *Phys. Rev. B*, 30:527–543, 1984. (Cited on page 75.)

[119] Gábor Zala, B. N. Narozhny, and I. L. Aleiner. Interaction corrections at intermediate temperatures: Longitudinal conductivity and kinetic equation. *Phys. Rev. B*, 64:214204, 2001. (Cited on page 75.)

[120] D. Belitz and T. R. Kirkpatrick. The Anderson-Mott transition. *Rev. Mod. Phys.*, 66:261–380, 1994. (Cited on page 75.)

[121] E. Abrahams, S. V. Kravchenko, and M. P. Sarachik. Metallic behavior and related phenomena in two dimensions. *Rev. Mod. Phys.*, 73:251–266, 2001. (Cited on page 75.)

[122] A. Richardella, P. Roushan, S. Mack, B. Zhou, D. A. Huse, D. D. Awschalom, and A. Yazdani. Visualizing critical correlations near the metal-insulator transition in $Ga_{1-x}Mn_xAs$. *Science*, 327(5966):665–669, 2010. (Cited on page 80.)

[123] F. Wegner. Inverse participation ratio in $2+\varepsilon$ dimensions. *Zeitschrift für Physik B Condensed Matter*, 36(3):209–214, 1980. (Cited on page 83.)

[124] V. I. Fal'ko and K. B. Efetov. Statistics of prelocalized states in disordered conductors. *Phys. Rev. B*, 52:17413–17429, 1995. (Cited on page 83.)

[125] V. E. Kravtsov and K. A. Muttalib. New class of random matrix ensembles with multifractal eigenvectors. *Phys. Rev. Lett.*, 79:1913–1916, 1997. (Cited on page 83.)